Femtomole Adsorption Calorimetry on Single-Crystal Surfaces

W. A. Brown, R. Kose, and D. A. King*

Department of Chemistry, University of Cambridge, Lensfield Road, Cambridge CB2 1EW, U.K.

Received September 11, 1997 (Revised Manuscript Received November 3, 1997)

Contents

I. Introduction

A unique instrument, a single-crystal adsorption calorimeter (SCAC), with sensitivity to femtomole quantities of reacting gas has been developed and deployed over the past 5 years, providing a significant new database for surface systems which have been spectroscopically and structurally well-defined. This instrument has been used in the first measurements of heats for molecules that adsorb irreversibly, which cannot be studied by thermal desorption or isosteric methods. This is the first comprehensive review of the instrument and the results obtained. Emphasis is placed on the extraction of chemisorption bond energies and interadsorbate lateral interaction energies from variations in adsorption heat with coverage obtained for CO, O_2, NO, C_2H_2, C_2H_4, CO/K, and O_2/K on single crystal surfaces of Ni, Pd, Pt, and Rh. The data uniquely provide an important benchmark for theoretical calculations of potential-energy surfaces for chemisorption, a new thermodynamic criterion for the onset of nondissociative adsorption (for NO), and a database for adsorption heats, average bond energies, and interaction energies for chemisorbed species on single-crystal surfaces.

Developments in the study of solid surfaces over the past 30 years[1−4] have dramatically transformed our understanding and control of the microscopic properties of the solid−vacuum interface. This is demonstrated by the accompanying revolution which has occurred in microchip technology, but these developments also herald a future transformation in environmental and industrial catalysis. Surface-sensitive diffraction and spectroscopic techniques[5,6] are now capable of providing detailed structural and electronic information; surface processes can be studied in atomic detail by scanning-probe microscopies;[7] and the dynamics of gas−solid scattering and the bond-making and -breaking processes associated with chemisorption and surface reactions are under attack.[8] Finally, advances in theory, together with the development of high-speed computers, have provided an unprecedented capability for reliably modeling surface properties.[9,10] The most critical test of these theoretical developments is the prediction of the total energy of the ground state of the adsorbate, but here there has been a distinct lack of experimental data. Indeed, from the viewpoint of surface reactivity and catalysis, the interaction energy be-

S0009-2665(97)00089-7 CCC: $30.00
Published on Web 03/07/1998

Wendy Brown is a Research Fellow at Peterhouse, Cambridge, and works with Professor David King in the Chemistry Department at Cambridge University, where she also studied for her Ph.D. Her research interests lie in the field of the energetics and dynamics of surface reactions. She will shortly be moving to the Chemistry Department at University College London.

Rickmer Kose is currently studying for his Ph.D. in the research group of Professor David King in the Chemistry Department at Cambridge University. He received his degree in Physics from the Berlin Technical University and did his Diploma Thesis with Professor Gerhard Ertl at the Fritz-Haber-Institute of the Max-Planck-Gesellschaft in Berlin.

David King is the 1920 Professor of Physical Chemistry in the Department of Chemistry at the University of Cambridge and is currently Head of Department. In 1995 he was elected Master of Downing College, Cambridge. His research covers structure and dynamics at surfaces and heterogeneous catalysis.

tween a molecule and the surface is arguably the most important parameter. The development of a reliable and accurate single-crystal calorimeter was therefore long overdue.

Since the first measurements by Tracy and Palmberg of CO on Pd{100},[11] Clausius−Clapeyron analyses of equilibrium adsorption isosteres and kinetic analyses of thermal desorption spectroscopy have been widely used to determine adsorption heats on well-defined single-crystal surfaces. The main disadvantage of these techniques, however, is that they can only be used for studying adsorption systems that are fully reversible. In general, the majority of surface processes, such as dissociative and reactive adsorption, cannot be studied. As a result of the development of a single-crystal adsorption calorimeter in Cambridge,[12,13] it is now possible to accurately measure calorimetric adsorption heats on single-crystal surfaces for many types of surface processes.

Since adsorption processes are exothermic, we shall adopt the usual convention, assigning the differential molar adsorption heat, q, as the negative of the differential molar enthalpy change for the process. Isosteric adsorption heats, q_{st}, are determined under equilibrium conditions using the Clausius−Clapeyron equation:

$$q_{st}(\theta) = -R\left(\frac{\partial \ln P}{\partial(1/T)}\right)_{\theta}$$

where R is the gas constant, P is the pressure, T is the temperature, and θ is the fractional surface coverage. This technique is most often used for physisorbed species, but as long as a process is truly reversible, it can also be used for chemisorption.[11] Isosteres are usually obtained by determining the pressure and temperature required to give a known coverage, and it is therefore important to monitor the coverage. Most commonly, the work function, ϕ, or a convenient low-energy electron diffraction (LEED) pattern is used to calibrate the coverage. To obtain the heat of adsorption, either isotherms or isobars are used, and once several have been obtained, a Clausius−Clapeyron plot is derived. This technique is based on the sometimes questionable assumption that ϕ or the LEED pattern is temperature invariant; more reasonable is the assumption that the adsorption heat is also temperature invariant. The major disadvantage of this technique, however, is that it can never be used to measure the heat of adsorption for an irreversible process.

The second method widely employed to estimate adsorption heats is through the measurement of the desorption energy, E_d. This method is more straightforward and is, hence, more commonly used. It gives the adsorption heat provided that the reverse process of desorption is nonactivated, and hence q is equated to E_d. Usually E_d is estimated by studying a series of thermal desorption spectra at different initial coverages. Using these spectra, the rate of desorption of adsorbate per unit area can be calculated using the expression:[14]

$$-\frac{dN}{dt} = \left(\frac{V}{AkT}\right)\left(\frac{dP}{dt} + \left(\frac{S}{V}\right)P\right)$$

where N is the surface coverage, P is the partial pressure increase observed above the background on desorption, V is the volume of the desorption chamber, S is the system pumping speed, A is the

Table 1. A Summary of References to All the SCAC Adsorption and Reaction Systems Measured with the Cambridge Calorimeter to Date

				hydrocarbons			
surface	CO	O_2	NO	C_2H_4	C_2H_2	CO + O_2 reaction	coadsorption
Ni{100}	16−18	16, 18, 25−28	27, 30	31	31		16, 18, 26, 28, 39, 40
Ni{111}	17, 18	18, 28					26, 28, 40
Ni{110}	13, 17, 18	12, 13, 18, 28		32	32		26, 28, 41
Pt{100}	19, 20		20	19, 33			
Pt{110}	21	21	21	33, 34		38	
Pt{111}	22	22		35, 36		22	
Pd{100}	23		23	31	31		
Rh{100}	24	29		37	37		

adsorbate area, and T is the temperature of the adsorbate.

With a high pumping speed and a low heating rate, β, the desorption rate can be shown to be proportional to the observed pressure increase, P. The Redhead equation[14] for first-order desorption is then used to relate E_d to the temperature at which a desorption peak occurs:

$$\frac{E_d}{RT} = \ln\left(\frac{\upsilon T}{\beta}\right) - 3.64$$

where υ is the frequency factor for the desorption process. Formally, this only applies when E_d and υ are independent of θ. Hence, the desorption energy can be determined at various initial coverages. This method is simple but has several disadvantages. It requires a precise knowledge of the desorption rate law, and this must also include information about how all of the kinetic parameters vary with coverage. It is limited to systems where desorption is first order and is the dominant pathway. A critical review of this method was given by King,[15] and this article also presents a more reliable direct method for analyzing a family of desorption spectra.

Directly measuring the heat of adsorption and reaction is clearly desirable. Using calorimetry, there are, in principle, no restrictions to the systems that can be studied. A summary of all of the adsorption systems examined to date with the SCAC is given in Table 1.[12,13,16−41] The experimental method has recently been extended to enable studies to be made of metal adsorption on metal surfaces.[42]

In this paper, we first briefly cover the history of calorimetry experiments and the thermodynamic quantities involved. What follows is a comprehensive review of single-crystal adsorption calorimetry measurements performed to date by our group and more recently by Campbell's group.[42] The measurements are described in various categories: reversible molecular adsorption (CO), completely dissociative adsorption (O_2), partially dissociative adsorption (NO), reactions with surface products (hydrocarbon adsorption), reactions with gas-phase products, coadsorption systems, and metal adsorption.

II. Brief History of Adsorption Calorimetry

Techniques for studying calorimetry on surfaces have been around for about 60 years. The first calorimetric measurements of the heat released when gases are adsorbed on metal wires were made in Cambridge in the 1930s by J. K. Roberts,[43−46] and since then the technique has progressed through various stages leading to the development of the SCAC in Cambridge in the 1990s.[12,13] A detailed review of the history of surface calorimetry has been recently given by Černý,[47] and the reader is referred there for more details.

All of the initial experiments by Roberts involved the adsorption of gases on metal wires.[43−46] The substrate wire itself was used as a resistance thermometer to measure the temperature rise occurring on adsorption. This method was revived some 20 years later by Kisliuk[48] who used metal ribbons as a substrate. Again, the ribbons were used as a thermometer to measure the adsorption heat. Similar experiments were also performed by Yamazaki et al.,[49] but there was little agreement from one laboratory to another.

Further developments in calorimetry on wires were made by many groups including Yamazaki and coworkers,[50] Eley and Norton,[51, 52] Norton and Richards,[53] and Couper and John.[54−56] The main problem with all of these experiments was the polycrystalline nature of the surface which made interpretation of the data difficult and also led to nonreproducibility between different sets of data.

The next development was a calorimeter for studying adsorption on thin polycrystalline films deposited in a vacuum. These calorimeters were more widely applicable to many adsorption systems and allowed higher precision measurements to be made. The thin-film calorimeter, developed by Beeck,[57−61] consisted of a thin-walled glass vessel mounted in an evacuable jacket. The film to be studied was evaporated onto the inside of the vessel from a filament. A thermometer was wound around the outside of the calorimetry vessel. Doses of gas were admitted incrementally, allowing a coverage-dependent determination to be made. The Beeck method was developed and refined in many laboratories, especially those of Wahba and Kemball,[62] Bagg and Tompkins,[63] Klemperer and Stone,[64] Brennan et al.,[65−70] Wedler et al.,[71−75] and Černý et al.[76,77] A further development was recently made by Černý and co-workers[78−80] who applied a pyroelectric heat detection method to adsorption on polycrystalline films. All of these experiments were, however, of limited use due to the unhomogeneous nature of the film.

The first attempt to make a calorimetric measurement on a single-crystal surface was by Kyser and Masel[81,82] on the surface of a Pt{111} crystal. The temperature rise observed on adsorption was measured by two thermistors fitted into holes in the side of the crystal. Coverage-dependent studies on clean

surfaces were difficult as the system required 10−12 h for thermal equilibration before an experiment. Unfortunately, this meant that the sample was significantly contaminated before experiments began. Quite simply, the large thermal mass of a standard single crystal and the small amount of heat liberated when a fraction of a monolayer was adsorbed at the surface proved to be insurmountable obstacles.

The most recent advance in calorimetry on surfaces was the development of a single-crystal adsorption calorimeter by our group,[12,13] which provided the first opportunity to measure accurate, coverage-dependent adsorption heats on well-defined surfaces, where a direct correlation with structural and spectroscopic results could be made. In particular, in many instances the unequivocal assignment of a heat of adsorption to a specific surface structure has enabled the first reliable measurements of substrate-adatom bond energies to be made. The development of the SCAC technique has opened up accurate heat measurement to many different surface processes which have not been measured before. Very recently, a SCAC has been built by Campbell and co-workers[42] specifically to measure metal vapor adsorption and another is currently being developed by Dixon-Warren et al.[83] These will help to further establish SCAC as one of the regular analytical tools used for investigating surface processes.

III. Thermodynamics

In a calorimetry experiment the heat produced in a substrate of known heat capacity during adsorption is quantitatively measured, as is the amount of gas adsorbed. The heat released per mole of gas adsorbed is closely related to the adsorbate−substrate bond strength and, hence, can be used to give the strength of the interaction between the adsorbate and the surface in detail. Thermodynamic definitions for the heat of adsorption were developed by Hill[84] and by Young and Crowell[85] in the 1950s. A detailed description of the thermodynamics of adsorption is given by Černý.[86]

To define the heat of adsorption, it is necessary to distinguish between different expressions that describe it. The total energy per mole released when adsorption occurs on a clean surface to a fixed coverage is the *integral* heat of adsorption over that coverage range. In SCAC, it is the energy released during the adsorption of a small increment of adsorbate at a fixed coverage, the *differential* heat, q_d, that is measured. The differential heat measured in a SCAC experiment for a reversible adsorption system can be related thermodynamically to the isosteric and desorption heats measured by other groups. A detailed comparison of these quantities is given by Stuckless et al.[17]

The energy released during adsorption, minus any work done by the system, is spent as heat warming the adsorption system and/or its surroundings and is measured in a SCAC experiment. The term "differential heat" refers to the change in internal energy between the adsorbed and gaseous states following a path in which no work is done, i.e., $q_d = U_g - U_a$, where U_g is the molar internal energy of the gas and U_a is the molar internal energy of the adsorbate. The sign convention for q_d is such that an exothermic process, such as adsorption, has a positive heat.

In a calorimetry experiment, the adsorbate surface area is constant and the substrate is assumed to be thermodynamically inert so that the only work done is the gas-phase pressure−volume work, the heat of compression, q_c. Its exact value depends upon whether the process is isothermal, adiabatic, etc. It is given by the expression:

$$q_c = -P\frac{dV_g}{dn_a} \approx RT$$

Here, P and V_g are the gas-phase pressure and volume and n_a is the number of moles of adsorbate. Since q_c is of the order of RT, the calorimetric heat, q_{cal}, measured in an experiment for a fully reversible process is

$$q_{cal} = q_d + RT$$

Assuming that the solid substrate is inert, then at equilibrium the chemical potential, μ, of the adsorbate and the gas phase should change identically for any perturbation of the system. The adsorbed gas-phase chemical potential can be given with respect to temperature, T, pressure, P, adsorbate area, α, and the number of adsorbate molecules, n_a, as

$$d\mu_a = -S_a\,dT + V_a\,dP + \left(\frac{\partial\mu}{\partial\alpha}\right)_{T,P,n_a} d\alpha + \left(\frac{\partial\mu}{\partial n_a}\right)_{T,P,\alpha} dn_a$$

where S_a is the differential entropy and V_a is the differential volume with respect to n_a at fixed temperature, pressure, and adsorbate surface area. If we apply the isosteric constraint that the adsorbate surface area and the number of adsorbate atoms are constant, the last two terms vanish. For the gas phase:

$$d\mu_g = -S_g\,dT + V_g\,dP$$

At equilibrium, $d\mu_a = d\mu_g$ and, hence:

$$\Delta V_{g-a}\left(\frac{\partial P}{\partial T}\right)_{\alpha,n_a} = \Delta S_{g-a}$$

where ΔS_{g-a} and ΔV_{g-a} are the entropy and volume change that occur upon adsorption. If we assume that the gas is ideal and neglect the volume of the adsorbate, then the Clausius−Clapeyron relationship is obtained:

$$-R\left(\frac{\partial \ln P}{\partial(1/T)}\right)_{\alpha,n_a} = T\Delta S_{g-a}$$

The term on the right-hand side is equal to the heat released in a reversible phase change, and this corresponds to a path for which the only work done is gas expansion at constant temperature and pressure. Hence, $T\Delta S_{g-a} = q_d + RT$. The term on the left-hand side is the isosteric heat, q_{st}, measured in

an experiment at equilibrium. Hence, calorimetric heat measurements can be directly compared with isosteric measurements, provided that both measurements refer to equilibrium conditions. Isosteric measurements are necessarily conducted at relatively high temperatures, where the desorption rate is significant, but calorimetric measurements may be conducted at much lower temperatures, where metastable states may be formed and the degree of order and island formation may be quite different. Comparisons should, therefore, always be made with care.

We now examine the formal relationship between the activation energy for desorption, E_d, and q_{cal}. If the desorption process is nonactivated, then E_d can be directly equated to the energy of adsorption. The desorption rate, r_d, may be equated to $k\theta^x$, where x is the reaction order (here the reaction is assumed to be first order), and k the rate constant given by

$$k = \upsilon(\theta)\exp\left(\frac{-E_d(\theta)}{RT}\right)$$

where υ is the coverage-dependent frequency factor for desorption. Even this expression, commonly deployed, only applies to a disordered adlayer;[15] the desorption rate is unlikely to follow such an elementary rate law. However, on the basis of this expression, the Arrhenius desorption energy and the isosteric heat can be readily related to one another. At equilibrium, equating rates of adsorption and desorption yields

$$\theta\upsilon\ \exp\left(\frac{-E_d}{RT}\right) = \frac{p\sigma}{(2\pi mkT)^{1/2}}$$

where m is the mass of the adsorbing or desorbing molecule, k is the Boltzmann constant, and σ is the sticking probability. At a fixed coverage:

$$q_d + RT = q_{st}$$

$$= E_d - T\left(\frac{\partial E_d}{\partial T}\right)_{\alpha,\theta} + \frac{1}{2}RT - R\left(\frac{\partial \ln(\upsilon/\sigma)}{\partial(1/T)}\right)_{\alpha,\theta}$$

If we make the further assumption that E_d, υ, and σ are temperature independent, then $E_d = q_{st} - 0.5RT$. On this basis it would seem to be valid to compare measured calorimetric heats with Arrhenius desorption energies as well as with isosteric heat measurements. Once again, however, the comparison should be treated with caution in view of the simplifying assumptions used. Fortunately, in many cases there is good agreement between isosteric, calorimetric, and kinetic measurements for well-defined systems at low coverages, indicating the validity of making comparisons between the various different sets of data.

IV. The Single-Crystal Adsorption Calorimeter

The design of the ultrahigh-vacuum single-crystal adsorption calorimeter has been described in detail,[12,13,40,87] and modifications and improvements to the original design were described in a recent paper.[88]

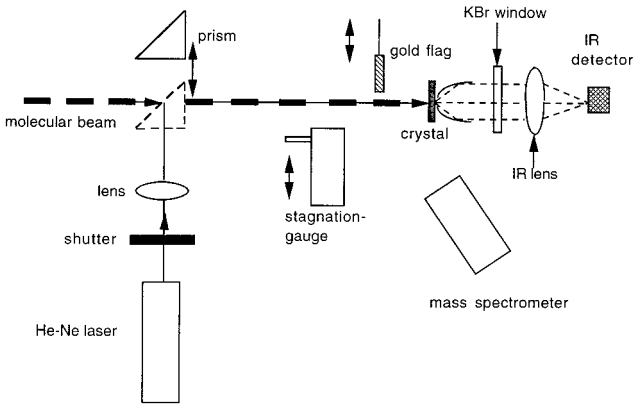

Figure 1. Schematic diagram showing the most important components of the Cambridge single-crystal adsorption calorimeter (SCAC). (Reprinted with permission from ref 88. Copyright 1996 Elsevier.)

A summary of the important elements of the experiment is given here.

The essence of a calorimetry experiment is shown in Figure 1. During an experiment, a pulsed molecular beam is directed at the front face of a single-crystal film. A proportion of these molecules adsorb at the surface and cause the liberation of adsorption heat within the surface region. As demonstrated in the experiments of Masel,[81,82] the large heat capacity of a normal single crystal, a disk 10 mm in diameter and 1 mm thick, is impractical due to long temperature equilibration times and the very small temperature rise with adsorption. For this reason, ultrathin (~2000 Å thick) crystals[89] mounted on a polycrystalline metal ring of the same metal are used. The central 4 mm diameter region of the crystal is unsupported and has a low heat capacity (~1 μJ K^{-1}). Adsorption is confined to this central region of the crystal by dosing with a molecular beam generated gas pulse of 50 ms duration and 2 mm diameter. The thinness of the crystal means that heat conduction between the front and back faces is rapid, but conduction to the crystal support ring is relatively inefficient. Hence, cooling of the crystal occurs mostly by radiation into the surroundings. The temperature of the crystal is measured remotely to avoid increasing its heat capacity. For this purpose, the back face of the crystal is coated thinly with amorphous carbon from a candle flame, giving it a high emissivity. Most of the radiation, therefore, occurs from the back face of the crystal, and this emitted infrared light is collected and focused onto a mercury cadmium telluride (MCT) detector which is mounted outside the experimental chamber. The adsorption of a molecular beam pulse equivalent to ~1% of a monolayer leads to a temperature rise of the crystal of ~0.1 K, which gives a significant signal at the infrared detector. Typical results showing the detector response during adsorption and during calibration with a laser pulse are shown in Figure 2.

The availability of thin-film single crystals is the key to the experiment. These crystals are grown epitaxially by evaporation onto the appropriate polished crystal plane of a radiation-hardened NaCl

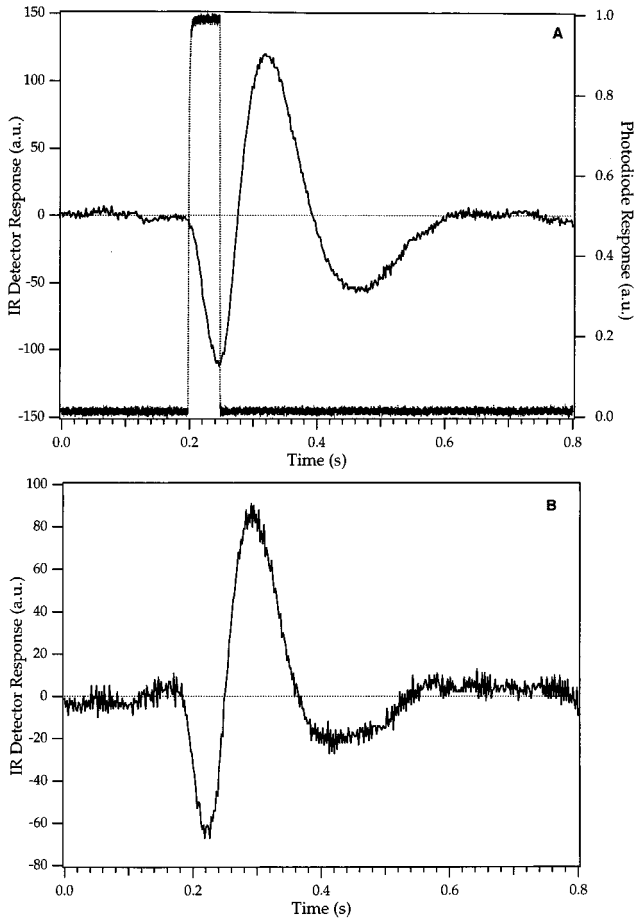

Figure 2. A typical SCAC detector response (A) to the calibrating laser pulse and (B) during an experiment. Note the similar shape in both cases. Also shown in A is the profile of the laser pulse from the output of the photodiode.

single crystal.[89] The NaCl is dissolved away in water to leave the metal crystal floating on the water. The support ring, made of the same metal as the crystal, is etched in hot acid to remove surface oxide, rinsed in distilled water, and then used to lift the crystal off the surface of the water. Gentle pressure is then applied to expel the water between the crystal and the ring and pull the film flat and taut. This results in a permanent cold weld which gives good mechanical support and electrical contact.

Some portion of the incoming gas pulse is not adsorbed and reflects back into the gas phase, producing a partial pressure rise in the experimental chamber. This is detected by a quadrupole mass spectrometer and, by comparison with the amount of gas that reflects from an inert, gold surface, allows the sticking probability to be measured absolutely. This is the King and Wells reflection−detection technique for measuring the sticking probability, s.[90] The coverage increment for each gas pulse is the product sQ, where Q is the integrated flux per pulse. Q is measured using a stagnation gauge, consisting of a thin pipe through which the molecular beam passes without scattering to enter an otherwise enclosed volume containing an absolute pressure gauge, a spinning rotor gauge. The beam pulses into the volume until a steady-state pressure is achieved, at which point the flux into and out of the thin pipe is equilibrated. From the conductance of this pipe, it is easy to calculate the inward flux intensity of the molecular beam.

The amount of heat generated by an adsorption pulse is calibrated by pulsing a known amount of power into the sample using a HeNe laser. The laser beam pulse mimics the spatial and temporal profile of the molecular beam gas pulse to allow an accurate reference signal to be obtained. The calorimeter is recalibrated for every experiment, since sputtering during sample cleaning cycles thins the crystals somewhat, lowering the heat capacity and increasing the sensitivity. In early experiments on Ni surfaces,[16−18,28,39−41] the HeNe beam was chopped with a mechanical rotating disk, but this was subsequently replaced with a liquid crystal shutter.[88] The laser beam passes through a biconvex lens to give a slightly divergent beam which is then passed into the system, and a prism reflects it down the molecular beam axis. It is thus cropped by the same collimating apertures as the beam itself to give the same spot profile at the crystal.[88] The infrared signal resulting from heating of the crystal by the HeNe seen in Figure 2 is collected and analyzed in the same way as the adsorption signal. The laser power is measured outside the KBr window using an absolutely calibrated photodiode.

Prior to any experiment, the sample surface is cleaned by gentle Ar ion bombardment (1 μA cm^{-2}) for approximately 10 min and annealed to ~700 K using a focused lamp. Chemical cleaning procedures can also be used where necessary.

Modifications to the original design[88] mean that the SCAC is capable of measuring molar adsorption heats for systems with a high sticking probability down to a detection limit of ~10 kJ mol^{-1}, with an estimated absolute accuracy of ~6% for adsorption heats greater than ~80 kJ mol^{-1}. This estimate is given strong support by the comparisons of low coverage calorimetric heats for CO on a range of metals with isosteric and desorption energy measurements from the literature, shown in Table 2.[91−114]

The infrared remote sensing technique is not readily adapted for measurements with the crystal at low temperatures. The detection of a temperature rise ΔT during adsorption is based on the change in the radiated power ΔP, which is proportional to $T^3\Delta T$. As the substrate temperature, T, is decreased, ΔP is rapidly attenuated. It is useful to be able to perform calorimetric measurements at low temperatures, since for many systems the heat of adsorption is too low for adsorption to be observed at 300 K and it is also important to study metastable states formed. For these reasons, an alternative pyroelectric detection technique has also been developed. It was originally used in a study of calorimetry on polycrystalline surfaces by Černý et al.[79] and has been adapted for low-temperature measurements on single-crystal surfaces.[25] In this work, all other aspects of the calorimeter were identical with that based on infrared remote sensing. The thin-film crystal is cold-welded onto the pyroelectric material. The detector consists of a $LiTaO_3$ wafer clamped onto

Table 2. Comparison of Isosteric Desorption Energies and Calorimetric Heats of Adsorption for CO on Various Surfaces[a]

system	ref	coverage (ML)	q^0_{cal} (kJ mol^{-1})	E_d (kJ mol^{-1})	q_{st} (kJ mol^{-1})
CO/Ni{111}	Stuckless et al.[17]	0.05	130		
	Ibach et al.[91]				149
	Froitzheim et al.[92]			127	
	Miller et al.[93]			130	
	Christmann et al.[94]				123
CO/Ni{110}	Stuckless et al.[17]	0.05	132		
	De Angelis et al.[95]			130	
	Feigerle et al.[96]			126	
	Madden et al.[97]				127
	Love et al.[98]			128	
CO/Ni{100}	Stuckless et al.[17]	0.1	122		
	Tracy[99]				126
	Bordoli et al.[100]				129
	Labohm et al.[101]				129
	Benziger et al.[102]			115	
	Kiskinova et al.[103]			119	
	Koel et al.[104]			138	
	Klier et al.[105]				109
CO/Pt{110}	Wartnaby et al.[21]	0.2	193		
	Jackman et al.[106]				170
	Engstrom et al.[107]			150	
	Fair and Madix[108]			148	
CO/Pt{111}	Yeo et al.[22]	0.04	187		
	Ertl et al.[109]				135
CO/Pt{100}-hex	Yeo et al.[20]	0.03	193		
	Thiel et al.[110]				115
	Hopkinson et al.[111]		105		
CO/Pt{100}-(1×1)	Yeo et al.[20]	0.01	220		
CO/Pd{100}	Yeo et al.[23]	0.05	163		
	Behm et al.[112]				160
	Tracy et al.[113]				150
	Szanyi et al.[114]				165

[a] Specific coverages were chosen to allow a direct comparison between calorimetric heats and heats obtained by isosteric or desorption energy measurements. It is clear that the agreement is good in most cases.

a special mount which is attached to the end of the sample manipulator in the UHV chamber. A schematic diagram is shown in Figure 3.

The pyroelectric experiments were compared with infrared measurements on the same adsorption system, and the detection system was shown to work well.[25] However, there were problems with microphonic noise in the pyroelectric experiments, and a compensating detector system is currently being developed which will be considerably less sensitive to this noise. Measurements were performed for O_2 on Ni{100} using the pyroelectric detection technique, and these are discussed in detail in the results section of this article. We note, however, that this system does require ca. 1 h to reach a stable temperature, and it is difficult to avoid background contamination over this time scale. The remote sensing detector system does not suffer from this problem.

In a calorimetry experiment, the sticking probability and the differential heat of adsorption are measured as a function of coverage. In all SCAC experiments there is apparently a constant nonzero sticking probability and heat at high exposures. This is referred to as the "steady-state" sticking and heat and usually arises due to the desorption of molecules from the surface between gas pulses. A steady state is reached in which the adsorption during a pulse exactly balances the desorption between pulses, and this leads to an apparent infinite uptake of gas onto the surface. Additional information can be extracted from the calorimetric heat measured at steady state. At this point, an equilibrium is achieved with an almost constant coverage, as mentioned earlier. The

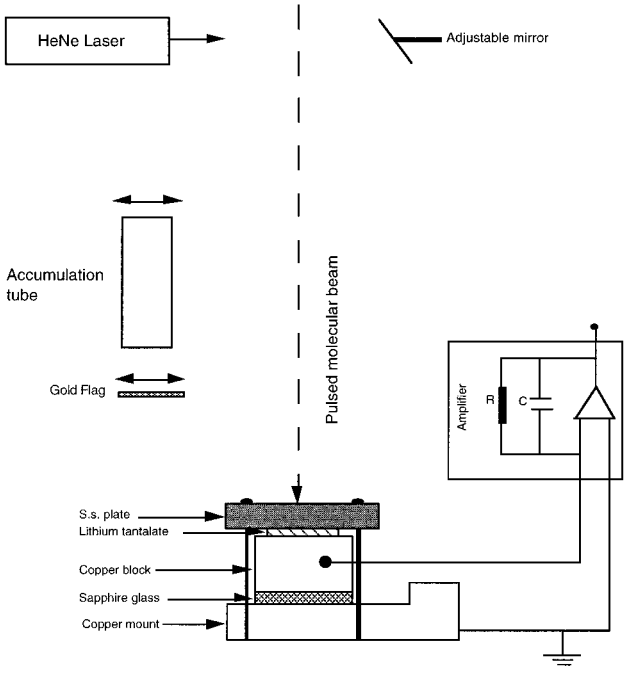

Figure 3. Schematic diagram showing the setup of the original pyroelectric-detector-based SCAC. (Reprinted with permission from ref 25. Copyright 1994 Elsevier.)

differential entropy of the adsorbate can, therefore, be calculated[115] using the equation:

$$S_a = S_g^\circ - R \ln\left(\frac{p}{p^\circ}\right) - \frac{q}{T}$$

where the standard state is 1 atm of pressure and $S_g^\circ = 198$ J mol^{-1} K^{-1} for CO. At steady state, the observed adsorption can be equated with the average rate of desorption, and hence, the frequency factor for desorption can also be calculated.

For all the data presented here where the shape of the sticking probability curve as a function of coverage shows precursor-mediated adsorption, the Kisliuk expression[116]

$$\frac{s}{s_o} = \left(1 + \frac{\theta/\theta_s}{1 - \theta/\theta_s}K\right)^{-1}$$

has been used to fit the data. This enables the usual "apparent coverage" scale to be converted to actual coverage and allows values for the saturation coverage to be obtained directly. This was not possible for all systems, and it is indicated where a fit has been performed. In all cases, a line has been put through the heat data simply to guide the eye. It is not meant as a fit to the data.

The data presented in this article is, in some cases, slightly different from the published data. This is due to the fact that two errors were found in the analysis program, which have now been corrected. This led to an error of ca. 10−30 kJ mol^{-1} in some of the previously published data. The raw experimental data was unaffected and was available on file for reanalysis to give the corrected values for heats of adsorption given in this review article. We also note that the calibration relies on a knowledge of crystal reflectivity. Reflectivity values used here were obtained from Weaver.[117]

V. From Adsorption Heats to Average Bond Energies

Bond dissociation energies are fundamental quantities in thermochemistry, and it would be useful to extend this capability to surface studies. In particular, the metal−carbon bond strength is a fundamental quantity of particular interest in surface reactivity and catalysis, and single-crystal calorimetry at last provides experimental access to this parameter. The determination of bond strengths from experimental data requires clear definitions of bond dissociation energies and a consideration of all energy changes occurring at the surface due to adsorption and any surface reaction, as discussed in a recent paper.[36]

There are two ways to define the bond dissociation energy, the difference being related to the final state of the gaseous and surface products of the dissociation process. For the *adiabatic* bond dissociation energy, the final state corresponds to the ground electronic states of the gaseous species and the surface, whereas for the *diabatic* bond dissociation energy, the final state is the gaseous species and the surface in the electronic states corresponding to those in the initial state. As an example,[36] consider the reaction which occurs on Pt{111} at 300 K, described in detail in section VI.E of this review:

$$Pt_n + C_2H_4(g) \rightarrow Pt_nCCH_{3(a)} + {}^1/_2H_2(g) \qquad \Delta H_{rn}$$

from which the standard heat of formation of adsorbed ethylidyne is

$$\Delta H^\circ_f(Pt_nCCH_{3(a)}) = \Delta H_{rn} + \Delta H^\circ_f(C_2H_4(g))$$

The bond dissociation energy refers to the reaction

$$Pt_nCCH_{3(a)} \rightarrow Pt_n + CCH_3(g)$$

where the adiabatic value refers to CCH_3 in its lowest energy electronic state (^{2}E, with one unpaired electron) and a fully relaxed clean surface, and the diabatic value refers to the ^{4}E electronic state of gaseous CCH_3 (with three unpaired electrons, the electronic state corresponding to ethylidyne with covalent bonds to each of the three surface Pt atoms in the 3-fold hollow site) and the Pt surface in the unrelaxed state. These definitions are closely tied to two methods for determining metal−carbon single-bond energies; the average bond energy (abe) method and the quasi-empirical valence bond (qvb) method.

The abe method, based on the principle of bond additivity,[118] is widely used in inorganic and organic chemistry to predict the thermochemistry of proposed reactions. In the first-order approximation, values are assigned to different types of bonds, distinguishing C−C from C=C, etc., and improvements can be achieved by distinguishing among each type, for example a C−C bond next to a single or a double bond. For simple molecules, this additivity of bond energies works within a confidence limit of ±8 kJ mol^{-1}. The second-order approximation involves the assignment of partial values of molecular bond energies to particular groups and then summing these group properties; this implies the availability of a very large database.[119] We should note that in this method there is no distinction between adiabatic and diabatic bond dissociation energies, since, for example, the method does not distinguish between the ^{2}E and the ^{4}E electronic states of CCH_3(g).

The qvb method was developed by Carter and Koel[120,121] for estimating heats of adsorption and adsorbate−surface bond strengths. It involves a determination of the local electronic state of the adsorbate when bonded to the metal surface and a calculation of the heat of formation of the gaseous species in the electronic state which is closest to that of the adsorbed species on the surface. Then, from heats of adsorption, the diabatic bond dissociation energy can be determined provided that the accompanying change in the energy of the surface is negligible.

Gross et al.[36] have analyzed recent calorimetric data for ethylene adsorption on Pt{111}[35] using both methods and produced very similar values for the Pt−C bond strength: 243 kJ mol^{-1} (abe method) and 237 kJ mol^{-1} (qvb method), corresponding to the single bond energy for a carbyne C atom triply bonded to three Pt atoms in a 3-fold hollow site. The agreement between the two approaches in this case

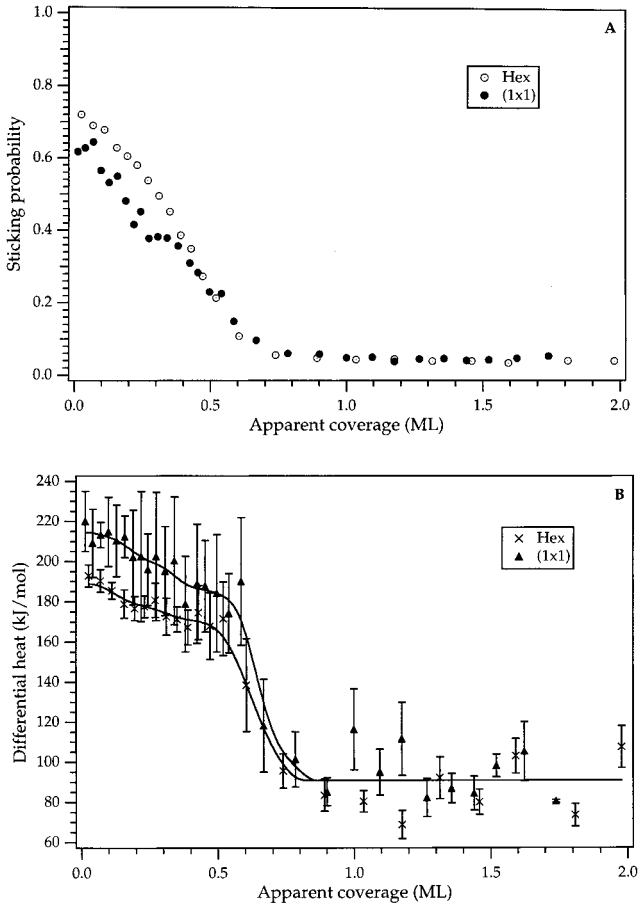

Figure 4. Sticking probability (A) and heat of adsorption (B) as a function of coverage for the adsorption of CO on Pt{100}−(1×1) and hex surfaces. Note how the heat and sticking signals coincide above 0.5 ML coverage, showing the production of the same final state. (Adapted from ref 20.)

is good, but the limitations of the abe method should be noted. It does not, for example, distinguish between adiabatic and diabatic bond dissociation energies, since it gives "spin-impure" results. In general, the abe method was used for the M−C bond energies calculated in this review.

VI. Summary of Results

A. Determination of the Energy Difference between Two Solid Surfaces

One of the most important results obtained with the SCAC was the first experimental measurement of the energy difference between two structural phases of a solid surface.[19,20] This was a benchmark experiment for theoretical calculations but also provides an example of the energy associated with adsorbate-induced restructuring. The clean Pt{100} surface can be prepared in a metastable (1×1) structure which is stable at 300 K. When this surface is heated above 500 K, it reconstructs to a more stable structure which is hexagonal. This is known as the Pt{100}−hex phase. Adsorption of various small molecules such as CO and NO lifts this reconstruction and the surface reverts to the (1×1) phase. Since the SCAC allows heats of adsorption to be measured, it is possible to construct a thermodynamic cycle that

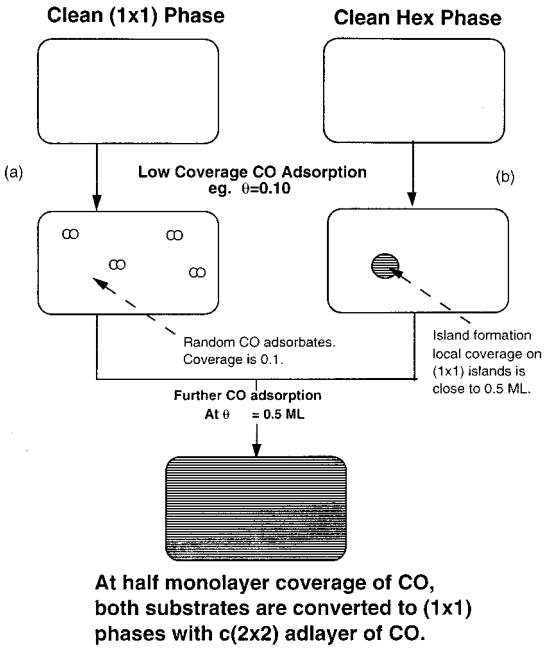

Figure 5. Schematic diagram showing the two initial states of Pt{100}: clean hex and clean (1×1), and the different CO adsorption pathways, a and b, with island formation along b and the identical final state, Pt{100}−(1×1)-c(2×2)CO. The difference in integral adsorption heat along the two paths is the energy difference between the two clean initial states. (Reprinted with permission from ref 20 Copyright 1996 American Institute of Physics.)

allows the heat for the reconstruction process to be calculated from various experimental measurements.

The hex and (1×1) surfaces were prepared by standard procedures,[19,20] and the heat of adsorption for CO as a function of coverage was measured on both surfaces. The heat of adsorption and the sticking probability for CO adsorption on the hex and (1×1) surfaces can be seen in Figure 4. The differential heat of adsorption on the (1×1) surface is initially 220 kJ mol^{-1} and has a steady-state value of ~90 kJ mol^{-1}. The heat for the hex surface is initially 193 kJ mol^{-1}, and above 0.5 ML it decreases to the same value seen for the (1×1) surface. In fact, at coverages above 0.5 ML, the two heat curves overlap. At these coverages, the sticking curves also coincide.

This can be rationalized by considering what happens upon adsorption of CO in both cases. For the hex surface, adsorption of CO leads to conversion to the (1×1) phase so the final state at coverages of 0.5 ML is the same in both cases. Evidence for this comes from the observation of corresponding LEED patterns from the surface. At 0.5 ML coverage after adsorption on the hex surface, the hexagonal LEED pattern has disappeared and been replaced by a c(2×2) LEED pattern.[110] Adsorption on the (1×1) surface also results in the production of a c(2×2) LEED pattern at 0.5 ML coverage. Further evidence that the final states are the same is provided by an infrared study by Gardner et al.[122] Of course, the heat of adsorption and sticking curves are further evidence that the same final state is reached in both cases. The difference between the two integral heats of adsorption is, therefore, the difference in the surface energies of the two different initial states,

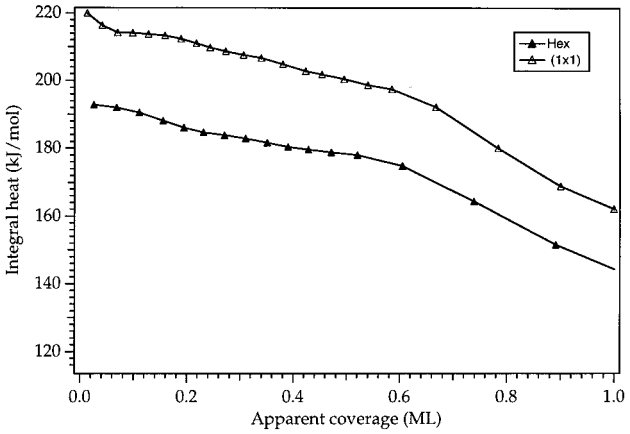

Figure 6. Integral heats of adsorption for CO/Pt{100}−(1×1) and hex. The difference in the integral heats at 0.5 ML coverage gives the energy difference between the two initial phases: here, 12 kJ mol^{-1}. (Adapted from ref 19.)

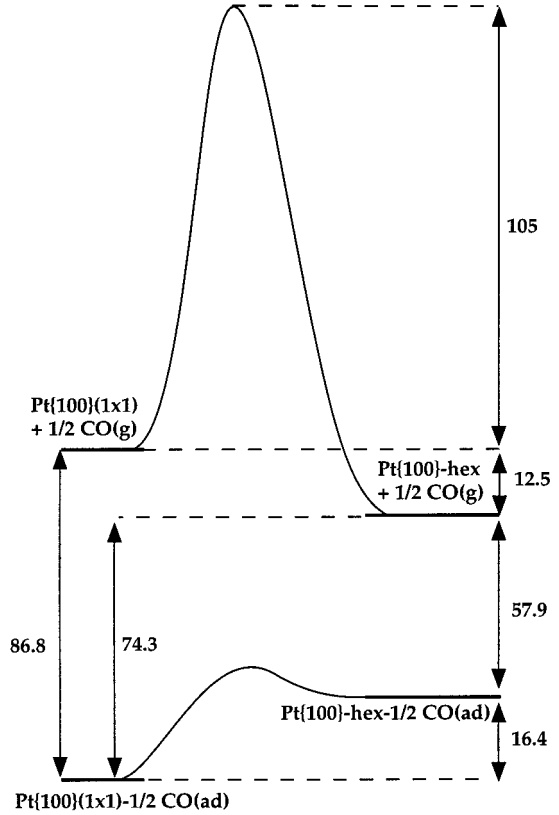

Figure 7. Schematic energy diagram illustrating the clean hex to (1×1) phase transition upon adsorption of CO on Pt{100}. All energies quoted are in units of kJ/mol/(1×1) unit cell area. (Adapted from ref 19.)

(1×1) and hex phases of the clean surface, shown schematically in Figure 5. The difference can be expressed in terms of the integral heat, which is calculated from

$$\Delta H_{\mathrm{in}} = \frac{\int \Delta H_{\mathrm{diff}}\, \mathrm{d}\theta}{\int \mathrm{d}\theta}$$

and shown in Figure 6. The difference between the integral heats on the (1×1) and hex surfaces at 0.5 ML coverage multiplied by the coverage (0.5 ML) is

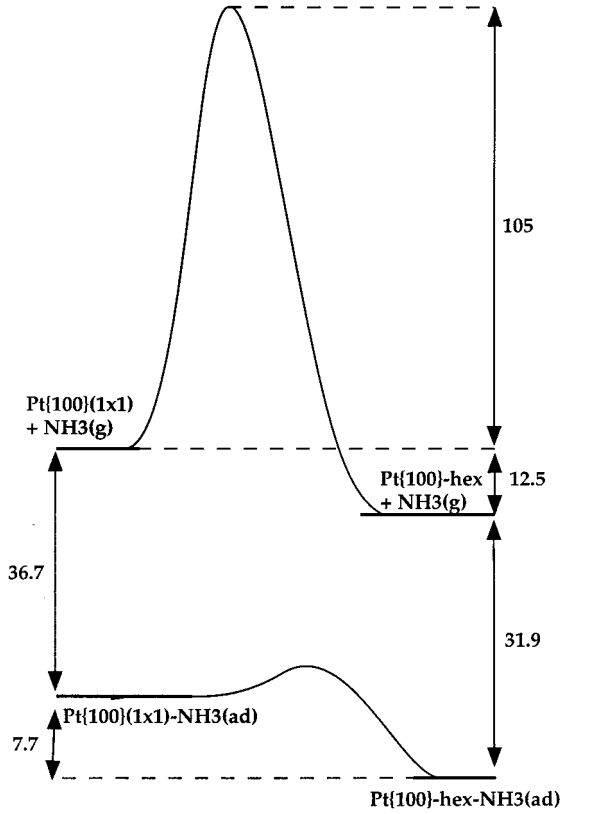

Figure 8. Schematic diagram for NH_3 adsorption on the Pt{100} hex surface. Here, the energy of the adsorbed species on the (1×1) phase is larger than that on the hex phase, and therefore, the reconstruction is not lifted by adsorption of NH_3. Energies are again quoted in units of kJ/mol/(1×1) unit cell area.

the energy difference corresponding to the surface phase transition (q_{spt}) between the two clean surfaces. This heat is expressed in terms of the number density of surface Pt atoms, Pt_s, and is equal to $q_{\mathrm{spt}} = 12 \pm 2$ kJ (mol of Pt_s)$^{-1}$. Effectively, the adsorption of any molecule which lifts the hex reconstruction to give an identical final state to adsorption on the (1×1) surface should give the same answer.

At very low coverages of CO on the hex phase, the rate of transformation to the (1×1) surface is negligibly small due to the nonlinear growth power law.[111,123] Hence, at very low coverages, it is possible to measure the heat of adsorption on the hex phase by isosteric or desorption measurements.[111,123] It was not possible to measure this heat with the SCAC due to adsorption of CO from the background in the chamber which immediately lifted the hex reconstruction. A value of 115 kJ (mol of CO)$^{-1}$ was measured for the hex phase.[110] This can be compared with the heat on the (1×1) phase (see Figure 4) which is much larger. This obviously represents the driving force for the adsorbate-induced lifting of the hex reconstruction, as can be seen from the energy diagram shown in Figure 7. Not all molecules lift the hex reconstruction upon adsorption: for example, NH_3 does not.[124] The reason for this is evident from the energy diagram for NH_3 adsorption on Pt{100} seen in Figure 8. Here the energy of $NH_{3(a)}$ on the hex surface is lower than that on the (1×1) phase, and there is no driving force back to the (1×1) surface phase.

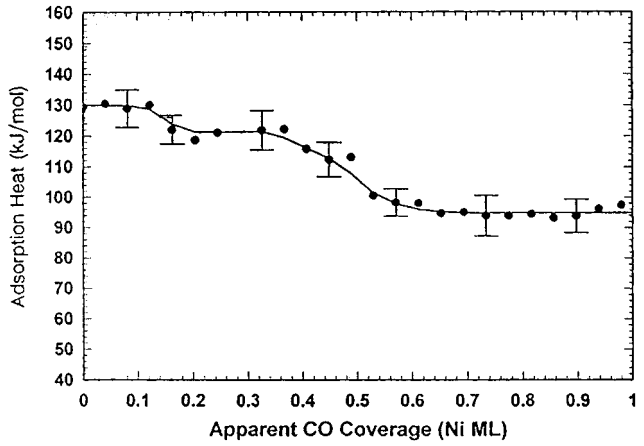

Figure 9. The heat of adsorption of CO on Ni{111} at 300 K as a function of coverage. (Reprinted with permission from ref 17. Copyright 1993 American Institute of Physics.)

This measurement highlights the fact that, to a first approximation, surface relaxation energies can be neglected when using adsorption heat measurements to calculate, for example, M−O and M−C bond strengths as in sections VI.C and VI.E, respectively. The reconstruction of the Pt{100} surface from a hex to a (1×1) phase involves a total rearrangement of the surface atoms and a large change in surface-atom density, and yet, the energy difference between these two phases is measured to be only 12 kJ mol^{-1}. Relaxation of the top layer of surface atoms generally occurs upon adsorption, but the energy change associated with this relaxation is relatively small and can, therefore, be neglected in calculations from the measured data.

B. Reversible Molecular Adsorption: CO

A molecule which undergoes reversible molecular adsorption on many metal surfaces is CO and it is for this reason a useful benchmark adsorbate as the results can be directly compared with those measured using isosteric and Arrhenius methods (see Table 2),[17] providing a test for the performance of the SCAC.

a. CO on Ni Surfaces

The first calorimetric measurement of the heat of adsorption of CO on a single-crystal surface was made by Al-Sarraf et al.[16] for the adsorption of CO on Ni{100}. This work was followed by adsorption on the other singular faces of Ni. Several overviews of this work have been given,[13,16,18,26] but the most detailed account is given in a paper by Stuckless et al.[17]

The initial sticking probabilities for CO on Ni{110} and {100} were measured to be 0.75 ± 0.02, and on Ni{111} it was found to be slightly smaller at 0.72 ± 0.02.[17] In all cases, the shape of the sticking probability curve showed precursor-mediated, nondissociative, adsorption and could be fitted by the Kisliuk expression.[116]

The heats of adsorption were measured for CO on the same three Ni surfaces. An example heat of adsorption curve for CO on Ni{111} is shown in Figure 9. The initial heat of adsorption for CO on Ni{111} was found to be 130 ± 3 kJ mol^{-1}, and the steady-state heat was about 95 kJ mol^{-1}. The observed detailed variations in the heat with coverage can be understood by comparison with changes in LEED and infrared spectra observed by other groups[93,125,126] where a site shift of the CO is observed at 0.2 ML.[125] LEED showed a $(\sqrt{3}\times\sqrt{3})R30°$ structure at 0.11 ML, which splits at 0.32 ML as a compressed structure is formed. Changes in the heat of adsorption probably arise due to changes in adsorbate−adsorbate interactions in these two states.

For the adsorption of CO on the Ni{110} surface, the initial adsorption heat is very similar to that on Ni{111}: 132 ± 3 kJ mol^{-1}. This is in good agreement with isosteric[97] and desorption heat measurements.[95,96,98] The heat drops continuously with increasing coverage until it reaches a steady-state value of 110 kJ mol^{-1} at coverages above 0.6 ML. The sticking probability for this system was not, however, observed to reach steady state until above 1 ML coverage. It is thought that this is due to the formation of anti-phase domain walls.[127] Although there is good agreement with this measurement and others at low coverage, at coverages above 0.3 ML large discrepancies appear between the calorimetric heat measurement and the other heat measurements. This could be due to errors in the other techniques or could be a real effect of the high temperature at which Arrhenius and isosteric heat measurements are performed.

The initial heat of adsorption for CO on Ni{100} is slightly lower than that for the other two surfaces at 122 ± 2 kJ mol^{-1}. The heat was observed to drop with increasing coverage between 0.25 and 0.65 ML. This time there is a reasonably good agreement in the coverage dependence between the calorimetric heat and other measurements.[99,128]

b. CO/Pt{100}

As well as information about the heat of adsorption, the SCAC data can also be used to get information on lateral interactions that occur between adsorbates. This was calculated for the adsorption of CO on Pt{100}−(1×1) (see section VI.A) using Monte Carlo simulation techniques to model the heat and sticking curves by varying the pairwise lateral interaction energies.[20] These are very important as they influence the differential heat of adsorption and, thus, affect the shape of the heat versus coverage curve, as seen by looking at the heat of adsorption curve in Figure 4. The fall in the heat at coverages greater than 0.25 ML is due to interadsorbate repulsions.[129−131] Lateral interactions between molecules can arise due to three main causes: (1) Dipole−dipole (through-space) interactions; (2) Substrate-mediated (through-bond) interactions; (3) Pauli repulsion between filled orbital states.

Apart from site blocking, the main interaction between molecules adsorbed on a surface is substrate-mediated. A general description of the Monte Carlo methodology, used to extract lateral interactions from experimental heat curves, can be found in ref 20. This was applied for all of the adsorption experiments in which simulations were used to get an understanding of the results.

It is necessary to make approximations in order to perform a Monte Carlo simulation. It is assumed that the heat of adsorption for CO on the (1×1) phase of Pt{100} is the same for bridge and atop sites. This is supported by the fact that both sites are occupied at low coverage. The second assumption is that the interaction energy between CO molecules is site independent. To perform the simulation, it is necessary to equilibrate the lattice and then determine the heat of adsorption for a molecule on this lattice. A small (8×8) lattice was chosen for the Pt{100}−(1×1) system to keep the computing time for the simulation down to a sensible level, and it was found that this did not cause any problems until high coverages, because periodic boundary conditions are included to avoid finite size effects. At high coverages, the energy change resulting from adsorption has large statistical errors due to the small amount of sites available for adsorption.

For CO on Pt{100}−(1×1), the energy corresponding to each configuration of molecules was calculated as follows. Each CO molecule was assigned an adsorption energy of 217 kJ mol^{-1}, taken from the experimental results at a coverage of 0.1 ML. Two molecules adsorbed on next-nearest-neighbor (nnn) diagonal sites have a repulsive interaction energy, ω_2, which accounts for the fall in heat seen at 0.25 ML coverage when these sites are first filled. There is also a high pairwise repulsive energy, ω_1, due to molecules on nearest-neighbor (nn) sites. This prevents the coverage reaching 1 ML. When the simulation is performed, it is found that a value of $\omega_2 = 5$ kJ mol^{-1} gives a good fit to the experimental data. As the coverage approaches 0.5 ML, a c(2×2) structure develops as expected.

The situation for adsorption on the hex surface is more complicated due to the CO-induced restructuring to the (1×1) phase. Since (1×1) island growth occurs with a high local CO coverage on the islands and low coverage elsewhere, a constant differential heat of adsorption is expected. This is what is observed (see Figure 4), with the heat of adsorption changing by only 25 kJ mol^{-1} over the first 0.5 ML. Adsorption on the hex surface must lift the reconstruction immediately, otherwise an abrupt change in the differential heat would be observed at the point where the reconstruction is supposed to initiate. Thus, in this experiment, even the first dose of CO on the hex surface induces reconstruction. Hopkinson et al.[123] showed that the hex to (1×1) adsorbate-induced restructuring is strongly nonlinear in the CO coverage on the hex phase and that only for coverages below ~0.02 ML is the rate essentially negligible. Background CO adsorption on the crystal prior to the start of the experiment takes the coverage above this minimum, so that the first CO pulse induces a rapid transformation to the (1×1) phase.

At coverages above ~0.5 ML, the (1×1) and hex surfaces have the same behavior. This is to be expected as, at these coverages, the hex surface has completely restructured, and hence, adsorption occurs onto the same phase. At these high coverages, the small distance between adsorbed CO molecules leads to a large decrease in the heat of adsorption due to large intermolecular repulsions.

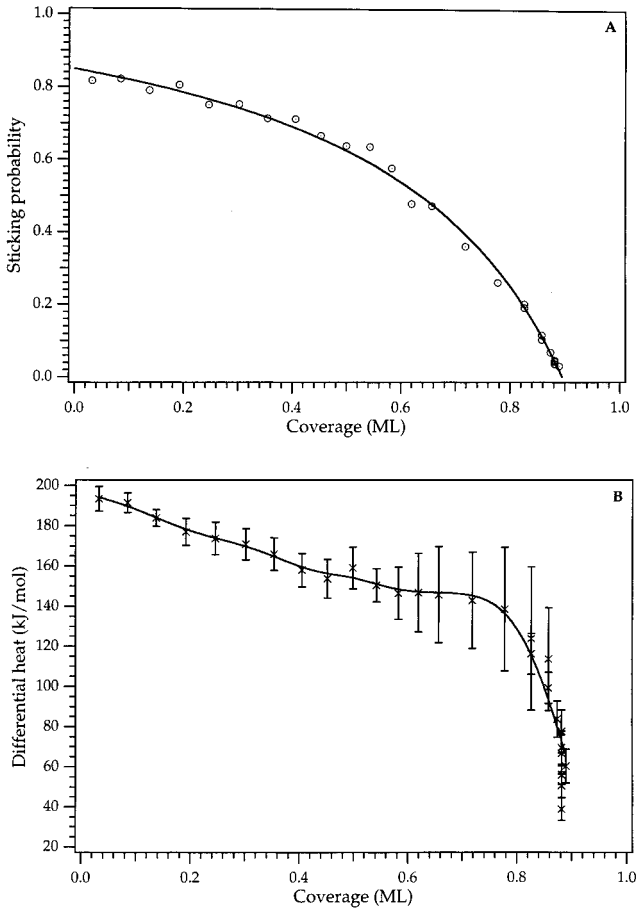

Figure 10. Sticking probability (A) and differential heat of adsorption (B) as a function of coverage for the adsorption of CO on Pt{110} at 300 K.[21] A Kisliuk fit to the sticking probability has been performed, and this has been used to give an absolute coverage scale.

c. CO/Pt{110}

The adsorption heat for CO on Pt{110} has also been determined.[21] The initial heat of adsorption for CO on Pt{110} is 193 ± 6 kJ mol^{-1}. The heat of adsorption and sticking curves obtained as a function of coverage for this system are shown in Figure 10. The sticking probability as a function of coverage shows precursor-mediated behavior and is well-fitted by the Kisliuk expression[116] (see Figure 10). The coverage scale has, therefore, been converted to an absolute scale. The steady-state heat is 70 kJ mol^{-1}. These data show remarkably good agreement with the isosteric data of Jackman et al.,[106] suggesting that the calibrations performed in the SCAC experiment (beam intensity, laser power, and crystal reflectivity) are very accurate. The data can also be compared with the phase diagram of Hofmann et al.[132,133] After 0.2 ML of CO adsorption, further adsorption should lead to reconstruction to a (1×1) phase on the Pt{110} surface. However, scanning tunneling microscopy (STM) results[134] indicate that the reconstruction has a longer time scale than the SCAC experiment. Hence, reconstruction is probably seen in this experiment because the heat of adsorption on the (1×2)

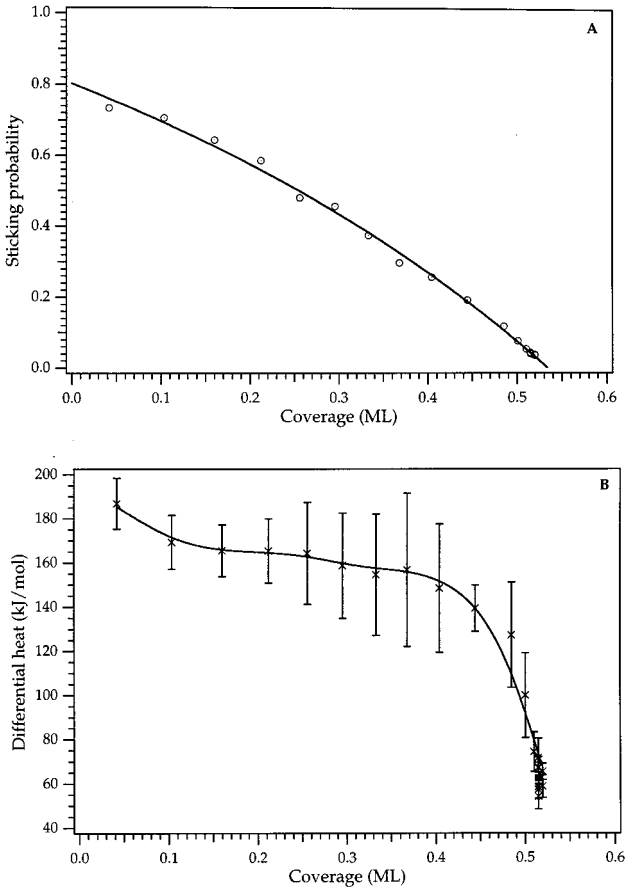

Figure 11. Sticking probability (A) and heat of adsorption (B) for the adsorption of CO on Pt{111} at 300 K.[22] Again, a Kisliuk fit has been performed to convert the scale to actual coverage.

surface drops rapidly, rather than the falling heat, indicating a lower adsorption heat on the reconstructed surface. Although this measurement shows reasonably good agreement with the work of Jackman et al.,[106] the measured calorimetric heat is higher than the measurements of the desorption energy performed by Engstrom et al.[107] and Fair and Madix.[108] This may be because of the assumptions made when using temperature-programmed desorption (TPD) to calculate desorption energies.

d. CO/Pt{111}

CO adsorption has also been investigated on the third singular Pt face, Pt{111}.[22] The heat of adsorption and sticking probability for this system can be seen in Figure 11. The initial heat of adsorption at 300 K was found to be equal to 187 ± 11 kJ mol^{-1}, and it declines to its steady-state value of 60 kJ mol^{-1} at the expected saturation coverage of 0.5 ML.[22] Again, a Kisliuk fit has been performed on the sticking data to allow conversion of the coverage scale to an absolute coverage. The gradient of the heat curve was observed to change at 0.4 ML coverage, and this is consistent with previous LEED measurements[109,135] which show that adsorption at 300 K leads to the development of a ($\sqrt{3}\times\sqrt{3}$)R30° LEED structure at $\theta = 0.33$ ML and a c(4 × 2) structure at $\theta = 0.5$ ML. The steady-state heat achieved at the saturation coverage of 0.5 ML was 60 ± 4 kJ mol^{-1}.

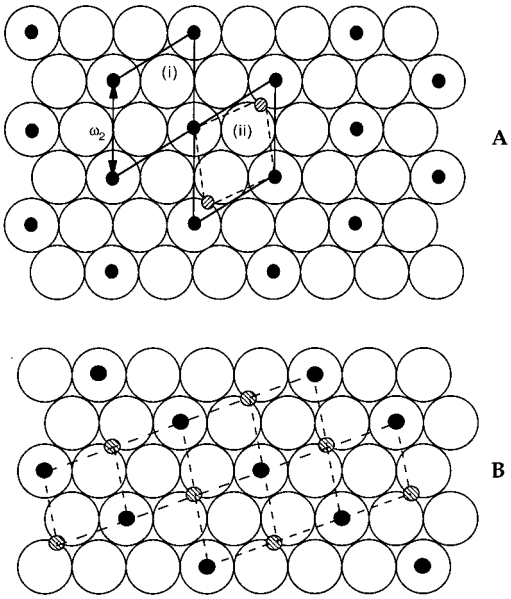

Figure 12. Ordered structures formed during the adsorption of CO on Pt{111} at 300 K. (A) i. Plan view of the ($\sqrt{3}\times\sqrt{3}$)*R*30° ordered structure at $\theta = 0.33$ ML. At this coverage, each CO is surrounded by 6 nnn and the second nearest-neighbor interaction is ω_2, as shown in the diagram. ii. The ($\sqrt{3}\times\sqrt{3}$)*R*30° structure shown uniaxially compressed to give the c(4×2) structure with increasing coverage of CO. CO molecules move from on-top sites (filled circles) to bridge sites (shaded circles). (B) The c(4×2) structure formed at $\theta = 0.50$ ML. Each adsorbate is now surrounded by four CO molecules on bridge sites and four CO molecules on on-top sites. The interaction energy between CO on on-top and bridge sites is given by ω_b. (Reprinted with permission from ref 22. Copyright 1997 American Institute of Physics.)

Using the coverage-dependent heat of adsorption, a simple analysis was performed to extract the magnitude of the interaction between adjacent adsorbates. At a coverage of 0.33 ML, a ($\sqrt{3}\times\sqrt{3}$)R30° ordered layer forms,[109,135] and this corresponds to a heat of 155 kJ mol^{-1}. The observed structure is shown in Figure 12a. At this coverage, each CO is surrounded by 6 nnn, so the nnn interactions, ω_2, can be approximately estimated as

$$\omega_2 = \left(\frac{q_0 - q_{0.33}}{6}\right) = 5.3 \text{ kJ mol}^{-1}$$

The same calculation can be performed at 0.5 ML coverage where a c(4×2) structure is observed (Figure 12b). Each CO is now surrounded by four CO molecules on bridge sites and four CO molecules on on-top sites. Hence, $q_{0.5}$ is

$$q_{0.5} = 0.5q_0(\text{on-top}) - 2\omega_2 - 2\omega_b + 0.5q_0(\text{bridge}) - 2\omega_2 - 2\omega_b$$

where q_0(on-top) is the heat of adsorption on the on-top sites (the initial heat of adsorption), q_0(bridge) is the heat of adsorption on the bridge sites, and ω_b is the interaction energy between CO on an on-top and a bridge site. Hence,

$$q_0(\text{bridge}) - 8\omega_b = 95.4 \text{ kJ mol}^{-1}$$

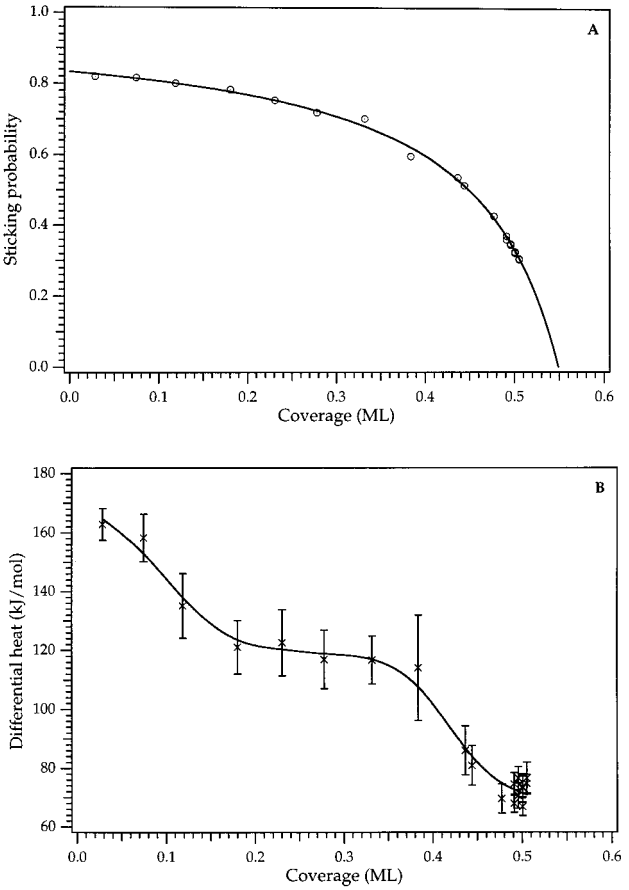

Figure 13. Sticking probability (A) and heat of adsorption (B) for the adsorption of CO on Pd{100} at 300 K. Again, an absolute coverage scale has been obtained via a Kisliuk fit. (Adapted from ref 23.)

The sticking probability curve is somewhat similar to that observed on Pt{110}, with a zero-coverage value of 0.80. The sticking probability as a function of coverage also shows precursor-mediated behavior readily fitted by the Kisliuk expression up to a coverage of 0.5 ML. Above this coverage, the observed steady-state sticking probability can be used to convert the coverage scale to actual coverage. Data from Persson et al.[136] showed that ordered LEED structures were observed at coverages above 0.5 ML, due to compression structures, even though saturation had apparently been achieved.

Isosteric heat measurements by Ertl et al.[109] can be compared with these calorimetric adsorption heat measurements. There is reasonably good agreement at high coverage, but at low coverage, the calorimetric heats are consistently higher than the isosteric heats.[22]

e. CO/Pd{100}

The only Pd surface upon which CO adsorption was studied is Pd{100}.[23] Again, the measurements made using the SCAC were used to give information about the magnitude of the lateral interactions that occurred between adsorbates. Figure 13 shows the heat of adsorption and the sticking probability as a function of coverage for CO on clean Pd{100}. The heat of adsorption decreases reasonably linearly with coverage, and no ordered structures were observed

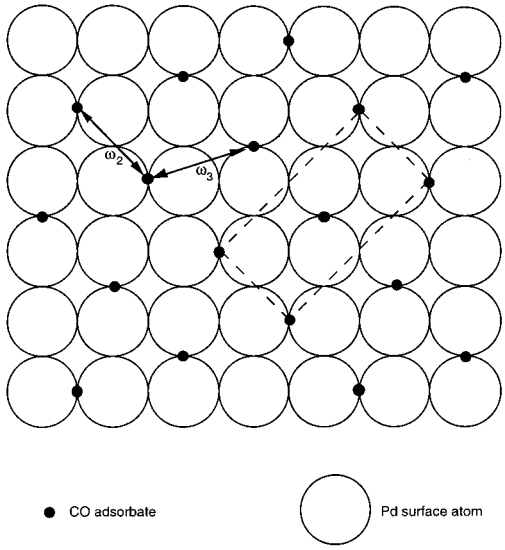

Figure 14. The c($2\sqrt{2}\times\sqrt{2}$)R45° structure formed at 0.5 ML coverage after the adsorption of CO on Pd{100} at 300 K. This structure can be used as the basis for an estimate of the nnn repulsion energy, ω_2, between adjacent adsorbates. (Reprinted with permission from ref 23. Copyright 1997 American Institute of Physics.)

by LEED until a coverage of 0.5 ML was achieved. At 0.5 ML, Tracy and Palmberg[113] observed a c($2\sqrt{2}\times\sqrt{2}$)R45° LEED pattern. This structure was used to estimate the magnitude of pairwise interactions between adsorbates and is shown in Figure 14; it is characterized by an infinite nearest-neighbor pairwise repulsion. The observed fall in heat from 163 to 70 kJ mol^{-1} at 0.5 ML coverage implies a nnn repulsion, ω_2, of 23 kJ mol^{-1}. The c($2\sqrt{2}\times\sqrt{2}$)R45° structure also implies that third nearest-neighbor (nn) interactions, ω_3, must be important if only pairwise (not three-body) interactions are taken into account. The sticking probability for this system is initially 0.82 and shows typical precursor-mediated behavior which can be fitted by the Kisliuk expression. A steady-state sticking of 0.32 is achieved at coverages above 0.5 ML.

The influence of C on CO adsorption was studied because other authors[112−114] state this as a reason for the disagreement between different data sets. The decreasing heat of adsorption with coverage on the clean Pd{100} surface agrees with isosteric measurements taken by Tracy and Palmberg[113] and Szanyi et al.[114] Results taken by Behm et al.[112] are in disagreement with the SCAC data.

Preadsorbed C hardly affects the initial sticking probability but changes the coverage dependence of the sticking probability significantly.[23] At large C precoverages, it seems that the role of the precursor is eliminated and the steady-state sticking probability and coverage are reduced. The effect of C coverage on the heat of adsorption is much more marked. On the clean surface, the initial heat of adsorption is 163 kJ mol^{-1}, this decreases almost linearly with coverage until a plateau is reached at ~0.20 ML, and it then decreases linearly to a steady-state value of 70 kJ mol^{-1} at about 0.5 ML coverage.[23] Even 0.05 ML precoverage of C reduces the initial heat measurably, and with 0.07 ML of C, the initial

Table 3. O_2 Initial Adsorption Heats, q_0, and Initial Sticking Probabilities, s_0, on Various Surfaces[a]

surface	q_0 (kJ/mol)	M−O (kJ/mol)	s_0
Ni{110}[28]	475	485	0.78
Ni{111}[28]	440	470	0.23
Ni{100}[28]	550	520	0.63
Pt{110}[21]	360	427	0.34
Pt{111}[22]	316	405	0.06
Rh{100}[29]	386	427	0.74

[a]Also given is the strength of the M−O single bond formed upon initial adsorption.

heat is reduced markedly from the clean surface value. This could be explained by very long range repulsions between C atoms and CO molecules. The coverage dependence of the heat of adsorption is also dramatically changed by the presence of C. This dependence of the adsorption heat on CO coverage at different C coverages is consistent with the presence of two C phases on the surface: a dilute C phase and a higher coverage phase.[23] Hence, CO adsorbs on the low C coverage phase initially, where interactions between CO molecules are dominant. It then adsorbs on the higher C coverage area, where interactions between CO molecules are screened out. On the basis of these studies with the calorimeter, it is now concluded that the older results could not be faulted on the basis of C contamination.

C. Irreversible Molecular Adsorption: O_2

Many molecules undergo irreversible adsorption on a surface. This may be due to dissociation, decomposition, or surface reaction. Oxygen undergoes irreversible adsorption since dissociation usually occurs upon impact on a surface. In many cases, O atoms also dissolve into the bulk and oxide film formation occurs. For all of these cases, Arrhenius and isosteric heat measurements are impossible due to the irreversible nature of the adsorption. This is, therefore, an adsorption system that can only be studied successfully with the SCAC.

A summary of all of the calorimetric heats measured for oxygen adsorption to date can be seen in Table 3. Also included are the metal−O bond energies derived from the adsorption data according to the reaction

$$O_2(g) + 2M_s \rightarrow 2M{-}O_s$$

a. O_2 on Ni Surfaces

The first single-crystal calorimetric measurement[12,13] made with the SCAC was a study of the adsorption of O_2 on a Ni{110} surface. This system was chosen because of the expected high heat of adsorption due to the dissociative nature of the adsorption. Subsequent measurements for the adsorption of O_2 on Ni surfaces were performed by Al-Sarraf et al.,[16,18,26] and a detailed account of the adsorption of O_2 on the three singular planes of Ni is given in a recent paper by Stuckless et al.[28] The adsorption of O_2 on Ni{100} was also studied using pyroelectric detection techniques to determine the temperature dependence of the adsorption.[25,28] For all three Ni surfaces, the initial adsorption of O_2 is

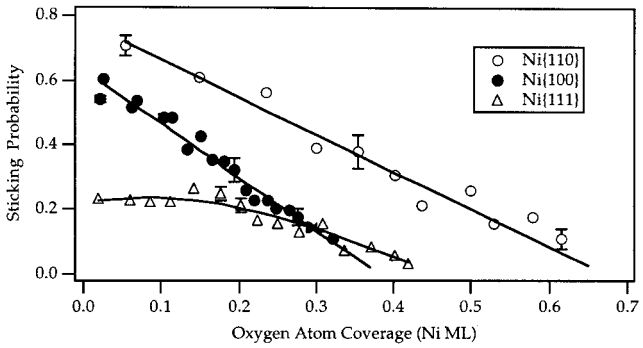

Figure 15. Sticking probability as a function of coverage in the chemisorption regime for O_2 adsorption on the three Ni surfaces at 300 K. (Reprinted with permission from ref 28. Copyright 1997 American Institute of Physics.)

dissociative and subsequent adsorption leads to the formation of oxide films several layers thick on the metal surface. These measurements were the first single-crystal data for the heat of surface oxidation.

The sticking probability of O_2 on the three Ni low index planes in the chemisorption regime is shown in Figure 15. The three Ni surfaces obviously show different behavior. For Ni{100}, there is a linear drop in sticking from an initial value of 0.63 down to ~0.05 at the "saturation" coverage of 0.38 ML. The ideal c(2×2) structure that forms upon O adsorption[28] should saturate at 0.5 ML, but the empty site array required for dissociation is extremely demanding and prevents total completion of the ordered structure.

For the Ni{110} surface, again the sticking probability drops linearly with coverage from an initial value of 0.78 to ~0.05 at the saturation coverage of 0.67 ML. The most obvious interpretation of the linear fall in sticking with coverage is that ordered filling of a chemisorption overlayer that saturates at 0.67 ML occurs, and further dissociative sticking is prohibited once this structure has been completed. A weak (3×1) LEED pattern is observed[137] on this surface, which corresponds to a saturation coverage of 0.64 ML.

For Ni{111}, the initial sticking probability is somewhat lower at 0.23. The sticking probability rises slightly as the coverage increases to 0.16 ML and then decreases at a saturation coverage of 0.45 ML. The sticking curve is similar to that usually found for precursor-mediated adsorption kinetics and can be fitted by a modified Kisliuk equation similar to that derived by Winkler and Rendulic.[138] Most other studies for the adsorption of O_2 on Ni{111} agree that the saturation coverage of chemisorbed O on this surface is 0.33 ML, corresponding to a $(\sqrt{3}\times\sqrt{3})$R30° LEED pattern. The saturation coverage of 0.45 ML seen here can probably be attributed to the initiation of oxidation, which cannot be distinguished from chemisorption.

As the exposure of oxygen increases, the sticking probability does not actually reach zero at the saturation coverage but instead oxide film formation occurs on the surface. On all of the Ni surfaces investigated, the sticking probability (after chemisorption is complete) remains low for a short time and then rises as oxide film formation starts. A few layers of oxide form during a period of rapid uptake,

and further oxidation is then extremely slow at 300 K. It is thought[139] that Ni oxidation starts at nucleation points on the surface and continues by island growth. Oxygen is only incorporated at the island edges, and therefore, the uptake slows as the islands get larger. This is the point where the sticking probability is equal to zero and the oxide layer growth stops. We, therefore, expect to see a maximum in the oxygen sticking probability curves.

Figure 16 shows the sticking probability for oxide formation on the three nickel surfaces. The island growth mechanism suggested by Holloway and Hudson[139] provides a reasonable fit to the sticking data for Ni{100}[28] shown by the solid line through the data. For island growth in two dimensions from islands of fixed thickness, an appropriate function is[139]

$$\theta = \theta_{ad} + \Delta\theta_{oxide} \quad (1)$$

where

$$\Delta\theta_{oxide} = (\theta_{sat} - \theta_{ad})(1 - \exp[-K_i N_o (L - L_o)^2]) \quad (2)$$

with θ_{sat} being the oxygen saturation coverage, L is the oxygen dosage, L_o is the exposure when oxide nucleation starts and $K_i N_o$ is the oxidation rate constant. Differentiating eq 1 including eq 2 gives an equation for the sticking as a function of coverage which fits the data well. Once the amount of reversible adsorption has been determined by this fit, then the net uptake can be determined, and this is used to adjust the heat data to take into account transient adsorption onto the oxide.

Data for the sticking of O_2 on Ni{111} and {110} are also shown in Figure 16, at higher coverages, and the fit parameters for oxidation according to the above equation are given in Table 4. Fits were optimized for the high exposure region where oxidation is occurring. At intermediate coverages, the situation is more complex as chemisorption and oxide island nucleation occur simultaneously.

For Ni{111}, oxidation occurs (shown by an increase in the sticking) above 0.45 ML, and for Ni{100}, the sticking probability rises at 0.68 ML. Both of these are somewhat higher than the coverages quoted in the literature as the onset of oxidation. For Ni{110}, the sticking is more erratic with a minimum at 0.9 ML, rising, and then falling to another minimum at 1.2 ML. This could be due to the formation of the (9×4) "pseudo oxide" structure seen by other groups.[140−142] The amount of oxide created on each surface is approximately four layers thick[28] and depends on the exact orientation of the NiO film.

We now summarize the adsorption heat data, again for both the chemisorption and oxide film formation regime. These are the only heat measurements available for oxide film formation. Table 3 shows the initial heats of adsorption and sticking probability along with the Ni−O bond strengths for all of the Ni surfaces. Figure 17 shows the heat of adsorption curves for oxygen adsorption on the three Ni surfaces in the chemisorption regime.

For the Ni{100} surface, the initial heat measured at 300 K is 550 kJ mol^{-1} and it falls rapidly with

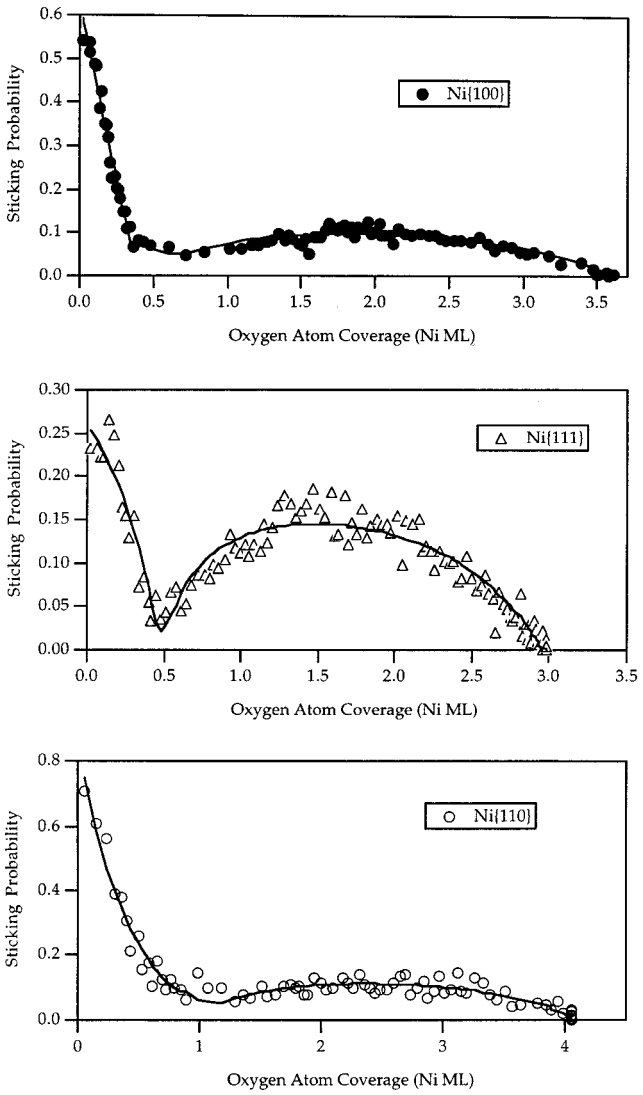

Figure 16. Sticking probability for O_2 on the three singular Ni surfaces during oxide formation at 300 K. Note that a decrease is seen in the sticking followed by an increase as oxide formation steps in. (Reprinted with permission from ref 28. Copyright 1997 American Institute of Physics.)

Table 4. Data for the Oxidation Growth on the Three Ni Surfaces[a]

	oxidation rate constant $K_i N_o$ (L^{-2})	saturation coverage θ_{sat} (ML)	oxidation onset (ML)	saturation sticking s_{rev}
Ni{100}	0.0002	3.6	0.68	0.062
Ni{111}	0.002	3.0	0.45	0.059
Ni{110}	0.0005	4.1	0.8−1.2	0.072

[a] The meaning of the various parameters is given in the text.

increasing oxygen coverage. The pyroelectric detection technique was used to extend the study of oxygen on Ni{100} to various different temperatures.[25,28] This allowed the effects of temperature on adsorption energy to be investigated, an experiment which is not possible using the standard infrared detection technique. The 300 K measurements allowed a direct comparison with infrared measurements to be made, and this is shown in Figure 18. The points in the figure represent the data obtained pyroelectrically, while the line is for the previous data measured with

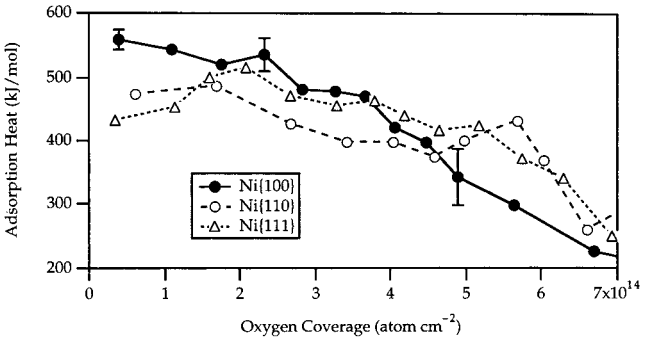

Figure 17. Heat of adsorption of O_2 as a function of coverage in the chemisorption regime at 300 K for all three Ni singular surfaces. (Reprinted with permission from ref 28. Copyright 1997 American Institute of Physics.)

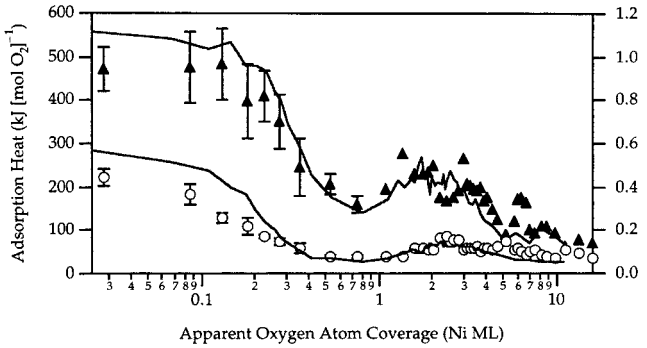

Figure 18. Comparison of the data obtained using the pyroelectric and infrared techniques for oxygen on Ni{100} at 300 K. A log scale is used so that both chemisorption and oxidation regimes can be seen in detail. The filled triangles represent adsorption heat, the empty circles represent the sticking probability for the pyroelectric data, while the solid lines represent the corresponding data obtained using the infrared emission technique. (Reprinted with permission from ref 28. Copyright 1997 American Institute of Physics.)

the infrared detection technique. The agreement between the two sets of data is excellent. There is a slight difference in the heats measured pyroelectrically at low coverage and those measured by infrared emission. This is probably due to the long thermal equilibration time required in a pyroelectric experiment during which background gas can contaminate the crystal, thus leading to slightly lower initial heats.

The coverage-dependent heats for three temperatures are seen in Figure 19. Immediate differences between the adsorption at the three temperatures are observed. The initial adsorption heat falls as a function of temperature from 490 kJ mol^{-1} at 410 K to 470 kJ mol^{-1} at 300 K to 440 kJ mol^{-1} at 100 K. This trend becomes stronger with increasing coverage, so that the heat at the highest temperature increases with coverage while at the lowest temperature the heat decreases sharply. All three curves are approximately coincident at 0.3 ML, after which the opposite trend is seen. Hence, the highest heat is now seen for the lowest temperature data.

These trends can be understood since the O−O interaction on Ni{100} is weakly attractive at the third nearest-neighbor separation so that p(2×2) island formation is preferable up to the saturation

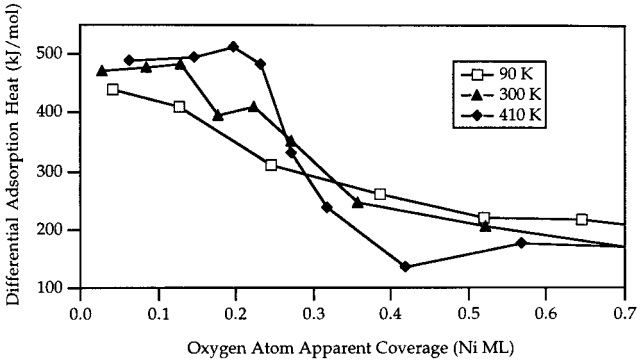

Figure 19. Temperature dependence of the heat of adsorption as a function of coverage for O_2 on Ni{100} measured with the pyroelectric detector. All of these adsorption heats are for the low coverage regime. (Reprinted with permission from ref 28. Copyright 1997 American Institute of Physics.)

coverage of 0.25 ML. After this, the c(2×2) structure forms which has strong repulsive interactions between O adatoms. Hence, for the thermodynamically preferred structure, there should be an increase in heat until the p(2×2) structure is completed and thereafter a sharp decrease should be observed. This is what is observed for adsorption at 410 K. However, at 100 and 300 K, the overlayer is not in thermodynamic equilibrium on the time scale of the measurement and lower heats of adsorption occur due to disorder. Essentially, the mobility of the O adatoms is only sufficient to achieve the thermodynamically stable adatom distribution at higher temperatures. The second and third nearest-neighbor interactions between O adatoms were quantified using a Monte Carlo simulation in a manner similar to that described earlier.[28] For the data obtained at 410 K, values of $\omega_2 = 30 \pm 5$ kJ mol^{-1} and $\omega_3 = -1.5$ kJ mol^{-1} were obtained. These are consistent with LEED and STM studies showing an attractive interaction in the p(2×2) structure.

For adsorption on the {110} surface, the initial heat is 475 kJ mol^{-1}, and the heat does not drop as rapidly as on the {100} surface. This can be attributed to the adlayer geometry on the {110} surface where Ni−O chains are formed[143] in the added-row model. The O atoms are well-shielded from one another by the intervening top layer Ni atoms so that less repulsion occurs and, therefore, the heat drops more slowly.

For the {111} surface, the initial heat is relatively low (at 440 kJ mol^{-1}), corresponding to adsorption in 3-fold hollow sites. The heat initially increases with exposure at the same time as the precursor effect is observed in the sticking curve. The heat then falls with increasing coverage, and this again is attributable to repulsive interactions between adatoms.

For adsorption in the thin oxide film regime, the heats obtained at 300 K are shown in Figure 20. All of the Ni surfaces behave in a similar manner with the heats dropping during chemisorption, then leveling off or rising during oxidation before dropping to a steady-state value. All of the heat curves have a contribution from the reversible adsorption of oxygen on the oxide film, equal to about 87 kJ mol^{-1}. This can be used to give a desorption frequency factor, υ (see earlier), of 1×10^{14} s^{-1}.

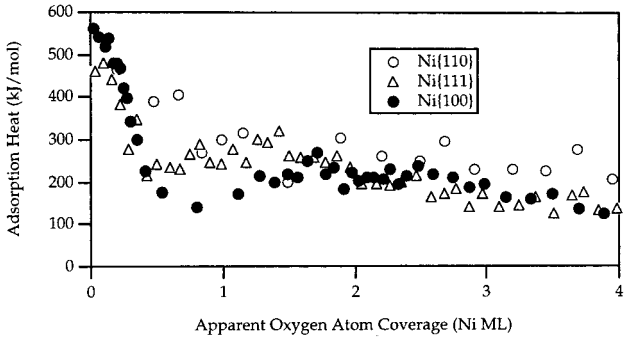

Figure 20. Heat of adsorption of O_2 as a function of coverage in the oxide film formation regime for all three singular Ni surfaces. (Reprinted with permission from ref 28. Copyright 1997 American Institute of Physics.)

The stability of the different oxide films is related to the height of the maximum observed during film growth. If the data is integrated over coverage, then the integral heat for oxide formation can be determined and compared with the bulk heat of formation of NiO. The integral heats are 220 kJ mol^{-1} for Ni{100}, 290 kJ mol^{-1} for Ni{110}, and 320 kJ mol^{-1} for Ni{111}.[28] These values are all considerably less than the bulk heat of formation of NiO (479 kJ mol^{-1}). This is not surprising considering that the oxide films were only about 4 layers thick and would, therefore, have considerable defects, giving a lower heat of oxide formation.

b. O_2/Pt{110}

The adsorption of O_2 on Pt{110} was studied as part of a wider study of CO, NO, and O_2 adsorption on this surface.[21] The initial adsorption heat is 360 ± 8 kJ mol^{-1}, decreasing rapidly to 250 ± 20 kJ mol^{-1} at 0.35 ML and reaching a steady-state value of 145 ± 40 kJ mol^{-1}. The initial sticking probability is equal to 0.34, and the steady-state sticking probability is only 0.029. The adsorption heat is much larger than previous estimates from thermal desorption spectroscopy[144−146] but in reasonable agreement with polycrystalline measurements of Brennan et al.[65] The steady-state adsorption heat of 145 ± 40 kJ mol^{-1} is too high for spontaneous desorption, but since the sticking probability is very low, it is possible that background CO could be removing the adsorbed O atoms between gas pulses, leaving empty sites for adsorption. Alternatively, this high heat could be as a result of incorporation of oxygen into the Pt{110} crystal.

c. O_2/Pt{111}

The adsorption of O_2 has also been measured on the Pt{111} surface[22] as part of a study of the CO oxidation process. The initial heat of adsorption for O_2 is somewhat similar to that on Pt{110}, 316 ± 34 kJ mol^{-1}. The heat of adsorption declines very rapidly with coverage to reach 180 kJ mol^{-1} at 0.1 ML and 115 ± 8 kJ mol^{-1} at the steady state. The sticking probability is low and ranges from 0.064 at zero coverage to only 0.02 at steady state. Using an initial heat of 316 kJ mol^{-1}, the Pt−O bond energy on this surface is calculated as 405 kJ mol^{-1}. This is smaller than that observed on most Ni surfaces (see Table 3) but somewhat similar to the value observed for Pt{110}.

Again, a Monte Carlo simulation was performed to evaluate the lateral interactions between adatoms on the surface. In the simulation, the first 0.02 ML of adsorption was neglected as it was assumed that this was due to adsorption on defect sites.[22] In the range of coverage from 0.02 to 0.2 ML, the differential heat of adsorption decreases continuously with coverage, suggesting that the adsorbate is immobile upon adsorption at 300 K. The observed saturation coverage is below 0.25 ML, indicating that the occupation of nn and nnn sites is forbidden. The main contribution to the observed decrease in the adsorption heat must, therefore, be due to adatoms adsorbed in third nn positions. A (2×2) LEED pattern is observed for this system, at which the coverage of each adatom has six other atoms in third neighbor positions. The magnitude of this pairwise interaction is, thus, estimated as $\sim(q_0 - q_{0.25})/6 \approx 27$ kJ mol^{-1}. A better estimate of the lateral interactions is given by a Monte Carlo simulation. Only a small number of adatom hops are allowed before equilibration of the atom with the surface, and this is the "immobile adsorbate" limit. Since the adsorbate is immobile, the saturation coverage observed is lower than that for an ideal (2×2) overlayer. The differential heat and sticking probability can be simulated, and in general, good agreement between theory and experiment are observed. A best fit to the data is obtained using the values $q_0 = -305$ kJ mol^{-1}, $\omega_3 \approx 22$ kJ mol^{-1}, $s_0 = 0.05$. The lattice was also allowed to equilibrate for a longer time (the "mobile adsorbate" limit), and in this case, the simulated data did not fit the experiment well. This, therefore, confirms that at this temperature the adsorbate is immobile.

d. O_2/Rh{100}

Results have also been recently obtained for the adsorption of O_2 on the Rh{100} surface.[29] For this system, the initial sticking probability is 0.74 and the initial heat is 386 kJ mol^{-1}, giving a value for the Rh−O bond strength of 440 kJ mol^{-1}. Two phases were observed in both the heat and sticking curves which correspond to different structures seen by LEED.[29]

D. Intermediate Adsorption: NO

NO is a molecule which can adsorb either dissociatively or molecularly depending on the metal and on the conditions of adsorption. For many systems adsorption is irreversible, and hence, it has not been widely studied by isosteric or thermal desorption techniques. Table 5 shows the initial heat of adsorption, q_0, and initial sticking probability, s_0, for the

Table 5. NO Initial Adsorption Heats, q_0, and Initial Sticking Probability, s_0, on Various Surfaces at 300 K

surface	q_0 (kJ/mol)	s_0
Ni{100}[27,30]	385	0.80
Pt{100}-(1×1)[20]	191	0.68
Pt{100}-hex[20]	187	0.86
Pt{110}[21]	162	0.87
Pd{100}[23]	110	0.85

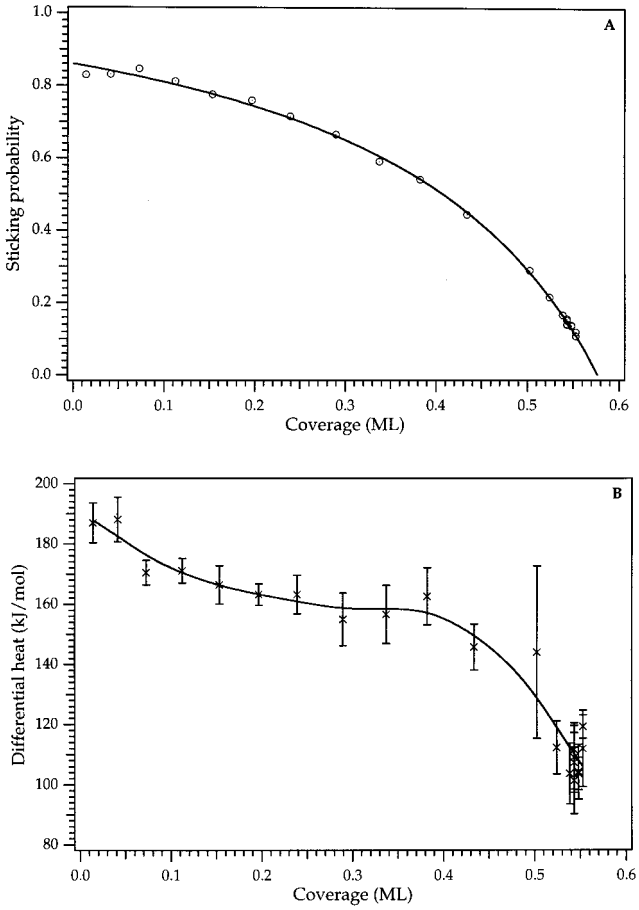

Figure 21. Sticking probability (A) and differential heat of adsorption (B) as a function of coverage for NO adsorbed on Pt{100}−hex at 300 K. A Kisliuk fit to the sticking has been performed, and the coverage scale is therefore absolute. (Adapted from ref 20.)

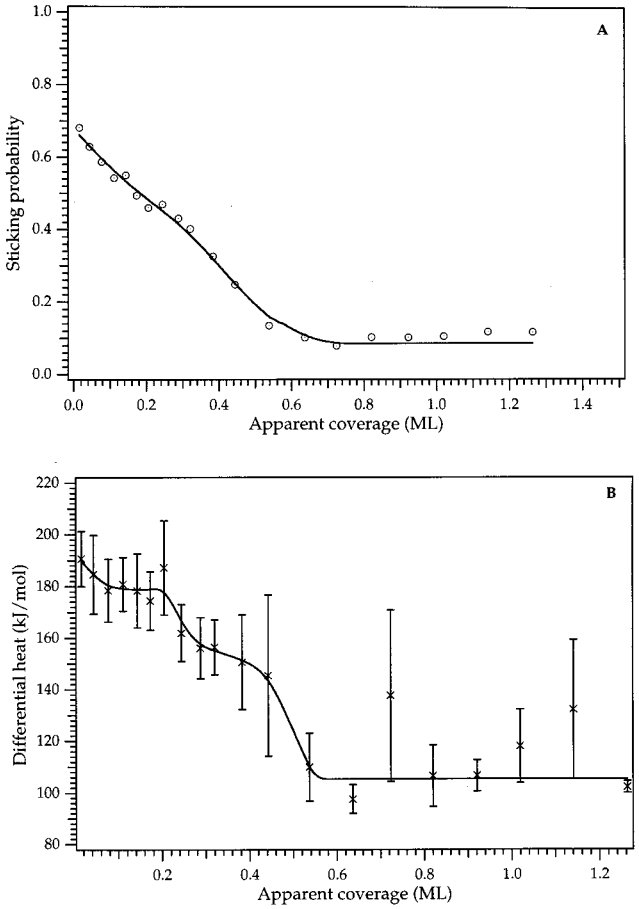

Figure 22. Sticking probability (A) and differential heat of adsorption (B) as a function of coverage for NO adsorbed on Pt{100}−(1×1) at 300 K. (Adapted from ref 20.)

adsorption of NO on all of the surfaces calorimetrically investigated to date.

a. NO/Pt{110}

For the adsorption of NO on Pt{110}[21] there are two regions to the heat curve, and this two-stage adsorption is consistent with previous electron-energy-loss spectroscopy (EELS) experiments.[147] The initial heat is 162 kJ mol^{-1}, and the steady state heat is ∼95 kJ mol^{-1}. Adsorption at 300 K is molecular, as expected.[148] The sticking data are described by the Kisliuk equation, indicating precursor mediated adsorption, and this again allows absolute saturation coverages to be estimated. The initial sticking probability is 0.87, dropping to a value of 0.09 at steady state. An equilibrium analysis can be performed on the steady-state data to extract a frequency factor and the differential entropy for adsorption.[21]

b. NO/Pt{100}

NO adsorption has also been studied on Pt{100}.[20] As was the case for CO, NO lifts the hex reconstruction on the Pt{100} surface and, hence, the possibility arises that its adsorption can be used to measure the energy difference between the clean hex and (1×1) surfaces. Monte Carlo simulations were performed to determine the magnitude of the lateral interactions to explain the coverage dependence of the heat of adsorption curves and the differences between the observed saturation coverages of CO and NO.

The adsorption heat and sticking probability as a function of coverage for NO on the hex and (1×1) surfaces can be seen in Figures 21 and 22, respectively. The true saturation coverage of NO on the hex surface is ∼0.55 ML, and after this point the sticking and heat are steady-state values. The initial adsorption heat on the hex surface is 187 kJ mol^{-1}, and this decreases linearly to ∼150 kJ mol^{-1} at 0.44 ML coverage. The steady-state value of 100 kJ mol^{-1} occurs above 0.5 ML coverage. The behavior of the heat curve for the (1×1) surface is different. The initial heat is higher, at 191 kJ mol^{-1}, and remains approximately constant up to 0.20 ML, at which point a small decrease is observed to about 160 kJ mol^{-1}. The heat again remains constant to 0.40 ML, at which point a rapid decrease occurs. At saturation, the heat is identical to that seen on the hex surface.

The initial sticking probability for the hex surface is 0.86, and the coverage dependence demonstrates precursor-mediated adsorption which can be fitted by the Kisliuk expression. The initial sticking on the (1×1) surface is lower (0.68) and decreases linearly to a steady-state value of 0.13 (the same as for the hex surface). This system does not show precursor-mediated adsorption. In contrast to the situation for CO, the sticking and heat curves at saturation (0.5

ML) on the hex and (1×1) surfaces do not coincide exactly, suggesting that the final states of the two surfaces are not identical. It is possible that NO does not totally lift the hex reconstruction, hence this experiment cannot be used to estimate the energy difference between the (1×1) and hex surfaces on Pt{100}.

It is assumed that NO does not dissociate on this surface on the basis of previous measurements.[149,150] The high initial adsorption heat for NO on the (1×1) surface is, therefore, attributed to adsorption at defect sites. The heat of adsorption on the (1×1) surface shows two approximate plateaus in the heat at 180 and 155 kJ mol^{-1}, separated by a sharp fall at ~0.2 ML coverage, and then followed by a decrease between 0.4 and 0.55 ML coverage. This can be accounted for by considering lateral interactions between adsorbate molecules. For NO adsorption on the (1×1) surface, the only ordered structure observed is a c(2×4) structure close to saturation, unlike the case for CO where c(2×4) and c(2×2) structures were observed. This implies that the repulsion between molecules in nnn positions along the diagonal of the lattice is larger than that for molecules in nn positions. It cannot be energetically favorable to have a molecule with four second neighbors (as for c(2×2)), and therefore, a molecule with only two second neighbors is a preferable structure. The absence of a p(2×2) structure at $\theta = 0.25$ was taken to imply that the c(2×4) structure involves "chains" of molecules on the surface.[20]

A possible structure for NO on Pt{100}−(1×1) is shown in Figure 23. To explain the behavior of the differential heat as a function of coverage, up to 0.2 ML coverage no large repulsions occur and above this coverage filling of nnn sites incurs a decrease in the measured heat. A similar process without further large repulsions is completed at 0.40 ML, and from then on large repulsions lead to the final drop in the heat. The model in Figure 23 possesses three adsorbed molecules in adjacent positions (configuration T in the figure) with a lower repulsion than either 2 nn (C) or 2 nnn (D). When the triplets are next to each other in line (configuration TT), then strong triplet−triplet repulsions occur.

This model was simulated using Monte Carlo techniques, and interaction energies were calculated by fitting the observed experimental data. High repulsions were assigned to molecules in configurations C and D, and a small repulsion (ϵ_t) was applied to each triplet to generate the observed fall in adsorption heat at 0.25 ML. A large repulsion is assigned to a triplet pair (ϵ_{tt}) to account for the final drop in heat above 0.4 ML. A reasonably good fit to the data is obtained with $q_0 = 200$ kJ mol^{-1}, $\epsilon_t = 20$ kJ mol^{-1}, and $\epsilon_{tt} = 80$ kJ mol^{-1}.

The adsorption of NO on the hex surface can be analyzed using the equation:[20]

$$q_{\text{diff}} = \left(\frac{-q_{\text{spt}}}{\theta_l}\right) + q_{\text{int}}(\theta_l)$$

where q_{spt} is the energy of the surface phase transition, $q_{\text{int}}(\theta_l)$ is the integral heat of adsorption at coverage θ on the (1×1) phase, and θ_l is the local coverage. The change in adsorption heat over the first 0.45 ML is 47 kJ mol^{-1}, so it cannot be assumed that the local coverage is constant. Using q_{spt} as calculated earlier for CO (12 kJ mol^{-1}) and assuming that the local coverage is a function of total coverage, it is possible to calculate the expected differential heat, q_{diff}. All calculations give an initial heat lower than that measured experimentally, and hence, defects must play a much larger role on the hex surface than on the (1×1) surface, probably because defects are created during the reconstruction process in addition to those present on the clean surface. This leads to a contribution of defects to the integral heat and, hence, to a correction on q_{spt}. Therefore, the final states obtained from adsorption on the hex and (1×1) surfaces are not the same, as confirmed by other studies[149,151,152] and by the observation that the final sticking probabilities are not identical.

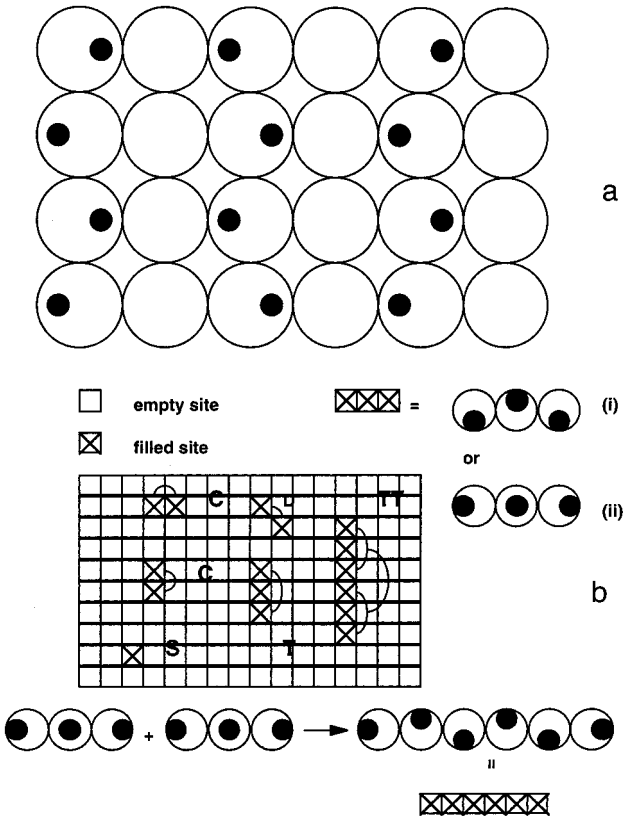

Figure 23. (a) The structure for NO/Pt{100}−(1×1). The large white circles are Pt atoms, and the small black circles are NO molecules. (b) Some of the possible configurations considered in the Monte Carlo simulations, as explained in the text. (Reprinted with permission from ref 20. Copyright 1996 American Institute of Physics.)

c. NO/Ni{100}

The only Ni surface upon which NO adsorption has been studied is Ni{100}.[27,30] This is an important system as on this surface NO adsorbs both dissociatively and molecularly and there is a threshold coverage at which the switch in the adsorption mode takes place. This is shown by the heat of adsorption data in Figure 24: there is a marked break at 0.16 ML. The calorimetry data demonstrates that the

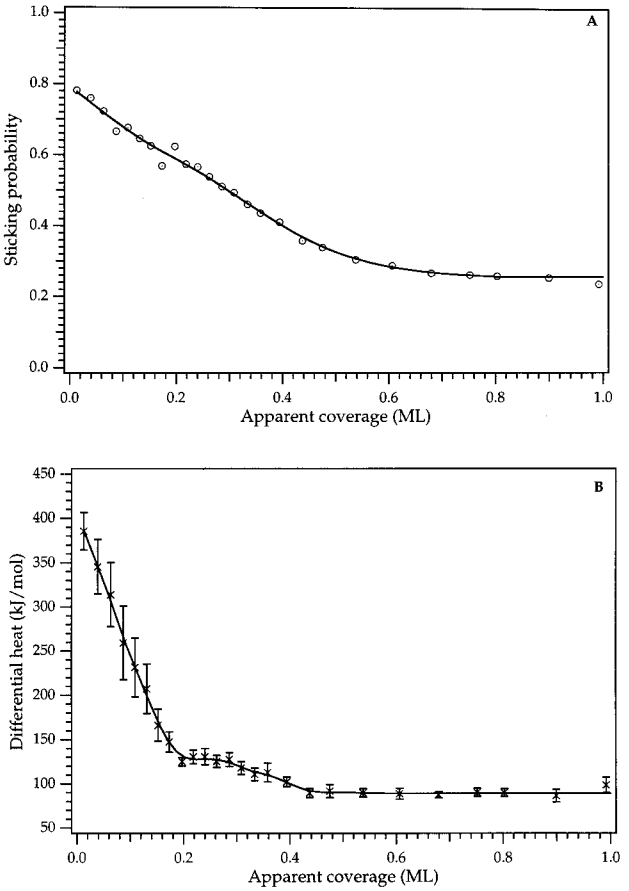

Figure 24. Sticking probability (A) and heat of adsorption (B) for NO on Ni{100}. Note the sudden change in the slope of the heat curve at 0.16 ML coverage. This is where further adsorption ceases to be dissociative and becomes molecular. (Adapted from ref 27.)

switch from dissociative to molecular adsorption is attributable to the magnitude of lateral interactions between N and O atoms in the adsorbed layer. The adsorption of NO was also investigated in the presence of a preadsorbed layer of O,[27] and these measurements were used to give information on the expected dissociative adsorption of N_2. The initial heat of adsorption on the clean surface is 385 kJ mol^{-1}, and it decreases smoothly with coverage up to 0.16 ML. At this point, there is a large slope change and the heat then decreases until a plateau is observed at 100 kJ mol^{-1}. When NO is dosed onto an oxygen precovered layer, the initial heat is lower and the plateau in the adsorption heat at 100 kJ mol^{-1} is reached at a lower NO coverage.[27] The sticking probability shows somewhat different behavior. On the clean surface, the initial sticking probability is 0.8 and decreases almost linearly with coverage. On an oxygen predosed surface the initial sticking is slightly lower and also decreases linearly.

The high initial adsorption heat for NO on Ni{100}[27] is consistent with dissociative adsorption. Using the measured initial value of the adsorption heat for NO (385 kJ mol^{-1}) and O_2 (see earlier, 550 kJ mol^{-1}), it is possible to calculate the initial heat of N_2 dissociative adsorption on Ni{100}; this cannot be measured directly due to a negligibly small sticking probability for N_2 dissociative adsorption. The reactions that are important in this calculation are

$$\mathrm{NO(g) + 2Ni \rightarrow Ni{-}O + Ni{-}N} \qquad -q_{(\mathrm{NO})}$$

$$\mathrm{Ni{-}O \rightarrow Ni + O(g)} \qquad {}^1/_2(D(\mathrm{O_2}) + q(\mathrm{O_2}))$$

$$\mathrm{N(g) + O(g) \rightarrow NO(g)} \qquad -D(\mathrm{NO})$$

$$\mathrm{Ni + N(g) \rightarrow Ni{-}N} \qquad -{}^1/_2(D(\mathrm{N_2}) + q(\mathrm{N_2}))$$

where $D(N_2)$ (942 kJ mol^{-1}), $D(O_2)$ (494 kJ mol^{-1}), and D(NO) (628 kJ mol^{-1}) are the gas-phase dissociation energies of the molecules involved. This gives a value of $q(N_2)$ of 40 kJ mol^{-1}. The desorption energy[153] of N_2 is approximately 195 kJ mol^{-1}, giving an activation energy for adsorption of ~155 kJ mol^{-1}, explaining why the sticking probability at 300 K is negligibly small. This is an important example of how calorimetry data can be used to extract information about species upon which experiments cannot be performed.

On the clean Ni{100} surface there is a large change in the slope of the differential heat of adsorption of NO at ~0.16 ML coverage. When the plateau in the adsorption heat at 100 kJ mol^{-1} is reached, the sticking probability still remains high and this is attributed to molecular adsorption, in agreement with spectroscopic data. The coverage independence of the heat in this range implies that there are only weak interactions between the adsorbed molecules, contrasting with the strong interactions between N and O adatoms. From the decrease in the heat of adsorption observed with increasing NO coverage at $\theta = 0.16$ ML, it is possible to estimate the pairwise repulsive interactions between adatoms. The three important interactions are those between O−O, O−N, and N−N atoms. O−O interactions were calculated from O_2 adsorption data and are assumed to be the same for NO adsorption. It is noted that the maximum observed coverage is lower than 0.5 ML, and hence, repulsions between first neighbor adatoms are prohibitively high. If a very simplified simulation is undertaken with the same repulsions between all adatoms, an average value for second neighbor repulsive interactions, ω_2, of 60 kJ mol^{-1} is obtained. This is higher than that obtained for O−O alone (40 kJ mol^{-1}) and implies that N−N and N−O interactions are larger than O−O interactions. A more refined simulation[27] gave N−N and O−N interactions to be ~100 kJ mol^{-1}. This gives a reasonable fit to the observed integral heats.

The strength of the lateral interactions between the adatoms is such that the differential heat falls very sharply with coverage, and at $\theta > 0.16$ ML, it falls below the value for non-dissociative adsorption; thus, dissociative adsorption is favored at low coverages, and molecular adsorption is favored at $\theta > 0.16$ ML. Changing the O adatom precoverage controls the relative amounts of dissociated and molecularly adsorbed NO[30] observed on the surface. This is particularly relevant to catalytic situations where oxygen may act as a poison or promoter depending on the

Table 6. Hydrocarbon Adsorption Heats, Initial Sticking, and M−C Bond Strengths[a]

system	initial heat (kJ mol^{-1})	initial sticking probability	surface species	no. of M−C bonds	M−C single bond energy (kJ mol^{-1})
C_2H_4/Pt{110}[33,34]	235	0.85	≡C−CH_2-	4	229
			≡C−CH_3	3	239
			−CH_2−CH_2−	2	257
C_2H_4/Pt{111}[35]	195	0.67	≡C−CH_3	3	238
			=CH−CH_3	2	250
C_2H_4/Pt{100}-hex[33]	213	0.79	quad-σ C_2H_2	4	223
			≡C−CH_3	3	230
			di-σ C_2H_4	2	249
C_2H_4/Pt{100}-(1×1)[33]	305	0.69	quad-σ C_2H_2	4	246
			di-σ C_2H_4	2	253
C_2H_4/Pd{100}[31]	73 (steady-state adsorption only)	0.75			
C_2H_4/Ni{100}[31]	203	0.81	≡CH	3	205
			≡CCH	π interaction	74−189
C_2H_2/Pd{100}[31]	112	0.83	di-σ C_2H_2	2	171
C_2H_2/Ni{100}[31]	264	0.81	≡CH	3	204
			≡CCH	π interaction	51−165

[a] It can be seen that hydrocarbon adsorption leads to the formation of many different species on the surface. In general, good agreement is achieved for calculated M−C bond energies whatever the nature of the adsorbate species.

reaction involved. It is possible to determine the amount of NO dissociation by changing the O predose, and it is therefore possible to influence the chemical reaction that takes place on the surface.

d. NO/Pd{100}

The adsorption heat for NO has also been determined on Pd{100}.[23] The initial heat of adsorption[23] is 110 kJ mol^{-1}, and a steady-state value of 80 kJ mol^{-1} is reached at a coverage of 0.5 ML. The sticking probability for this system[23] is initially 0.85 and as a function of coverage exhibits precursor-mediated adsorption which can be fitted by the Kisliuk expression before a high steady-state sticking of 0.45 is achieved. The differential heat of adsorption for NO on Pd{100} shows a very sharp decrease in the 0−0.05 ML coverage range, and this initial high adsorption heat is assigned to adsorption on defect sites.

E. Reactions with Surface Products: The Adsorption of Hydrocarbons

The adsorption of diatomic molecules is relatively simple, resulting in either non-dissociative molecular adsorption or dissociative atomic adsorption. No other products are observed on the surface at room temperature. The adsorption of hydrocarbons is more complex, with surface reactions often occurring upon adsorption at 300 K. Hydrocarbon reactions are a fundamental part of many catalytic processes, and an understanding of the energetics of adsorption is essential. Due to the irreversible nature of the processes, no adsorption heats had been measured for hydrocarbons before the investigations described here. Some of the different species that can be formed upon adsorption of ethylene or acetylene onto a surface are shown in Figure 25. A summary of all of the microcalorimetric measurements of hydrocarbon adsorption to date is given in Table 6. In all cases, an attempt has been made to calculate the M−C bond energy for the different species formed on the surface, and these are also included in Table

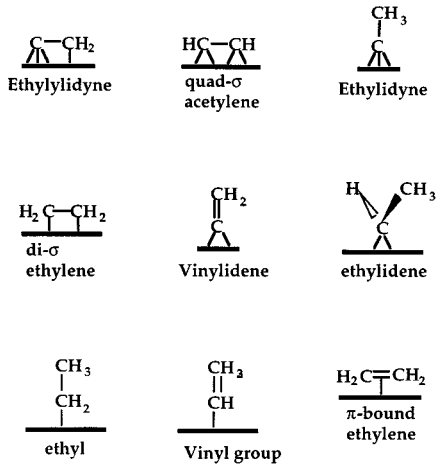

Figure 25. Some of the hydrocarbon species that can be formed upon adsorption of C_2H_2 and C_2H_4 on a surface. (Reprinted with permission from ref 35. Copyright 1996 Elsevier.)

6. There are two different methods of calculating M−C bond energies, outlined in section V of this review. The abe method was used to calculate all of the metal−C bond energies given in Table 6. The following values for the bond strengths have been used in all of the calculations: C≡C, C=C, C−C, and C−H bond strengths are taken as 962, 733, 376, and 412 kJ mol^{-1}, respectively.[154] Also required is the M−H bond energy (266 kJ mol^{-1} for the Ni surface, 270 kJ mol^{-1} for Pd, and 250 kJ mol^{-1} for Pt) which is calculated from the dissociation energy of H_2 (436 kJ mol^{-1}) and the metal−H_2 bond strength determined by TDS[155] to be 96, 103, and 63 kJ mol^{-1} for Ni, Pd, and Pt, respectively.

a. C_2H_4 /Pt{110}

A measurement of the heat of adsorption for C_2H_4 on the Pt{110}-(1×2) surface at 300 K has been made[33,34] and is shown in Figure 26. The initial heat is 235 kJ mol^{-1}, and there are then several distinct regimes before a steady-state heat of 140 kJ mol^{-1} is reached.[34] The heat can be interpreted by considering the nature of the different species observed on

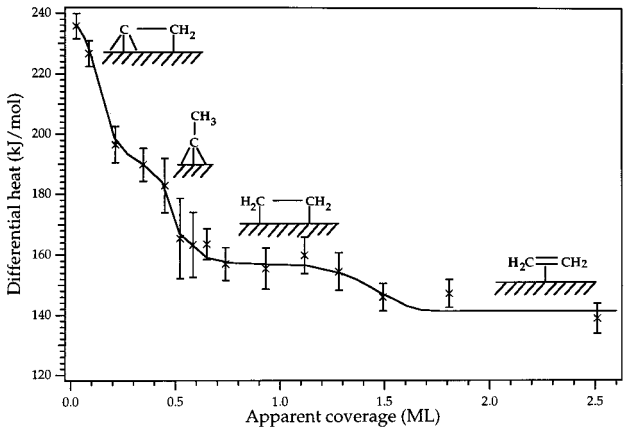

Figure 26. Heat of adsorption as a function of coverage for the adsorption of C_2H_4 on Pt{110} at 300 K. (Adapted from ref 34.)

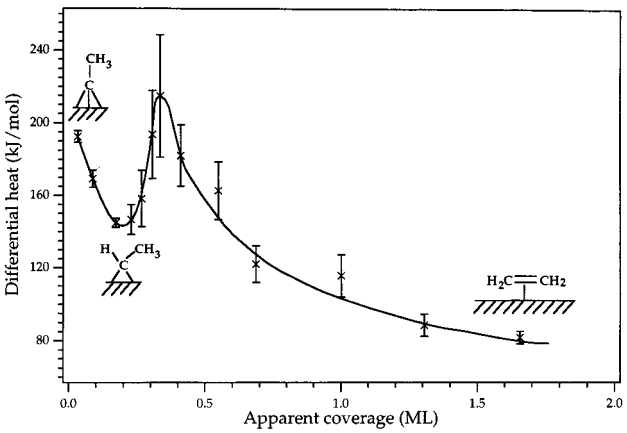

Figure 27. Heat of adsorption as a function of coverage for the adsorption of C_2H_4 on Pt{111} at 300 K. The minimum corresponds to $\equiv CCH_{3(a)} + {}^1/_2H_2(g)$; at zero coverage the species present are $\equiv CCH_{3(a)} + H_{(a)}$; and the maximum at a coverage of 0.35 ML corresponds to $=(CH)$-CH_3. (Adapted from ref 35.)

the surface. By comparison with other authors,[156−159] it is suggested that the first species formed on the Pt{110} surface is ethylylidyne ($\equiv C-CH_2-$), which bonds to the surface in the troughs of the (1×2) missing-row reconstruction. The next species to be formed on the surface is ethylidyne ($\equiv C-CH_3$), probably on the {111} microfacets of the Pt{110} reconstructed surface.[34] Above 0.5 ML coverage, di-σ-bonded ethylene and then π-bonded ethylene are found on the surface. The coverage regimes where these species are present are indicated in Figure 26. The heats of reaction for the different species on the surface can be used to obtain average values for the C−Pt bond energies, and these are given in Table 6.

An example of how these values are calculated using the abe method is illustrated for ethylidyne. The C−Pt_s bond formation reaction is

$$3Pt_s + {}^{\bullet}C-CH_3(g) \rightarrow Pt_{3s}\equiv C-CH_3 \qquad \Delta H_0$$

and the enthalpy for this reaction can be obtained from the reaction heats of the following processes:

$$4Pt_s + H_2C{=}CH_2(g) \rightarrow Pt_{3s}\equiv C-CH_{3(a)} + Pt-H \qquad \Delta H_1 = -197 \text{ kJ mol}^{-1}$$

$$Pt_s-H \rightarrow Pt_s + H(g) \qquad \Delta H_2 = 250 \text{ kJ mol}^{-1}$$

$$H(g) + {}^{\bullet}C{=}CH_3(g) \rightarrow H_2C{=}CH_2(g) \qquad \Delta H_3 = -769 \text{ kJ mol}^{-1}$$

ΔH_1 was measured in the adsorption experiment, ΔH_2 is the heat of adsorption of H_2 on Pt{110}, and ΔH_3 was calculated from the average bond energies of the C=C, C−C, and C−H bonds as given above. Combining these gives $\Delta H_0 = -716$ kJ mol^{-1}, and hence, the C−Pt_s single-bond energy for ethylidyne on Pt{110} is estimated as 239 kJ mol^{-1}.

As seen in Table 6, there is good agreement in the C−Pt bond energies calculated for the different adsorption species and, as expected, there is a variation in the bond energy depending on the nature of the species. There is also a variation in the bond energy depending on how many bonds are formed to the Pt surface, with the bond energy decreasing with an increase in the number of bonds formed to the surface, as expected.

b. C_2H_4/Pt{111}

The adsorption of ethylene has also been investigated on the Pt{111} surface.[35] This investigation was very useful in helping to determine the decomposition pathway of C_2H_4 to ethylidyne ($\equiv C-CH_3$), which is the most stable adsorbed species seen at room temperature on Pt{111}.[35] The heat of adsorption versus coverage for C_2H_4 on Pt{111} is shown in Figure 27. The initial heat is 195 ± 4 kJ mol^{-1}, and there is a marked minimum in this curve before the steady-state heat of 80 ± 4 kJ mol^{-1} is reached. The sticking probability shows precursor-mediated behavior[35] with an initial sticking probability of 0.67. The sticking probability at coverages less than 0.2 ML can be fitted by the King and Wells expression.[160]

The remarkable observation of a minimum in the heat of adsorption curve at a coverage of 0.17 ML needs some explanation. The initial heat of adsorption on the Pt{111} surface can be attributed to the formation of ethylidyne. The sharp decrease in the adsorption heat to a minimum of 140 kJ mol^{-1} can be described by a mechanism where at low coverage adsorbed ethylene rapidly converts to the intermediate $=CHCH_3$, ethylidene, which is in equilibrium with ethylidyne and H on the surface. At low coverages, there is no net loss of H by recombination to $H_2(g)$ and, hence, the measured heat of adsorption is that for the reactions

$$C_2H_4(g) + 2^* \rightarrow =CHCH_{3(a)} \qquad \text{(Ia)}$$

$$=CHCH_{3(a)} + 2^* \rightarrow \equiv CCH_{3(a)} + H_a \qquad \text{(Ib)}$$

where an asterisk (*) is an empty site. This reaction sequence is energetically favored because the isomerization of adsorbed ethylene to ethylidene is exothermic (reaction Ia). At 0.17 ML, each C_2H_4 loses a H atom which combines with a preadsorbed H to give

H_2 during the time scale of the molecular beam pulse, i.e., the reaction

$$C_2H_4(g) + 3^* + H_{(a)} \rightarrow \equiv CCH_{3(a)} + H_2(g) \quad (II)$$

begins to occur and the heat at the minimum corresponds to this process. The desorption of H_2 is endothermic, so that the overall heat release in II is less than that in Ia and Ib: the measured heat decreases with coverage. Once all of the preadsorbed H has been used up, then the formation of ethylidyne (reaction Ib) occurs as this equilibrium is shifted to the right. As the ethylidyne islands grow, the availability of 3-fold sites decreases and only bridge sites (favorable for $=CHCH_3$ formation) are vacant. Hence, direct ethylidyne formation stops, and the only way it can form is via step Ia. Since no H_2 is lost from the surface, the measured heat rises. There is spectroscopic evidence for ethylidene formation on Pt{111},[161] and hence, this is a sensible candidate for an intermediate.

From the initial heats of reaction of ethylidyne and ethylidene on Pt{111}, the average C−Pt bond dissociation energies have been calculated in the same way as for Pt{110}. For ΔH_I equal to −195 kJ mol^{-1}, the M−C bond energy is calculated to be 238 kJ mol^{-1} (assuming ethylidyne formation only), and for ΔH_{II} equal to −142 kJ mol^{-1} at 0.17 ML coverage where reaction II occurs, the M−C bond energy is calculated as 250 kJ mol^{-1} (assuming ethylidene formation only). Since these two species are in equilibrium on the surface, the actual value lies somewhere between these two values. However, it is hard to distinguish these, fitting well with the assumption that they are in equilibrium. These values also compare very well with the average value of 242 kJ mol^{-1} obtained from the adsorption of C_2H_4/Pt{110}: within these error margins, the C−Pt bond energy is the same despite the difference in coordination of Pt surface atoms on the two surfaces.

c. C_2H_4/Pt{100}

The adsorption of ethylene has also been investigated on Pt{100},[33] which undergoes a reconstruction from the hex phase to a (1×1) phase on adsorption. The heat of adsorption and sticking probability as a function of coverage for adsorption on the initial hex phase is shown in Figure 28. The heat falls from an initial value of 213 ± 8 kJ mol^{-1} to reach a steady-state value of 130 ± 4 kJ mol^{-1}. Different species formed during the adsorption are marked on the figure. The initial sticking probability is 0.79. The heat of adsorption and sticking probability on the (1×1) surface are shown in Figure 29. This time the initial heat is 305 ± 14 kJ mol^{-1} and a drop occurs until the steady-state heat is the same as that on the hex phase, as would be expected if C_2H_4 lifts the hex reconstruction. The sticking probability on the (1×1) phase was initially 0.69. However, the sticking for the hex and (1×1) phases is not identical at high coverages, suggesting that the hex reconstruction is not totally lifted by C_2H_4. The energy difference between the (1×1) and hex phases of the clean surface can be calculated from the integral heats as

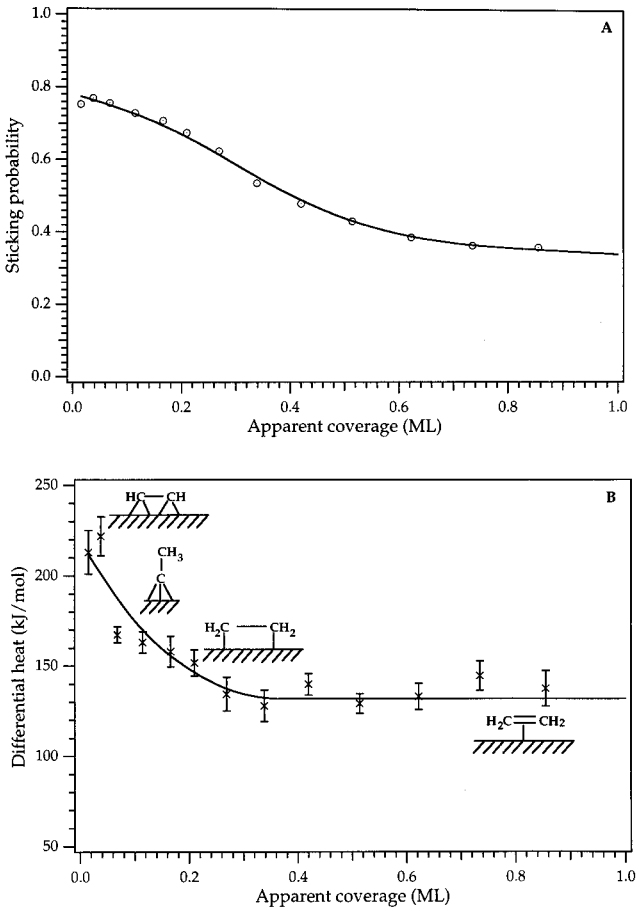

Figure 28. Sticking probability (A) and heat of adsorption (B) as a function of coverage for the adsorption of C_2H_4 on Pt{100}−hex at 300 K. (Adapted from ref 33.)

for CO and is found to be 13 ± 3 kJ (mol of Pt$_s$)$^{-1}$. This is slightly larger than that measured by CO adsorption, but this is not surprising if the same final state is not reached in both cases, as occurs for CO.

At low coverage on the Pt{100}−hex surface, acetylene is formed and is adsorbed in the form of quad-σ acetylene.[33] At coverages above 0.05 ML, the heat of reaction is similar to that expected for ethylidyne formation on Pt{111}[35] and Pt{110}[34] and, hence, it is assumed that this species is formed between 0.06 and 0.18 ML coverage on the Pt{100}−hex surface. At higher coverage still, it is assumed that di-σ ethylene is formed, at similar heats to those on Pt{110},[34] followed by π-bonded ethylene. These different species are shown on the heat of adsorption curve seen in Figure 28. For adsorption on the (1×1) phase, it is assumed that di-σ ethylene is again formed at high coverage. Ethylidyne cannot be formed on this surface due to the absence of 3-fold sites. The initial adsorption heat is again assumed to be due to the formation of acetylene on the surface.

As before, Pt−C bond dissociation energies can be calculated for the different species seen on the hex and (1×1) phases, and the results of this calculation are shown in Table 6. The calculated bond dissociation energy decreases systematically as the number of bonds per molecule increase, as expected. Again, good agreement exists with other Pt data (Table 6), and it is interesting to note that many similar species

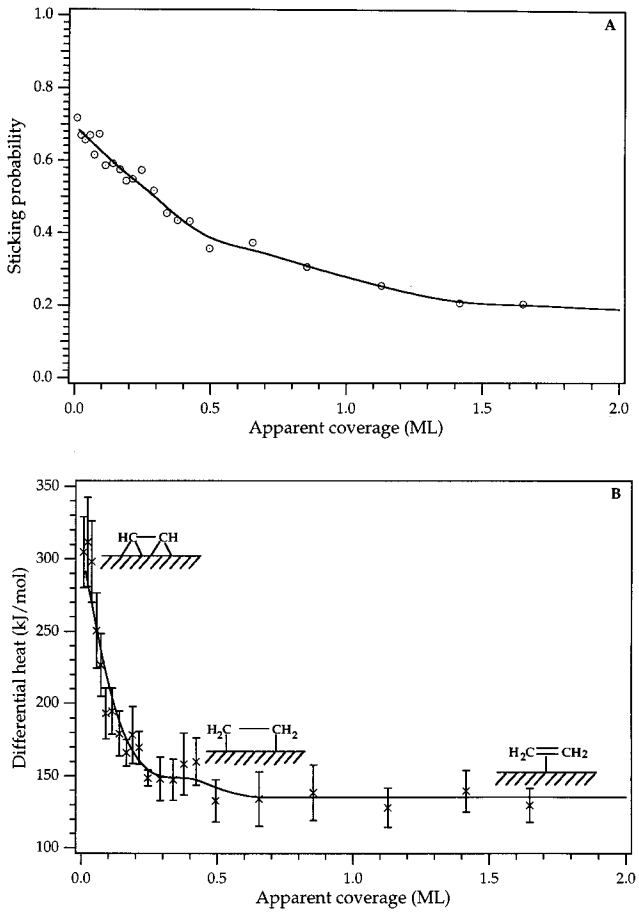

Figure 29. Sticking probability (A) and heat of adsorption (B) as a function of coverage for the adsorption of C_2H_4 on Pt{100}−(1×1) at 300 K. (Adapted from ref 33.)

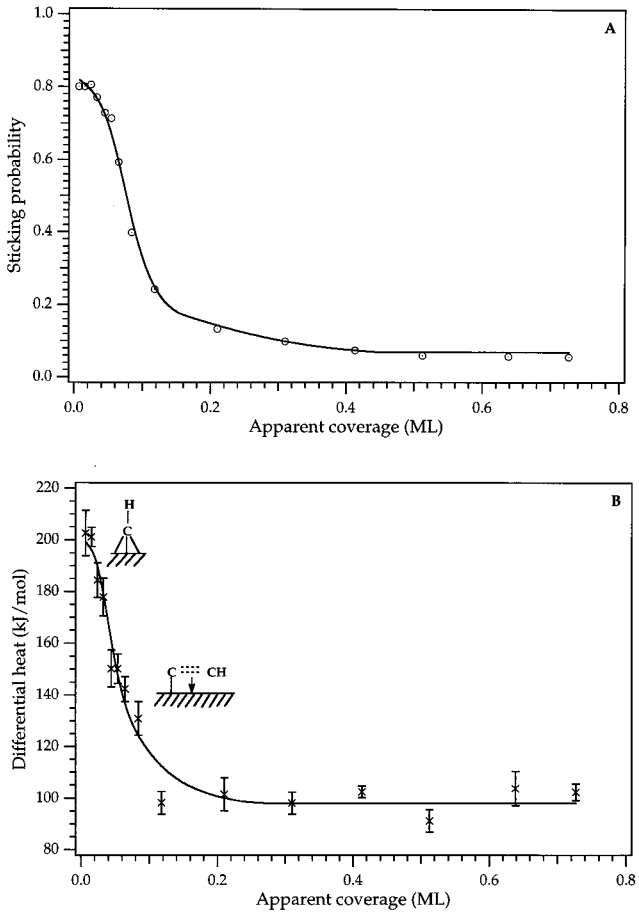

Figure 30. Sticking probability (A) and heat of adsorption (B) as a function of coverage for the adsorption of C_2H_4 on Ni{100} at 300 K. (Adapted from ref 31.)

are formed on the three different Pt surfaces despite the different surface structures.

d. C_2H_4/Ni{100}

An investigation of the adsorption of C_2H_4 on the Ni and Pd{100} surfaces has also been undertaken.[31] These provide a good comparison with hydrocarbon adsorption on Pt since different species are formed. Again, an attempt was made to identify the species present on the surface, and a calculation of the M−C bond energies was made (see Table 6). The heat of adsorption and sticking probability of C_2H_4 on Ni{100} as a function of coverage are shown in Figure 30. The initial heat is 203 ± 9 kJ mol^{-1}, and this decreases rapidly to a steady-state value of ∼100 kJ mol^{-1}. The sticking probability for this system exhibits typical precursor-mediated behavior[31] with an initial sticking probability of 0.81.

In the past, various authors have reported that C_2H_4 splits into either CH or CCH species upon adsorption on Ni{100} at room temperature.[162−166] Zaera and Hall[162] reported the presence of methylidyne (≡CH) on the surface, and it is this species which is assumed to give rise to the initial heat of adsorption on the Ni{100} surface. With increasing coverage, it is assumed that acetylide (CCH) is formed on the surface. With these assumptions, it is possible to calculate the Ni−C bond strength in exactly the same way described earlier for Pt surfaces, using the values given previously. If ≡CH is formed, then the Ni−C bond strength is estimated to be 205 kJ mol^{-1}. If CCH is formed, seen at about 0.07 ML coverage with HREELS,[162] then it is also possible to calculate the Ni−C bond energy for this species. This is not straightforward, however, as it has been suggested that the species bonds to the surface via its π electrons which interact strongly with the d electrons of the metal atoms, and hence, only an estimate can be made of the π-interaction energy. Depending on whether the CCH species contains C≡C or a C=C bond, then the π-interaction energy[31] is somewhere in the region of 74−189 kJ mol^{-1}. This is very low compared with a Ni−C σ interaction, but it must be noted that more work is required to unambiguously identify all of the species present on the Ni{100} surface upon adsorption of C_2H_4.

e. C_2H_4/Pd{100}

The adsorption of C_2H_4 on Pd{100} was very hard to measure as, at room temperature, only reversible (steady-state) adsorption occurred. The sticking and heat of adsorption for this system were 0.75 and 73 kJ mol^{-1}, respectively, and hence, it was not possible to extract a value for the Pd−C bond energy from these data. This is a system which would benefit greatly from experiments at lower temperatures

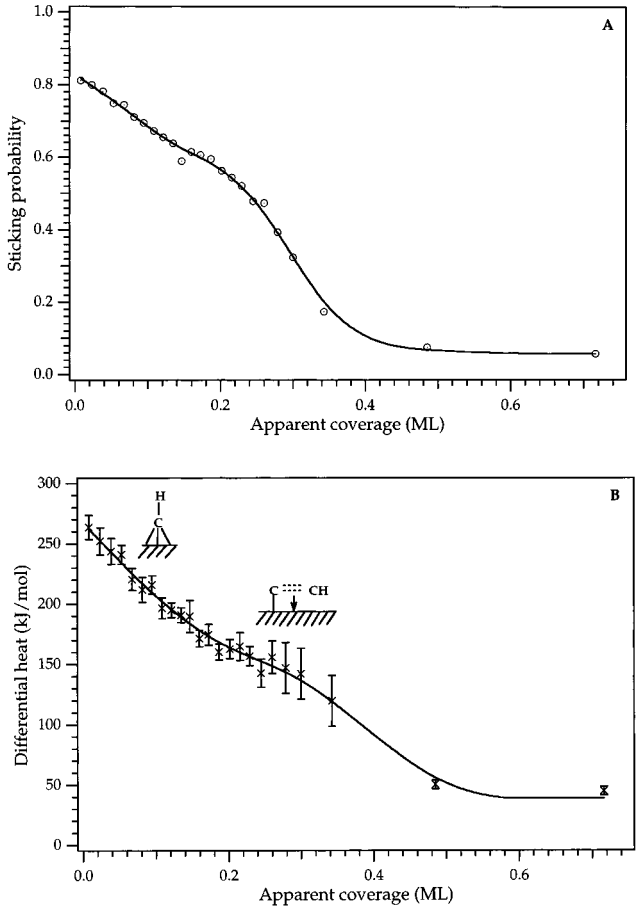

Figure 31. Sticking probability (A) and heat of adsorption (B) as a function of coverage for the adsorption of C_2H_2 on Ni{100} at 300 K. (Adapted from ref 31.)

where the reactive intermediates could be isolated on the surface.

f. C_2H_2/Ni{100}

The only other hydrocarbon which has been investigated calorimetrically is acetylene, C_2H_2, on Ni{100} and Pd{100}.[31] The heat of adsorption versus coverage for C_2H_2 on Ni{100} is shown in Figure 31. The initial heat of adsorption is 264 ± 10 kJ mol^{-1}, and this decreases linearly to ~0.2 ML where the heat is ~160 kJ mol^{-1}. At this point, a change in slope occurs and the heat then falls to a steady-state value of ~50 kJ mol^{-1}. The initial sticking probability on this surface is 0.81, with a steady-state value of 0.08. A change in the slope of the sticking curve is observed at the same time as a change is seen in the heat curve. For this system, it has been proposed again that CH and CCH species are observed on the surface upon adsorption of C_2H_2, as was the case for C_2H_4.[162,164] Again, as for C_2H_4 adsorption, the exact coverage dependence of the heat is hard to explain due to the uncertainty of the exact nature of the species observed. If the initial heat is associated with the formation of a CH species, then the average Ni−C bond energy can be estimated in the same way as for C_2H_4 to be 204 kJ mol^{-1}. At higher coverage where the change in the slope of the heat and sticking curve occurs, it is assumed that CCH species are formed on the surface and a π-interaction energy (analogous to that for C_2H_4 adsorption) can be calculated, which is found to be between 51 and 165 kJ mol^{-1}. These values are in excellent agreement with those calculated for C_2H_4 adsorption on this surface.

Table 7. Average M−C Bond Energy for Each Surface Derived from the Average of the Calculated Energies Given in Table 6

surface	average M−C single bond energy (kJ mol^{-1})
Pt{110}	242
Pt{111}	244
Pt{100}	240
Pd{100}	171
Ni{100}	205

[a]Note the excellent agreement between the M−C bond energies calculated for the three singular Pt surfaces.

g. C_2H_2/Pd{100}

For the adsorption of C_2H_2 on Pd{100}, the initial heat is 112 kJ mol^{-1}, it decreases slowly to 96 kJ mol^{-1} at 0.32 ML, and then decreases sharply to a steady-state value of 40 kJ mol^{-1}. The sticking probability again shows precursor-mediated behavior with an initial sticking probability of 0.83.[31] It can be fitted by the Kisliuk expression, and this was again used to convert the coverage scale into an absolute scale. Other authors have reported that acetylene does not decompose upon adsorption on Pd{100}, and hence, it is assumed that the C_2H_2 is bonded to the surface as di-σ acetylene. The Pd−C bond strength can, therefore, be extracted to be 171 kJ mol^{-1}.

It is suggested that a π-bonded acetylene species reversibly adsorbs in the steady-state regime with an adsorption heat of only 60 kJ mol^{-1}. For this adsorption system, as for most hydrocarbon systems, a definitive study of the species formed during surface decomposition reactions would aid the interpretation of the heat of adsorption as a function of coverage.

Several important points arise from these hydrocarbon measurements. First, the exact nature of the hydrocarbon species formed on the surface during the calorimetric measurements, in the time scale (~50 ms) of the experiment, is often difficult to ascertain, making it difficult to determine M−C bond strengths with confidence. However, good agreement is achieved when M−C bond energies are calculated for different species on the same metal surface; indeed, the heat measurement is itself an indicator of the nature of the adsorbed species formed. Table 7 shows the average M−C bond energy for each surface derived from the average of the calculated energies for each species on the surface.

There is good agreement between the values for the three Pt surfaces, and Table 6 also shows good agreement for M−C bond energies calculated for C_2H_4 and C_2H_2 adsorption on Ni{100} despite the difference in the initial adsorbate. It is, therefore, a valid calculation. Note also that similar species, e.g., ethylidyne, all appear at similar adsorption heat values on the different Pt surfaces: 203 kJ mol^{-1} for Pt{110}, 195 kJ mol^{-1} for Pt{111}, and 170 kJ mol^{-1}

for Pt{100} hex. The same is true of the di-σ ethylene species seen on these surfaces.

It is obvious that the interaction of ethylene and acetylene is stronger on Pt surfaces than on Pd or Ni surfaces. While the database for hydrocarbon adsorption energies is still very small, it shows that there are trends, with similar M−C bond energies being seen on the same metal surface despite the formation of different species. It also shows that similar species often have similar heats even though they are adsorbed onto different surface planes. Experiments to extend the database are continuing, and it is hoped that this will enhance our understanding of hydrocarbon adsorption on surfaces.

F. Reactions with Gas-Phase Products: The CO Oxidation Reaction

The SCAC can also be used to study surface reactions, which have gas-phase products, to determine the heat of reaction. Since a surface reaction is a non-reversible process, no previous measurements of reaction heats have been made. The reaction that has been studied with the calorimeter is the CO oxidation reaction where the product is gas-phase CO_2. These were the first measurements of the heat for a surface reaction, which was investigated on Pt{110}[38] and Pt{111}.[22]

a. CO Oxidation on Pt{110}

The measured heat deposited into the surface for the reaction on Pt{110} was compared with that expected for the reaction, and the excess energy removed by the product CO_2 gas-phase species was determined. The reaction was studied in two ways: by first dosing O_2 and then dosing CO and vice versa. Figure 32a shows the heat measured for the addition of CO to a Pt{110} surface already saturated with O_2. The heat measured is the heat deposited into the Pt{110} sample per mole of CO that reacts or adsorbs during the beam pulse. The heat of adsorption for O_2/Pt{110} is known, as are the gas-phase heats of formation of CO_2 and CO, and hence, the expected heat of reaction can be calculated.

The initial heat measured when CO is dosed onto an O-precovered surface is 177 ± 4 kJ mol^{-1}. The reaction is

$$CO(g) + O_{(Pt)} \rightarrow CO_2(g)$$

Hence, the heat of reaction, ΔH_r, is given by

$$\Delta H_r = \Delta H_f(CO_2(g)) - \Delta H_f(CO(g)) - \Delta H_f(O_{(Pt)})$$

$$= (-393.5) - (-110.5) - (-112)$$

The expected heat for the initial reaction is, therefore, 171 ± 16 kJ mol^{-1}, which would be measured if the CO_2 product did not remove any excess energy when leaving the surface. Hence, the CO_2 molecules leave with an average of 6 ± 17 kJ mol^{-1} of excess energy. The heat of formation of O_{ad} is obtained from an average of the oxygen adsorption heat between 0.35 and 0.5 ML, the range over which saturation of the surface occurs.[38]

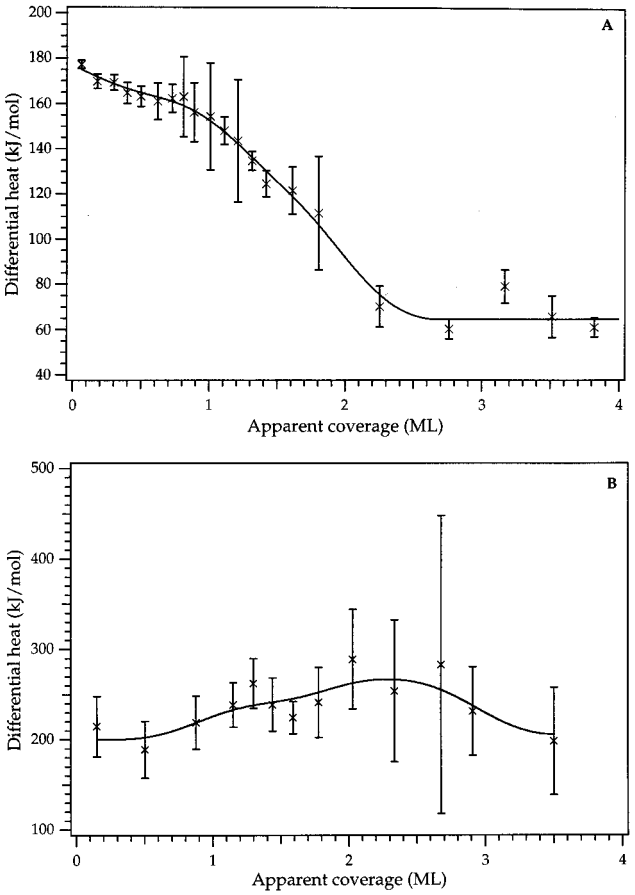

Figure 32. Reaction heat for the CO oxidation reaction on Pt{110}. The experiment was performed in two ways: (A) by dosing CO onto an O-saturated surface, and (B) by dosing O_2 onto a CO-saturated surface. (Adapted from ref 38.)

The result is different if the reaction is performed with preadsorbed CO, O_2 being beamed at the surface. The initial reaction heat was measured to be 190 ± 35 kJ mol^{-1} (Figure 32b). Again, the reaction heat expected if the product CO_2 is at the surface temperature can be calculated for the reaction:

$$O_2(g) + 2CO_{(Pt)} \rightarrow 2CO_2(g)$$

Here

$$\Delta H_r = 2\Delta H_f(CO_2(g)) - 2\Delta H_f(CO_{(Pt)}) - \Delta H_f(O_2(g))$$

$$= (2 \times -393.5) - (2 \times -250) - (0)$$

which yields, ΔH_r = 287 ± 24 kJ mol^{-1}. This is considerably larger than the measured heat, and it is concluded that the product CO_2 molecules carry away 49 ± 21 kJ mol^{-1} for each CO_2 molecule produced.

It is postulated that the excitation of gas-phase CO_2 only in the case of preadsorbed CO is due to the formation of "hot" O adatoms during the exothermic dissociation of O_2,[38] the existence of which has been previously postulated.[167−169] In the case where O_2 was predosed onto the surface, the O adatoms are thermally equilibrated with the surface and the product CO_2 is not excited. When CO is predosed

onto the surface, the hot O adatoms produced during the dissociation of O_2 react with CO molecules before they have time to lose their excess translational energy and, hence, highly excited gas-phase CO_2 is produced.

b. CO Oxidation on Pt{111}

The same reaction was investigated on Pt{111} by Yeo and co-workers.[22] The adsorption heats and sticking probabilities for the individual CO and O_2 molecules were also investigated and have been reported earlier in this article. The reaction was first investigated by beaming CO onto an O predosed surface and then vice versa.

For the addition of CO to a surface predosed with O adatoms, the initial heat of reaction is measured as 173 ± 2 kJ mol^{-1}. The reaction that occurs is similar to that on Pt{110} and ΔH_r is, therefore, given by:

$$\Delta H_r = \Delta H_f(CO_{2(g)}) - \Delta H_f(CO_{(g)}) - \Delta H_f(O_{(Pt)})$$

$$= (-393.5) - (-110.5) - (-98)$$

The heat of formation for O_{Pt} is again calculated to be the average for the adsorption range over which saturation is occurring. The calculated reaction heat is therefore 185 ± 8 kJ mol^{-1}, and hence, the CO_2 must again (as for Pt{110}) leave the surface with a small excess energy of 12 ± 8 kJ mol^{-1}.

Unfortunately, it was not possible to measure the reaction heat when O_2 was dosed onto an overlayer of preadsorbed CO as the sticking probability is negligibly small. Other authors[170,171] have indicated that CO_2 produced in this manner does not leave the surface with excess energy.

G. Coadsorption Systems

The coadsorption of alkali metals is very important in many catalytic reactions as they often act as promoters for the particular reaction in question. The mechanism by which this happens is often unclear, and therefore, it is essential to have a good understanding of the energetics of a particular surface process. This can be gained by using calorimetry to measure the heat of adsorption on a surface. The particular coadsorption systems that have been investigated calorimetrically are the coadsorption of K and CO and K and O_2 on the three singular faces of Ni. The former is an important model system for understanding the Fischer−Tropsch process, which often occurs on Ni, and is promoted by the presence of K on the surface. The presence of K has also been observed to increase the rate of surface oxidation on Ni. K is used as a promoter in many catalytic reactions, including ammonia synthesis, and it is important to measure the changes in bond energies involved.

a. K and CO Coadsorption

The preadsorption of K onto a Ni{100} surface has a marked effect on the heat of adsorption and the sticking probability for CO on this surface.[16,18,26,39,40] For alkali-metal adsorption on transition metals, the work function is observed to fall rapidly with increasing alkali-metal coverage (due to charge transfer to the metal) until a minimum is reached, at which point the work function increases until it reaches the value for the clean alkali itself. Hence, a low K precoverage corresponds to coverages of K below the work function minimum, and a high K precoverage corresponds to K coverages above the work function minimum. Figure 33a shows the interaction of CO with Ni{100} at low K precoverages. For a K precoverage of 0.035 ML, the initial heat of adsorption is increased dramatically from 124 kJ mol^{-1} for the clean surface to 210 kJ mol^{-1} and then falls to 130 kJ mol^{-1} with increasing CO coverage. At θ_K = 0.08 ML, the initial heat is also higher than the clean surface value and remains constant for 0.05 ML before falling to the clean surface value. Figure 33b shows the adsorption behavior for higher K precoverages (θ_K = 0.3 and 0.33 ML). Here, the initial heat is considerably higher at 250 kJ mol^{-1} and increases with CO coverage to a maximum of 310 kJ mol^{-1} before leveling off. The sticking probability, at low K precoverages, shows very similar behavior to that on the clean surface, with precursor-mediated adsorption being observed. As the precoverage of K increases beyond the work function minimum, the initial sticking probability falls very rapidly. At high K precoverages the sticking probability increases with increasing CO coverage from very low initial values.

Previous studies on K and CO adsorption on Ni{100}[172] have shown that the CO desorption temperature increases from a clean surface value of 450 K up to 680 K with preadsorption of K, which corre-

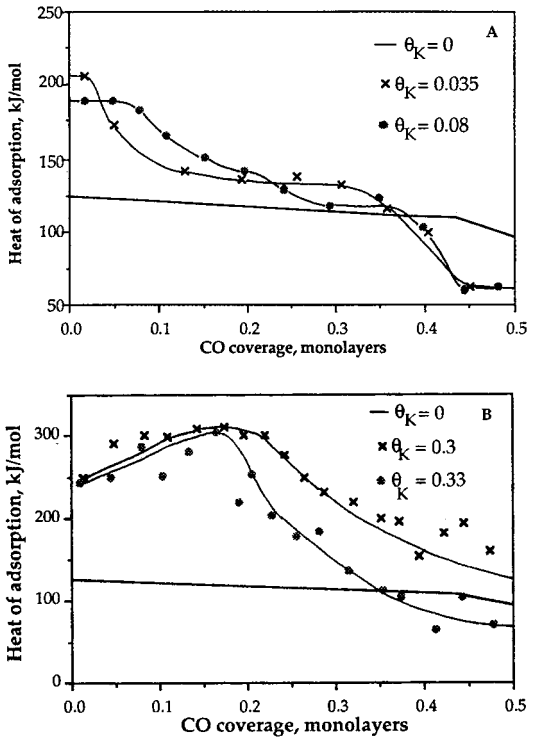

Figure 33. (A) Interaction of CO with Ni{100} at 300 K at low potassium precoverages. (B) Interaction of CO on the same surface at high potassium precoverages. (Reprinted with permission from ref 40. Copyright 1993 University of Cambridge.)

sponds to a 60 kJ mol^{-1} increase in the adsorption heat. This is in good agreement with observations at low K precoverages, but it is lower than values seen at high K coverages where the heat of adsorption increases by 195 kJ mol^{-1}. Differences in the heat of adsorption data can be correlated with the charge state of the K. At low θ_K, charge transfer to the Ni occurs to leave ionic K on the surface. This resembles a point charge. CO adsorbed near a point charge has its orbital energies electrostatically downshifted, thus taking the center of the $2\pi^*$ level in CO below the Fermi level and increasing its occupancy. This raises the CO adsorption heat due to an increase in the strength of the Ni−CO bond, but the C−O bond is weakened. The coverage dependence of the heat at low θ_K suggests that the interaction between the CO and the K is short range, and hence, the heat at high CO coverage for low θ_K corresponds to CO adsorbed on sites far away from K atoms.

At higher θ_K, a very large increase in the CO adsorption heat is observed. We might expect that this is due to dissociation, but spectroscopic evidence shows that this is not the case.[173] At high θ_K, the K bonding in the pure K adlayer becomes covalent, with a subsequently large decrease in the K adsorption energy. Adsorption of CO onto this covalent K adlayer screens K adatoms from each other and allows reionization, therefore increasing the K−substrate bond energy. The delayed maximum in the heat with coverage suggests a long-range electrostatic contribution as a charged CO lattice is formed. This lattice of $K^{\delta+}CO^{\delta-}$ will have a Madelung energy associated with it. Only as islands coalesce is the full Madelung energy realized, resulting in the observed increase in adsorption heat for high θ_K with increasing CO coverage. There are, therefore, several reasons for the observed increase in heat of adsorption at high K precoverages. The first is an increasing CO $2\pi^*$ occupation, and the second is ionization of K adatoms which leads to large islands of salt. This is shown in Figure 34. Good agreement between this study and the theory of Christensen and Nørskov[174] has been found, which supports this explanation of an increase in the heat of adsorption upon increasing K predose.

The coadsorption of CO and K on Ni{111} has also been investigated using SCAC.[26,40] The results are quite different to those seen on Ni{100}, especially at high θ_K. At low θ_K (0.039 ML), the initial heat of adsorption increases from the clean surface value of 130 to ~190 kJ mol^{-1}. Again, the CO adsorption heat levels off to the clean surface value with increasing coverage. For $\theta_K = 0.14$ ML, the CO heat no longer levels off but continues to fall up to the saturation coverage of CO of 0.5 ML. At higher K precoverages of 0.25 and 0.33 ML, the initial heat increases as for Ni{100}. It is raised to 210 and 255 kJ mol^{-1}, respectively, however, there is no evidence of an immediate increase after the initial adsorption heat value. Instead, the heat falls and then rises to a small peak. For the highest K precoverages, this effect is less pronounced. Unlike Ni{100}, the CO adsorption heat at high θ_K does not approach a particular value on Ni{111}. The initial sticking probability for CO/Ni{111} falls more rapidly with increasing θ_K than that for Ni{100}. Small increases with increasing CO coverage at high θ_K are seen, but they are not as large as those seen for Ni{100}.

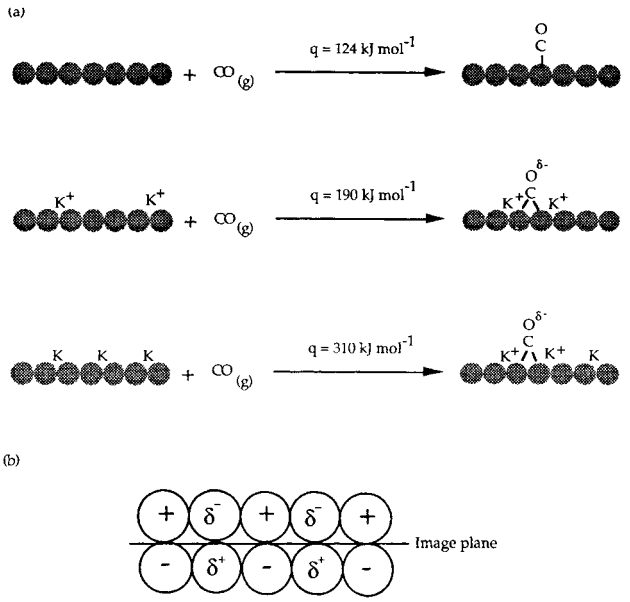

Figure 34. (a) Schematic diagram of the CO interaction as the precoverage of potassium is increased on Ni{100} and of the related heats of adsorption, q. (b) The image charge ionic bilayer lattice formed at high K precoverages. (Reprinted with permission from ref 39. Copyright 1992 Nature.)

A vibrational study of the CO/K/Ni{111} system[175,176] has shown that at high θ_K a very low stretching frequency peak is observed at 1435 cm^{-1}. With increasing CO coverage, a second peak at 1520 cm^{-1} appears which then shifts toward the zero K precoverage frequency as more CO is adsorbed while the 1435 cm^{-1} peak disappears. This was attributed to a charged CO species and is in agreement with the heat of adsorption data. At very high θ_K and low coverages of CO, a very high heat of adsorption is observed and it drops very rapidly as a function of CO coverage. There is no evidence on this surface for the build up of salt islands at high θ_K. The heat of adsorption data actually suggests that repolarization occurs only at very low CO coverages. However, this is not the whole story as there is still evidence at high θ_K that the surface saturates at very high CO coverages. It therefore seems likely that repolarization does occur in the presence of CO but that the build up of 2D islands does not occur, in contrast to the results for the {100} plane. The differences in the adsorption observed for Ni{111} and Ni{100} are probably related to the different site occupancy on the two surfaces.

The coadsorption of CO with K has also been investigated on Ni{110}.[26,41] For this surface, two distinct regimes are observed which correspond to the K-induced surface reconstruction. For $\theta_K < 0.35$ ML, the Ni{110} surface undergoes a missing-row reconstruction, and above this coverage, the reconstruction is lifted. Due to this reconstruction, the desorption energy of Na showed very different behavior on Ni{110} to that observed on the other low-index planes of Ni.[177]

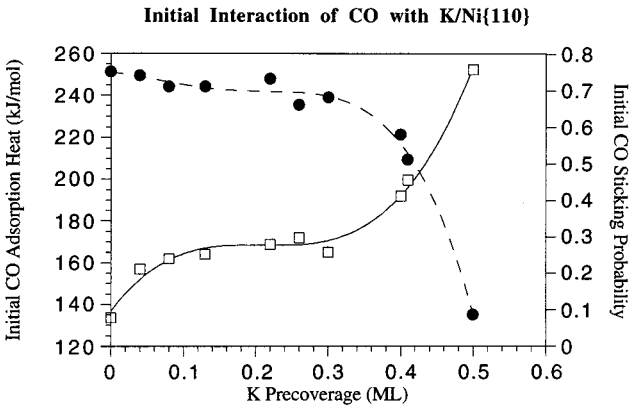

Figure 35. Initial adsorption heat and sticking probability for CO on Ni{110} as a function of potassium precoverage. The squares represent the initial heat of adsorption, and the circles represent the initial sticking probability. (Reprinted with permission from ref 41. Copyright 1994 World Scientific Publishing.)

Figure 35 shows that the initial heat of adsorption of CO increases progressively from 132 kJ mol^{-1} on the K-free surface to 160 and then to 250 kJ mol^{-1}. For very low K coverages, any promotion effect is seen only for the first 0.05 ML of CO adsorption. However, with larger K predoses, but still below θ_K = 0.4 ML where the reconstruction is lifted, the CO adsorption heat remains higher than the clean surface value up to a CO coverage of 0.25 ML. Generally, the CO adsorption heat remains high up to some CO coverage which increases with K precoverage. At θ_K = 0.4 ML, the initial sticking probability for CO decreases only slightly with increasing K coverage. However, the sticking probability falls more rapidly with CO coverage to a steady-state value, indicating a reduction in the CO saturation coverage as the K precoverage increases.

For K precoverages above the threshold for lifting the reconstruction, a dramatic change occurs in both the kinetics and the energetics of the CO adsorption process as seen in Figure 35. The CO adsorption heat increases further to 250 kJ mol^{-1}, and the sticking falls drastically to just 0.1.

The kinetics and energetics of CO on a K-promoted Ni{110} surface are strongly influenced by the K-induced missing-row reconstruction of the substrate; this highly corrugated surface gives very different behavior to that on the flatter {100} and {111} surfaces. On the reconstructed surface, CO sticking stays high, as there are many substrate atoms still exposed along the ridges, and the heat of adsorption is increased from 132 kJ mol^{-1} on the clean surface to 170 kJ mol^{-1}. This increase is small compared with that seen on the {100} surface. The corrugated nature of the {110} surface appears to prevent the formation of the salt islands seen on Ni{100}, but this difference can also be attributed to the fact that K binds more strongly to the Ni{110} and, therefore, gains less binding energy when CO is adsorbed. Above 0.35 ML of K, the missing-row reconstruction is lifted and at this point the kinetics and energetics of the CO uptake changes markedly. Once the reconstruction has lifted, the CO heat of adsorption rises to 250 kJ mol^{-1} and the sticking probability drops by a large amount. The decrease in sticking probability implies that less exposed Ni is seen by the impinging CO. The increased heat of adsorption is due to two effects: the strengthening of the Ni−K binding due to K−K screening by CO, and the formation of 2D islands of the $K^{\delta+}CO^{\delta-}$ salt on the flatter surface, in the same way as on Ni{100}.

b. K and O_2 Coadsorption

The coadsorption of O_2 and K has also been investigated on the same three Ni surfaces. It is well-known that alkali-metal adsorption often reduces the exposure of O_2 required to oxidize a transition metal, making this an interesting system to study. The heat of adsorption and sticking probability have been investigated for O_2 and K on Ni{100}.[16,26,28,40] Preadsorption of K has a large effect on the kinetics of O_2 uptake, and the coverage dependence of the sticking probability is influenced as the adsorbed alkali metal becomes more covalent. For low θ_K (<0.15 ML), the sticking probability is very similar to that on the unalkylated surface. However, above this coverage of K, two distinct plateaus in the sticking are observed as a function of O_2 coverage. In addition, the total oxygen exposure required to form a passivated oxide film is reduced with increasing θ_K. In general, the initial sticking probability rises with increasing θ_K and approaches a saturation value.

There are also changes observed in the oxygen adsorption heat with increasing θ_K. The initial differential heat is ~70 kJ mol^{-1} higher for θ_K = 0.15 ML than for the clean Ni{100} surface. With increasing θ_K, the initial heat starts to fall back toward that of the clean surface. For O_2 on Ni surfaces, minima in both the heat and the sticking are seen before the onset of oxide film formation begins (see section VI.C). Increasing the predose of K increases the value of the heat at this minimum in the sticking curve, from 80 kJ mol^{-1} on the clean surface to 170 kJ mol^{-1} at θ_K = 0.019 to 240 kJ mol^{-1} at θ_K = 0.11. For very high precoverages of K, there is no minimum in the heat curves.

To fully understand the effect of preadsorption of K on the O_2 adsorption heat and sticking probability on Ni{100}, it is essential to determine whether the primary O interaction is with the Ni substrate or with K. Using the influential factors which determine the mechanism of O_2 adsorption given by Kiskinova,[178] it is possible to determine the principle interaction that occurs when O_2 is adsorbed in the presence of K on Ni{100}. TPD[177,179] has shown that the K−Ni{100} bond strength varies as a function of the charge state of the K. At low θ_K (ionic K species present on the surface), the maximum value for the K adsorption heat is 295 kJ mol^{-1}. As θ_K increases to saturation, a drop in the adsorption heat of ~100 kJ mol^{-1} is measured as depolarization of the K occurs. For O_2 on clean Ni{100}, the heat of adsorption is 550 kJ mol^{-1}, and therefore, it seems reasonable to assume that the major O interaction on K predosed Ni{100} will be with Ni whatever the state of the K. Integral heats of adsorption[39] support this: the oxide heats of formation are unaf-

fected by the presence of K. Hence, the preadsorption of K has very little influence on the thermodynamics of O uptake, but it has a large effect on the kinetics.

The dependence of the O_2 uptake kinetics on θ_K can be understood by examining the influence of preadsorbed K on adsorbed dioxygen. Investigations by Kiskinova et al.[180] have shown that increased charge density in the surface region due to K adsorption encourages charge transfer from the metal to the $1\pi^*$ level of O_2, which in turn increases the rate of dissociation of the O_2 molecular precursor. Above $\theta_K = 0.15$, a molecular state is stabilized by the presence of K on the surface, which acts as a precursor to the dissociated state and increases the rate of oxidation of the Ni substrate.

The coadsorption of O_2 and K on Ni{111} has also been investigated.[26,28,40] The general behavior of the sticking probability as a function of increasing K coverage for O_2/K/Ni{111} is similar to that seen on Ni{100}. Initial sticking increases as a function of θ_K and reaches a plateau at an initial sticking value of 0.83 at $\theta_K = 0.08$ ML. There is no evidence for the presence of a molecular precursor for low θ_K despite its presence on the clean Ni{111} surface. For higher θ_K (0.15 and 0.38 ML), the initial sticking probability remains high out to quite high O coverages and at these θ_K the sticking probability does not decrease until an oxygen coverage of ~0.33 is reached. Unlike the case for Ni{100}, there is no evidence for a coverage shift of the minimum in the sticking at low θ_K, and this implies that chemisorption is complete at an oxygen coverage of 0.33 ML regardless of the K predose.

The adsorption heat for O_2 at low θ_K is similar to that on the clean surface; but as θ_K increases beyond that of the work function minimum, the heat shows a large increase. A maximum change of 130 kJ mol^{-1} is evident as the binding of the K switches from ionic to covalent. Overall, the interaction of O on a K-predosed Ni{111} surface proceeds in a manner similar to that on Ni{100}. At low θ_K, both substrates show features similar to those seen for the clean surface. As the dipole moment of the alkali layer changes and θ_K increases above the work function minimum, then the kinetics can be explained as a precursor-mediated adsorption process. Again, the main bonding of the O adatom is to the Ni substrate rather than to the K; the main influence of K is to change the kinetics of the interaction.

Unlike the case for Ni{100}, the preadsorption of K on Ni{111} has little effect on the saturation coverage for chemisorption, in agreement with previous studies.[181] A second difference occurs at high θ_K. A large increase in the adsorption heat occurs as a function of increasing θ_K, and the magnitude of this increase is very similar to that for CO and K coadsorption. It therefore seems sensible that this observed increase arises from repolarization of the K adatoms and the growth of islands of K^+O^-. It seems odd that this does not occur on Ni{100}, but we note that the geometric location of K adatoms on the two surfaces is remarkably different. On Ni{111}, O lies in an on-top position,[182] whereas on Ni{100}, O is in a 4-fold hollow site and is not available for island formation.

Finally, the coadsorption of O_2 and K has been briefly investigated on Ni{110}.[28] An increase in the initial heat of O_2 adsorption with θ_K is observed, as was the case for the {111} and {100} surfaces. It is interesting to determine whether this observed increase corresponds to the complete transfer of two electrons to the O adatom, and for this purpose, the work function of Ni{110} was measured by Norton et al.[183] as a function of increasing O precoverage. The work function increases linearly as a function of coverage up to 0.1−0.2 ML, beyond which it is no longer linear. This is the coverage at which the heat of adsorption starts to drop, implying a reduction in charge donated to oxygen. If this indirect interaction between oxygen atoms is responsible for the fall in adsorption heat rather than a direct local interaction with K, then a high coverage structure for O/Ni{110} with no K would be possible. This is not found, and a local interaction is suggested.

Without K, the heat of adsorption falls very rapidly with increasing O coverage on the {110} surface. With coadsorbed K, the fall in adsorption energy with oxygen coverage was curtailed due to local K−O attractions which compensate for the O−O repulsions, analogous to the results found for K/CO on Ni{100} and Ni{110}.

H. Metal Adsorption Heats

The final category of adsorption to be considered here is the adsorption of metal atoms onto other metal surfaces. Measuring metal adsorption energies is important in many applications including catalysis, molecular beam epitaxy (MBE), chemical vapor deposition (CVD), film growth, etc. Previous measurements have been performed using TPD on metal and oxide surfaces,[184−191] but this is often not accurate as the metal may diffuse into the bulk or not desorb at an accessible temperature. Generally, the often irreversible nature of metal adsorption renders it inaccessible to study by isotherms and TPD. Calorimetric measurements are, hence, a better alternative, and the new instrument developed by Campbell and co-workers[42] opens up the technique to such measurements. It also allows adhesion energies for the metal film to be calculated.

The design of Campbell's instrument is similar to that of the Cambridge calorimeter; a schematic diagram of the system is shown in Figure 36. In an experiment, a pulse of metal-atom vapor from a chopped atomic beam source impinges onto a thin-film crystal (~1 μm thick), producing a temperature rise. This is detected using a pyroelectric detector consisting of a 9 μm thick film of β-polyvinylidene fluoride coated with NiAl for electrical contact and shaped into a ribbon which forms an arch sticking out of the detector housing. During an experiment, this ribbon is placed into mechanical (and therefore thermal) contact with the back of the substrate film. The detector can be removed from the sample to allow high-temperature sample preparation to take place, which is not possible with the Cambridge system. However, the use of this detector requires the use of

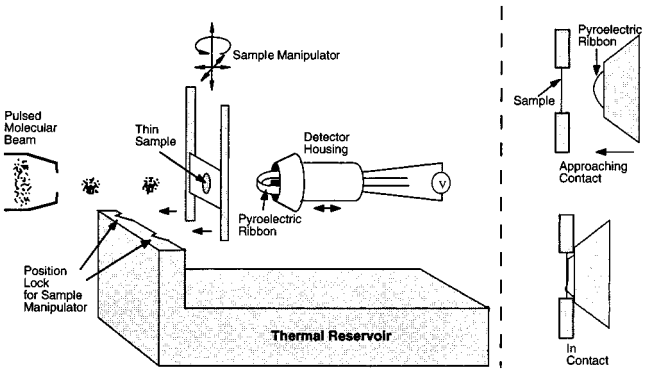

Figure 36. Schematic diagram of Campbell's calorimeter[42] showing the pyroelectric detector. The right side of the figure shows a close up of the pyroelectric film. (Reprinted with permission from ref 42. Copyright 1997 American Institute of Physics.)

thicker substrate films which, therefore, have a higher heat capacity. The technique can, in principle, also be used for measurements at low temperatures. As with the Cambridge system, calibration of the heat signal is achieved using a HeNe laser.

With this system, radiation from the hot source required to generate metal atoms also heats the sample and must be subtracted from the observed detector response. The amount of heat this corresponds to can be quite large (~67% of the total signal for Cu/O/W{100}[42]). A more important current problem is that the sticking probability is not measured, and therefore, it is not possible to derive the heat or a coverage scale without assumed values for the sticking probability.

Measurements were made for the heat of Pb adsorption on Mo{100}. The results obtained can be seen in Figure 37. A very high initial heat of ~340 kJ mol^{-1} is seen, and this abruptly decreases to a constant value very close to the sublimation energy of Pb (207.6 kJ mol^{-1}).[42]

The heat of adsorption of Pb on p(2×1)−O/Mo{100} was also measured.[42] In this case, the heat of adsorption for Pb in the first monolayer is drastically reduced, to ~150 kJ mol^{-1}. The heat rises with increasing coverage to again approach the sublimation energy of Pb. The heat of adsorption of Cu on O/W{100} was also measured, and again, the initial heat was low (300 kJ mol^{-1}) but increases to the bulk sublimation energy of Cu (362 kJ mol^{-1}) with increasing coverage.

These adsorption heats can be used to deduce adhesion energies using the thermodynamic cycle shown in Figure 38. The relationship

$$\sum_n \Delta H_{ads} = -n\Delta H_{sub} + A(2\gamma_{v/m} - E_{adh})$$

can be used to calculate adhesion energies.[42] In this expression, $\sum_n \Delta H_{ads}$ is the integral heat of adsorption over the first n adspecies, A is the area they cover, $\gamma_{v/m}$ is the surface energy of the clean bulk solid of the adspecies, and E_{adh} is the adhesion energy. Note that n/A must be large enough to allow the formation of a continuous film. Using data measured in the

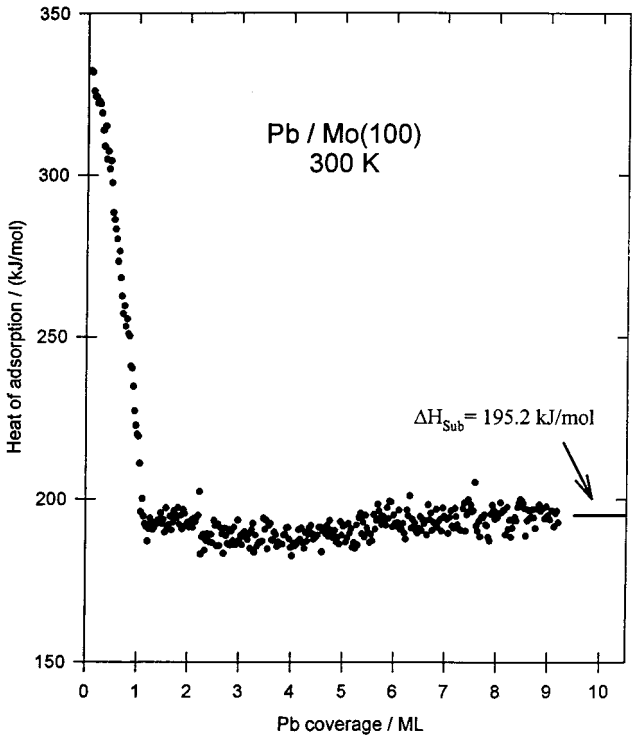

Figure 37. Heat of Pb adsorption on Mo{100} as a function of coverage at 300 K. (Reprinted with permission from ref 42. Copyright 1997 American Institute of Physics.)

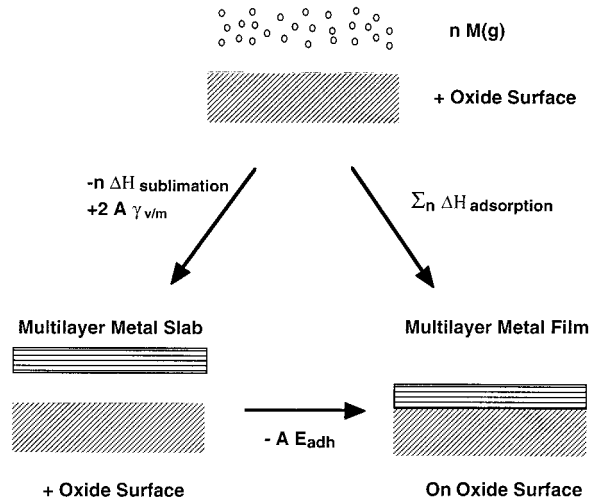

Figure 38. Thermodynamic cycle connecting adhesion energies to adsorption energies. (Reprinted with permission from ref 42. Copyright 1997 American Institute of Physics.)

experiment described,[42] the adhesion energy of Pb to Mo{100} was calculated to be 234 μJ cm^{-2} and that to O-covered Mo{100} was only 56 μJ cm^{-2}. Hence, a single monolayer of O is enough to prevent wetting of the surface with Pb. This is obviously an important point since surface cleanliness will affect the calculation of adhesion energies greatly. Similarly, adhesion energies were calculated for Cu to clean O/W{100} to be 236 μJ cm^{-2}. This was the first measurement providing adhesion energies, and much useful information about the energetics of metal adsorption can be anticipated from the instrument in the future.

VII. Summary and Conclusions

This review has demonstrated that single-crystal adsorption calorimetry has already provided a wide range of new data for well-defined systems, which, when compared with existing structural, kinetic, and spectroscopic data from the literature for these systems, fills an important gap in our knowledge. This is of particular importance to the understanding of surface reactivity and catalysis at metal surfaces.

For a number of reversible single-crystal adsorption systems, isosteric heats are available and generally good agreement has been found using the recently established calorimeter. The key advantage to the technique, which has already been widely exploited, lies in applications to irreversible systems, where adsorption, reaction heats, and bond energies have not been previously measurable for single-crystal surfaces. A summary of initial adsorption heats for systems studied to date is given in Table 8.

Some trends are beginning to emerge. For CO adsorption, initial heats are relatively insensitive to the crystal plane and the average values for the group VIIIA metals Ni, Pd, and Pt increase systematically, from 130 (Ni) to 160 (Pd) to 200 kJ mol^{-1} (Pt). On Pt, the highest heat was observed on the metastable {100}−(1×1) surface; the lower value for the initially hex surface is accounted for by the additional energy required to reconstruct this surface to (1×1) during the adsorption process. In turn, this provided the first experimental measurement of the energy difference between two clean surface structures with the same crystal plane orientation. For the dissociative adsorption of oxygen, the crystal-plane dependence of adsorption heat covers a wider range, for example, for Ni from 440 kJ mol^{-1} on the {111} plane to 550 kJ mol^{-1} on the {100} plane; but these values are significantly higher than the values found for Pt surfaces (360 kJ mol^{-1}). Measurement of the dissociative adsorption of NO on Ni{100} enabled an estimate to be made of the dissociative heat of adsorption of N_2 on Ni{100}, although the direct experiment cannot be performed because of the large activation energy barrier to N_2 dissociative adsorption on Ni. The large variability in heats of adsorption for ethylene and acetylene adsorption from one crystal plane to another, for the same metal, reflects the different nature of the stable species formed in each case. Where the structure and configuration of the stable species is known, from spectroscopic and diffraction studies, the adsorption heats for hydrocarbons have enabled estimates to be made of the metal−carbon bond energies, summarized in Table 7; the average single-bond energy from the three Pt surfaces is 242 kJ mol^{-1}.

Table 8. All of the Initial Adsorption Heats Measured to Date with the SCAC, for Comparison

surface	CO	O_2	NO	C_2H_4	C_2H_2
Ni{110}	132[17]	475[28] [a]		120[32]	180[32]
Ni{111}	130[17]	440[28] [a]			
Ni{100}	122[17]	550[28] [a]	385[27] [a]	203[31]	264[31]
Pt{110}	193[21]	360[21] [a]	162[21]	235[34]	
Pt{111}	187[22]	316[22] [a]		195[35]	
Pt{100} (1×1)	220[20]		191[20]	305[33]	
Pt{100} hex	193[20] [c]		187[20]	213[33]	
Pd{100}	163[23]		110[23]	73[31] [b]	112[31]
Rh{100}	115[24]	386[29] [a]		165[37]	210[37]

[a] Dissociative adsorption. [b] Steady-state sticking only. [c] With conversion to (1×1).

Perhaps the most important message from the calorimetric studies to date is the magnitude of adatom−adatom interaction energies, which have been determined from the detailed coverage dependencies of the calorimetric heats. For example, the heat of dissociative adsorption for oxygen on Ni{100} falls from a zero-coverage value of 500 kJ mol^{-1} to the low value of 150 kJ mol^{-1} at 0.5 ML. The dramatic fall in heat in this case is attributed to a second nearest-neighbor repulsive pairwise adatom−adatom energy of 40 kJ mol^{-1} with a very much larger value between first neighbors, which totally precludes their occupation. There are two major implications for surface reactivity and catalysis from these observations. First, the differential adsorption energy and, hence, the adatom to substrate bond energy and, in turn, the adsorbate reactivity can be dramatically altered by relatively small coverage changes. Second, the thermodynamically stable state of the adsorbed species can be altered. For example, for NO on Ni{100}, the stable state is dissociative ($O_a + N_a$) at coverages below 0.16 ML, but at higher coverages, due to strong adatom−adatom repulsive interactions, the more stable state is molecular (NO_a). In catalysis, this information can be utilized, depending on the desired product: for NO removal, the total (O + N) coverage should be kept below 0.16 ML, when N_2 will be favored; but for NO synthesis, for example, from NH_3 oxidation, a high (O + N) coverage is desirable to avoid dinitrogen production.

Coadsorption studies have also proved to be very revealing. Interaction energies between one adsorbate species and another can be attractive or repulsive, a good example of the former being the interaction between CO and K on Ni{100}; here, the CO calorimetric heat was found to rise from 124 kJ mol^{-1} on the clean Ni{100} surface to 250 kJ mol^{-1} with 0.3 ML preadsorbed K. Comparison with data for lower precoverages of K demonstrated that part of the increased adsorption heat is attributable to a strengthening of the CO bonding to the surface and partly due to a strengthening of the K bonding to the surface.

It must be expected that this new database for adsorption and bond energies, currently only on singular metal single-crystal surfaces, will be considerably extended during the coming decade. The Cambridge group has now initiated a series of studies on the high-index-stepped and step-kinked metal surfaces;[192] considerably more work also needs to be done on coadsorption heats and surface reaction heats, and to date, there have been no studies on alloy single crystals. Campbell's group has very recently pioneered calorimetric studies of metal vapor deposition on metal single-crystal surfaces,[42] which opens up an important new area for investigation. However, no studies have yet been made on the many important semiconductor and oxide surfaces, which

remain as a challenge for further instrumental development work.

VIII. Acknowledgments

We acknowledge Peterhouse, Cambridge, for a Research Fellowship to W.A.B. and the Oppenheimer Trust for a Studentship to R.K. The pioneering work of Dr. C. Borroni-Bird, assisted by Professor Stig Andersson and by Dr. N. Al-Sarraf, in establishing the SCAC technique, and the subsequent work in refining and applying the instrument by Drs. C. E. Wartnaby, J. T. Stuckless, Y. Y. Yeo, A. Stuck, St. J. Dixon-Warren, M. Kovar, and L. Vattuone are all gratefully acknowledged. The technical skills of J. Chevallier, University of Århus, in the preparation of the thin crystals is also acknowledged. Finally, we thank Professor C. T. Campbell for helpful discussions and for providing us with preprints of his recent work.

IX. References

(1) *The Chemical Physics of Solid Surfaces and Heterogeneous Catalysis*; King, D. A., Woodruff, D. P., Eds.; Elsevier: Amsterdam, 1980−95; Vols. 1−7.
(2) Somorjai, G. A. *Introduction to Surface Chemistry and Catalysis;* Wiley: New York, 1994.
(3) Zangwill, A. *Physics at Surfaces*; Cambridge University Press: Cambridge, 1992.
(4) Masel, R. I. *Principles of Adsorption and Reaction on Solid Surfaces*; Wiley: New York, 1996.
(5) Titmuss, S.; Wander, A.; King, D. A. *Chem. Rev.* **1996,** *96,* 1291.
(6) *Surface Science the First Thirty Years;* Duke, C. B., Ed.; Elsevier: Amsterdam, 1994.
(7) See, for example: Besenbacher, F. *Rep. Prog. Phys.* **1996,** *59,* 1737.
(8) *Dynamics of Gas−Surface interactions;* Rettner, C. T., Ed.; Cambridge University Press: Cambridge, 1991.
(9) See, for example: Ge, Q.; Hu, P.; King, D. A.; White, J. A.; Payne, M. C. *J. Chem. Phys.* **1997,** *106,* 1210.
(10) See, for example: Gross, A.; Scheffler, M. *Prog. Surf. Sci.* **1996,** *53,* 187.
(11) Tracy, J. C.; Palmberg, P. W. *Surf. Sci.* **1969,** *14,* 274.
(12) Borroni-Bird, C. E.; Al-Sarraf, N.; Andersson, S.; King, D. A. *Chem. Phys. Lett.* **1991,** *183,* 516.
(13) Borroni-Bird, C. E.; King, D. A. *Rev. Sci. Instrum.* **1991,** *62,* 2177.
(14) Redhead, P. A. *Vacuum* **1962,** *12,* 203.
(15) King, D. A. *Surf. Sci.* **1975,** *47,* 384.
(16) Al-Sarraf, N.; Stuckless, J. T.; Wartnaby, C. E.; King, D. A. *Surf. Sci.* **1993,** *283,* 427.
(17) Stuckless, J. T.; Al-Sarraf, N.; Wartnaby, C. E.; King, D. A. *J. Chem. Phys.* **1993,** *99,* 2202.
(18) King, D. A. *Phys. Scr.* **1993,** *T49,* 560.
(19) Yeo, Y. Y.; Wartnaby, C. E.; King, D. A. *Science* **1995,** *268,* 1731.
(20) Yeo, Y. Y.; Vattuone, L.; King, D. A. *J. Chem. Phys.* **1996,** *104,* 3810.
(21) Wartnaby, C. E.; Stuck, A.; Yeo, Y. Y.; King, D. A. *J. Phys. Chem.* **1996,** *100,* 12483.
(22) Yeo, Y. Y.; Vattuone, L.; King, D. A. *J. Chem. Phys.* **1997,** *106,* 392.
(23) Yeo, Y. Y.; Vattuone, L.; King, D. A. *J. Chem. Phys.* **1997,** *106,* 1990.
(24) Kose, R.; Brown, W. A.; King, D. A. Manuscript in preparation.
(25) Dixon-Warren, St. J.; Kovar, M.; Wartnaby, C. E.; King, D. A. *Surf. Sci.* **1994,** *307−309,* 16.
(26) Al-Sarraf, N.; King, D. A. *Surf. Sci.* **1994,** *307−309,* 1.
(27) Vattuone, L.; Yeo, Y. Y.; King, D. A. *J. Chem. Phys.* **1996,** *104,* 8096.
(28) Stuckless, J. T.; Wartnaby, C. E.; Al-Sarraf, N.; Dixon-Warren, St. J.; Kovar, M.; King, D. A. *J. Chem. Phys.* **1997,** *106,* 2012.
(29) Kose, R.; Brown, W. A.; King, D. A. *Surf. Sci.,* in press.
(30) Vattuone, L.; Yeo, Y. Y.; King, D. A. *Catal. Lett.* **1996,** *41,* 119.
(31) Vattuone, L.; Yeo, Y. Y.; Kose, R.; King, D. A. Manuscript in preparation.
(32) Brown, W. A.; Kose, R.; King, D. A. Submitted to *J. Mol. Catal.*
(33) Yeo, Y. Y.; Stuck, A.; Wartnaby, C. E.; Kose, R.; King, D. A. *J. Mol. Catalysis,* in press.
(34) Stuck, A.; Wartnaby, C. E.; Yeo, Y. Y.; King, D. A. *Phys. Rev. Lett.* **1995,** *74,* 578.
(35) Yeo, Y. Y.; Stuck, A.; Wartnaby, C. E.; King, D. A. *Chem. Phys. Lett.* **1996,** *259,* 28.
(36) Gross, H.; Koel, B. E.; Campbell, C. T.; King, D. A. To be submitted for publication.
(37) Kose, R.; Brown, W. A.; King, D. A. Manuscript in preparation.
(38) Wartnaby, C. E.; Stuck, A.; Yeo, Y. Y.; King, D. A. *J. Chem. Phys.* **1995,** *102,* 1855.
(39) Al-Sarraf, N.; Stuckless, J. T.; King, D. A. *Nature* **1992,** *360,* 243.
(40) Al-Sarraf, N. Ph.D. Thesis, University of Cambridge, 1993.
(41) Wartnaby, C. E.; Stuckless, J. T.; King, D. A. *Surf. Rev. Lett.* **1994,** *1,* 689.
(42) Stuckless, J. T.; Starr, D. E.; Bald, D. J.; Campbell, C. T. *J. Chem. Phys.* **1997**, *107,* 5547.
(43) Roberts, J. K.; Whipp, B. *Proc. Camb. Philos. Soc.* **1934,** *30,* 376.
(44) Roberts, J. K. *Proc. R. Soc. (London)* **1935,** *A152,* 445.
(45) Roberts, J. K. *Proc. R. Soc. (London)* **1935,** *A152,* 464.
(46) Roberts, J. K. *Proc. R. Soc. (London)* **1935,** *A152,* 477.
(47) Černý, S. *Surf. Sci. Rep.* **1996,** *26,* 1−59.
(48) Kisliuk, P. *J. Chem. Phys.* **1959,** *31,* 1605.
(49) Yamazaki, H.; Oguri, T.; Kanomata, J. *Jpn. J. Appl. Phys.* **1971,** *10,* 304.
(50) Yamazaki, H.; Oguri, T.; Kanomata, J. *Jpn. J. Appl. Phys.* **1971**, *10,* 1105.
(51) Eley, D. D.; Norton, P. R. *Proc. R. Soc. (London)* **1970,** *A314,* 301.
(52) Eley, D. D.; Norton, P. R. *Proc. R. Soc. (London)* **1970,** *A314,* 319.
(53) Norton, P. R.; Richards, P. J. *Surf. Sci.* **1974,** *44,* 129.
(54) Couper, A.; John, C. S. *J. Chem. Soc., Faraday Trans. 1* **1977,** *73,* 950.
(55) Couper, A.; John, C. S. *J. Chem. Soc., Faraday Trans. 1* **1977,** *73,* 961.
(56) Couper, A.; John, C. S. *J. Chem. Soc., Faraday Trans. 1* **1978,** *74,* 326.
(57) Beeck, O.; Smith, A. E.; Wheeler, A. *Proc. R. Soc. (London)* **1940,** *A177,* 62.
(58) Beeck, O. *Rev. Mod. Phys.* **1948,** *20,* 127.
(59) Beeck, O. *Rev. Mod. Phys.* **1945,** *17,* 61.
(60) Beeck, O.; Cole, W. A.; Wheeler, A. *Discuss. Faraday Soc.* **1950,** *8,* 314.
(61) Beeck, O. *Adv. Catal.* **1951,** *2,* 151.
(62) Wahba, M.; Kemball, C. *Trans. Faraday Soc.* **1953,** *49,* 1351.
(63) Bagg, J.; Tompkins, F. C. *Trans. Faraday Soc.* **1955,** *51,* 1071.
(64) Klemperer, D. F.; Stone, F. S. *Proc. R. Soc. (London)* **1957,** *A243,* 375.
(65) Brennan, D.; Hayward, D. O.; Trapnell, B. M. W. *Proc. R. Soc. (London)* **1960,** *A256,* 81.
(66) Brennan, D.; Hayward, D. O.; Trapnell, B. M. W. *J. Phys. Chem. Solids* **1960,** *14,* 117.
(67) Brennan, D.; Jackson, J. M. *Proc. Chem. Soc.* Dec **1963,** 375.
(68) Brennan, D. *Discuss. Faraday Soc.* **1966,** *41,* 106.
(69) Brennan, D.; Hayes, F. H. *Trans. Faraday Soc.* **1964,** *60,* 589.
(70) Brennan, D.; Graham, M. J. *Discuss. Faraday Soc.* **1966,** *41,* 95.
(71) Wedler, G. *Z. Phys. Chem. (Frankfurt)* **1960,** *24,* 73.
(72) Wedler, G.; Strothenk, H. *Ber. Bunsen-Ges. Phys. Chem.* **1966,** *70,* 214.
(73) Wedler, G. *Discuss. Faraday Soc.* **1966,** *41,* 104.
(74) Wedler, G. In *Thin metal films and gas chemisorption;* Wissmann, P., Ed.; Elsevier: Amsterdam, 1987; Vol. 32.
(75) Wedler, G. *J. Thermal Anal.* **1978,** *14,* 15.
(76) Černý, S.; Ponec, V.; Hladek, L. *J. Catal.* **1966,** *5,* 27.
(77) Hladek, L. *J. Sci. Instrum.* **1965,** *42,* 198.
(78) Kovar, M.; Černý, S. *Calorim. Anal. Therm. XX−XXI* (Proc. Conf. Assoc. Franc. Calorim. et Anal. Therm., Clermont-Ferrand, 14−17 mai 1990), 97.
(79) Kovar, M.; Dvorak, L.; Černý, S. *Appl. Surf. Sci.* **1994,** *74,* 51.
(80) Dvorak, L.; Kovar, M.; Černý, S. *Thermochim. Acta* **1994,** *245,* 163.
(81) Kyser, D. A.; Masel, R. J. *J. Vac. Sci. Technol.* **1986,** *A4,* 1431.
(82) Kyser, D. A.; Masel, R. J. *Rev. Sci. Instrum.* **1987,** *58,* 2141.
(83) Dixon-Warren, St. J. University of Boulder, CO.
(84) Hill, T. L. *Adv. Catal.* **1952,** *4,* 212.
(85) Young, D. M.; Crowell, A. D. *Physical Adsorption of Gases;* Butterworth: London, 1962.
(86) Černý, S. In *The Chemical Physics of Solid Surfaces and Heterogeneous Catalysis;* King, D. A., Woodruff, D. P., Eds.; Elsevier: Amsterdam, 1983; Vol. 2.
(87) Borroni-Bird, C. E. Ph.D. thesis, University of Liverpool, 1991.
(88) Stuck, A.; Wartnaby, C. E.; Yeo, Y. Y.; Stuckless, J. T.; Al-Sarraf, N.; King, D. A. *Surf. Sci.* **1996,** *349,* 229.
(89) Jacques Chevallier, Institute of Physics and Astronomy, Århus University, Denmark.
(90) King, D. A.; Wells, M. G. *Surf. Sci.* **1972,** *29,* 454.
(91) Ibach, H.; Erley, W.; Wagner, H. *Surf. Sci.* **1980,** *92,* 29.
(92) Froitzheim, H.; Köhler, U. *Surf. Sci.* **1987,** *188,* 70.

(93) Miller, J. B.; Siddiqui, H. R.; Gates, S. M.; Russell, J. N., Jr.; Yates J. T., Jr.; Tully, J. C.; Cardillo, M. J. *J. Chem. Phys.* **1987,** *87,* 6725.
(94) Christmann, K.; Schober, O.; Ertl, G. *J. Chem. Phys.* **1974,** *60,* 4719.
(95) De Angelis, M. A.; Glines, A. M.; Anton, A. B. *J. Chem. Phys.* **1992,** *96,* 8582.
(96) Feigerle, C. S.; Desai, S. R.; Overbury, S. H. *J. Chem. Phys.* **1990,** *93,* 787.
(97) Madden, H. H.; Küppers, J.; Ertl, G. *J. Chem. Phys.* **1973,** *58,* 3401.
(98) Love, C. A.; Schultz, S. L.; Feigerle, C. S. *Surf. Sci. Lett.* **1991,** *244,* L143.
(99) Tracy, J. C. *J. Chem. Phys.* **1972,** *56,* 2736.
(100) Bordoli, R. S.; Vickerman, J. C.; Wolsteholm, J. *Surf. Sci.* **1979,** *85,* 244.
(101) Labohm, F.; Engelen, C. W. R.; Gijzeman, O. L. J.; Geus, J. W.; Bootsma, G. A. *J. Chem. Soc., Faraday Trans. 1* **1982,** *78,* 2435.
(102) Benziger, J. B.; Madix, R. J. *Surf. Sci.* **1979,** *79,* 394.
(103) Kiskinova, M.; Goodman, D. W. *Surf. Sci.* **1981,** *108,* 64.
(104) Koel, B. E.; Peebles, D. E.; White, J. M. *Surf. Sci.* **1983,** *125,* 709.
(105) Klier, K.; Zettlemoyer, A. C.; Leidheiser, H., Jr. *J. Chem. Phys.* **1970,** *52,* 589.
(106) Jackman, T. E.; Davies, J. A.; Jackson, D. P.; Unertl, W. N.; Norton, P. R. *Surf. Sci.* **1982,** *120,* 389.
(107) Engstrom, J. R.; Weinberg, W. H. *Surf. Sci.* **1988,** *201,* 145.
(108) Fair, J.; Madix, R. J. *J. Chem. Phys.* **1980,** *73,* 3480.
(109) Ertl, G.; Neuman, M.; Streit, K. M. *Surf. Sci.* **1977,** *64,* 393.
(110) Thiel, P. A.; Behm, R. J.; Norton, P. R.; Ertl, G. *J. Chem. Phys.* **1983,** *78,* 7448.
(111) Hopkinson, A.; Bradley, J. M.; Guo, X.-C.; King, D. A. *Phys. Rev. Lett.* **1993,** *71,* 1597.
(112) Behm, R. J.; Christmann, K.; Ertl, G.; Van Hove, M. A. *J. Chem. Phys.* **1990,** *73,* 2984.
(113) Tracy, J. C.; Palmberg, P. W. *J. Chem. Phys.* **1969,** *51,* 4852.
(114) Szanyi, J.; Kuhn, W. K.; Goodman, D. W. *J. Vac. Sci. Technol.* **1993,** *A11,* 1969.
(115) Hayward, D. O.; Trapnell, B. M. W. *Chemisorption;* Butterworth: London, 1964; Chapter 9.
(116) Kisliuk, P. *J. Phys. Chem. Solids* **1957,** *3,* 95.
(117) Obtained from J. H. Weaver, Department of Chemical Engineering and Materials Science, University of Minnesota.
(118) McMillen, D. F.; Golden, D. M. *Annu. Rev. Phys. Chem.* **1982,** *33,* 493.
(119) Benson, S. W. *Thermodynamical Kinetics;* Wiley: New York, 1976.
(120) Carter, E. A. *Chem. Phys. Lett.* **1990,** *169,* 218.
(121) Carter, E. A.; Koel, B. E. *Surf. Sci.* **1990,** *226,* 339.
(122) Gardner, P.; Martin, R.; Tüshaus, M.; Bradshaw, A. M. *J. Electron Spectrosc. Relat. Phenom.* **1990,** *54*−*55,* 619.
(123) Hopkinson, A.; Guo, X.-C.; Bradley, J. M.; King, D. A. *J. Chem. Phys.* **1993,** *99,* 8262.
(124) Bradley, J. M.; Hopkinson, A.; King, D. A. *Surf. Sci.* **1997,** *371,* 255.
(125) Campuzano, J. C.; Greenler, R. G. *Surf. Sci.* **1979,** *83,* 301.
(126) Surnev, L.; Xu, Z.; Yates, J. T., Jr. *Surf. Sci.* **1988,** *201,* 1.
(127) Haq, S.; Love, J. G.; King, D. A. *Surf. Sci.* **1992,** *275,* 170.
(128) Lombardo, S. J.; Bell, A. T. *Surf. Sci.* **1991,** *245,* 213.
(129) Grimley, T. B. *Proc. Phys. Soc. (London)* **1967,** *90,* 75.
(130) Grimley, T. B.; Walker, S. M. *Surf. Sci.* **1969,** *14,* 395.
(131) Persson, B. N. J.; Tüshaus, M.; Bradshaw, A. M. *J. Chem. Phys.* **1990,** *92,* 5034.
(132) Hofmann, P.; Bare, S. R.; King, D. A. *Surf. Sci.* **1982,** *117,* 245.
(133) Bare, S. R.; Hofmann, P.; King, D. A. *Surf. Sci.* **1984,** *144,* 347.
(134) Gritsch, T.; Coulman, D.; Behm, R. J.; Ertl, G. *Phys. Rev. Lett.* **1989,** *63,* 1086.
(135) Wong, Y.-T.; Hoffmann, R. *J. Phys. Chem.* **1991,** *95,* 859.
(136) Persson, B. N. J.; Tüshaus, M.; Bradshaw, A. M. *J. Chem. Phys.* **1990,** *92,* 5034.
(137) Rieder, K. H. *Appl. Surf. Sci.* **1978,** *2,* 74.
(138) Winkler, A.; Rendulic, K. D. *Surf. Sci.* **1982,** *118,* 19.
(139) Holloway, P. H.; Hudson, J. B. *Surf. Sci.* **1974,** *43,* 123.
(140) Masuda, S.; Nishijima, M.; Sakisaka, Y.; Onchi, M. *Phys. Rev. B* **1982,** *25,* 863.
(141) Norton, P. R.; Tapping, R. L.; Goodale, J. W. *Surf. Sci.* **1977,** *65,* 13.
(142) Smeenk, R. G.; Tromp, R. M.; Van der Veen, J. F.; Saris, F. W. *Surf. Sci.* **1980,** *95,* 156.
(143) Besenbacher, F.; Stensgaard, I.; Barnes, C. J. in *The chemical physics of solid surfaces;* King, D. A., Woodruff, D. P., Eds.; Elsevier: Amsterdam, 1994; Vol. 7, Chapters 13 and 14.
(144) Wilf, M.; Dawson, P. T. *Surf. Sci.* **1977,** *65,* 399.
(145) Campbell, C. T.; Ertl, G.; Kuipers, H.; Segner, J. *Surf. Sci.* **1981,** *107,* 220.
(146) Coulston, C. W.; Haller, G. L. *J. Chem. Phys.* **1991,** *95,* 6932.
(147) Gorte, R. J.; Gland, J. L. *Surf. Sci.* **1981,** *102,* 348.
(148) Freyer, N.; Kiskinova, M.; Pirug, G.; Bonzel, H. P. *Appl. Phys. A* **1986,** *39,* 209.
(149) Pirug, G.; Bonzel, H. P.; Hopster, H.; Ibach, H. *J. Chem. Phys.* **1979,** *71,* 593.
(150) Zemlyanov, D. Y.; Smirnov, M. Y.; Gorodetskii, V. V.; Block, J. H. *Surf. Sci.* **1995,** *329,* 61.
(151) Bonzel, H. P.; Broden, G.; Pirug, G. *J. Catal.* **1978,** *53,* 96.
(152) Mase, K.; Murata, Y. *Surf. Sci.* **1991,** *242,* 132.
(153) Price, G. L.; Baker, B. G. *Surf. Sci.* **1980,** *91,* 571.
(154) *CRC Handbook of Chemistry and Physics* 73rd ed.; Lide, D. R., Ed.; CRC Press: Boca Raton, FL, 1992.
(155) Stuve, E. M.; Madix, R. J. *J. Phys. Chem.* **1985,** *89,* 105.
(156) Hatzikos, G. H.; Masel, R. I. *Surf. Sci.* **1987,** *185,* 479.
(157) Salmeron, M.; Somorjai, G. A. *J. Phys. Chem.* **1982,** *86,* 341.
(158) Yagasaki, E.; Backman, A. L.; Masel, R. I. *J. Phys. Chem.* **1990,** *94,* 1066.
(159) Boronin, A. I.; Bukhtiyarov, V. I.; Kvon, R.; Chesnokov, V. V.; Buyanov, R. A. *Surf. Sci.* **1991,** *258,* 289.
(160) King, D. A.; Wells, M. G. *Proc. R. Soc. London A* **1974,** *339,* 245.
(161) Windham, R.; Koel, B. E. *J. Phys. Chem.* **1990,** *94,* 1489.
(162) Zaera, F.; Hall, R. B. *J. Phys. Chem.* **1987,** *91,* 4318.
(163) Zaera, F.; Hall, R. B. *Surf. Sci.* **1987,** *180,* 1.
(164) Zhu, X. Y.; Castro, M. E.; Akhter, S.; White, J. M.; Houston, J. E. *Surf. Sci.* **1988,** *207,* 1.
(165) Demuth, J. E. *Surf. Sci.* **1980,** *93,* 127.
(166) Hutson, F. L.; Ramaker, D. E.; Koel, B. E.; Gebhard, S. C. *Surf. Sci.* **1991,** *248,* 119.
(167) Akerlund, C.; Zoric, I.; Kasemo, B. *J. Chem. Phys.* **1996,** *104,* 7359.
(168) Mieher, W. D.; Pelak, R. A.; Ho, W. *Surf. Sci.* **1996,** *359,* 23.
(169) Yamanaka, T.; Inoue, Y.; Matsushima, T. *Chem. Phys. Lett.* **1997,** *264,* 180.
(170) Becker, C. A.; Cowin, J. P.; Wharton, L.; Auerbach, D. J. *J. Chem. Phys.* **1977,** *67,* 3394.
(171) Poehlmann, E.; Schmitt, M.; Hoinkes, M.; Wilsch, H. *Surf. Sci.* **1993,** *287,* 269.
(172) Luftman, H. S.; Sun, Y.-M.; White, J. M. *Appl. Surf. Sci.* **1984,** *19,* 59.
(173) Sinniah, K.; Sands, W. D.; Yates, J. T., Jr.; Janda, K. C. *J. Am. Chem. Soc.* **1991,** *113,* 3684.
(174) Christensen, O. B.; Nørskov, J. K. *Chem. Phys. Lett.* **1993,** *214,* 443.
(175) Uram, K. J.; Ng, L.; Folman, M.; Yates, J. T., Jr. *J. Chem. Phys.* **1986,** *84,* 2891.
(176) Uram, K. J.; Ng, L.; Yates, J. T., Jr. *Surf. Sci.* **1986,** *177,* 253.
(177) Gerlach, R. L.; Rhodin, T. N. *Surf. Sci.* **1970,** *19,* 403.
(178) Kiskinova, M. In *Poisoning and promotion in catalysis based on surface science concepts and experiments;* Studies in surface science and catalysis; Elsevier: Amsterdam, 1992; Vol. 70.
(179) Gerlach, R. L.; Rhodin, T. N. *Surf. Sci.* **1969,** *17,* 32.
(180) Kiskinova, M.; Surnev, L.; Bliznakov, G. *Surf. Sci.* **1981,** *104,* 240.
(181) Brundle, C. R.; Broughton, J. Q. In *The Chemical Physics of Solid Surfaces and Heterogeneous Catalysis;* King, D. A., Woodruff, D. P., Eds.; Elsevier: Amsterdam, 1990; Vol. 3A.
(182) Fisher, D.; Li, Z.-T.; Diehl, R. D. *Surf. Sci.* **1991,** *259,* 85.
(183) Norton, P. R.; Binder, P. E.; Jackman, T. E. *Surf. Sci.* **1986,** *175,* 313.
(184) Campbell, C. T. *Annu. Rev. Phys. Chem.* **1990,** *44,* 775.
(185) Rodriguez, J. A. *Surf. Sci. Rep.* **1996,** *24,* 223.
(186) Bauer, E.; Poppa, H.; Todd, G. *Thin Solid Films* **1975,** *28,* 19.
(187) Tikhov, M.; Bauer, E. *Surf. Sci.* **1988,** *203,* 423.
(188) Goodman, D. W. *Surf. Rev. Lett.* **1995,** *2,* 9.
(189) Xu, X.; Szanyi, J.; Xu, Q.; Goodman, D. W. *Catal. Today* **1994,** *21,* 57.
(190) Peden, C. H. F.; Kidd, K. B.; Shinn, N. D. *J. Vac. Sci. Technol.* **1991,** *A9,* 1518.
(191) Campbell, C. T. *J. Chem. Soc., Faraday Trans.* **1996,** *92,* 1435.
(192) Kose, R.; Brown, W. A.; King, D. A. To be published.

CR9700890